CIVIL ENGINEERING STUDIES
STRUCTURAL RESEARCH SERIES NO. 162

NUMERICAL INTEGRATION FOR ONE-DIMENSIONAL STRESS WAVES

By
Rodney H. Smith
and
N. M. Newmark

A Technical Report
Of a Research Program
Sponsored by
THE OFFICE OF NAVAL RESEARCH
DEPARTMENT OF THE NAVY
Contract Nonr 1834(03)
Project NR 064-183

DEPARTMENT OF CIVIL ENGINEERING
UNIVERSITY OF ILLINOIS
URBANA, ILLINOIS
August 1958

NUMERICAL INTEGRATION FOR ONE-DIMENSIONAL STRESS WAVES

by

Rodney H. Smith and Nathan M. Newmark

A Technical Report
of a Research Program
Sponsored by

THE OFFICE OF NAVAL RESEARCH
DEPARTMENT OF THE NAVY

In Cooperation With

THE DEPARTMENT OF CIVIL ENGINEERING
UNIVERSITY OF ILLINOIS

Contract Nonr 1834 (03)
Project NR 064-183

Urbana, Illinois
11 August 1958

ACKNOWLEDGMENT

This report was prepared as a doctoral dissertation by 1st. Lt. Rodney H. Smith, CE, USA, submitted in partial fulfillment of the requirements for the degree of Ph.D. in Engineering in the Department of Civil Engineering at the University of Illinois, under the direction of Dr. Nathan M. Newmark, Professor and Head of the Department. The work was done as a part of the program of research sponsored by the Mechanics Branch of the Office of Naval Research.

The authors wish to acknowledge the suggestions and assistance of John W. Melin, Research Associate in Civil Engineering, and Mrs. Ann Ihrig, Statistical Clerk, in connection with the solutions obtained on the ILLIAC. Thanks are due Mr. Thomas G. Morrison, Mechanics Research Department, American Machine and Foundry Company, for permitting the use of some of the data originally submitted in a report to him.

Above all, acknowledgment is due the Digital Computer Laboratory of the University for the use of the ILLIAC, the University of Illinois High Speed Digital Computer.

TABLE OF CONTENTS

TABLE OF CONTENTS (CONT'D)

TABLE OF CONTENTS (CONT'D)

LIST OF TABLES

LIST OF FIGURES

LIST OF FIGURES (CONT'D)

LIST OF FIGURES (CONT'D)

LIST OF FIGURES (CONT'D)

NUMERICAL INTEGRATION FOR ONE-DIMENSIONAL STRESS WAVES

1. INTRODUCTION

1.1 Object and Scope

The purpose of this report is to develop a satisfactory dynamic model and numerical integration technique which will solve the problem of one-dimensional stress wave propagation in a wide variety of materials. Primary interest is in linear visco-elastic type materials, but materials which have purely elastic or nonlinear resistances are also treated. The one-dimensional bar of material being considered need not be homogeneous, but may vary in both density and stiffness with length.

In order to design intelligently underground structures to resist atomic bomb loadings which pass over the ground surface, a knowledge of the forces transmitted through the soil cover must be known. Field results are available in classified reports, but these results are not altogether consistent and include a very limited selection of unusual soil types. A theoretical means of solving the problem of blast wave transmission through soils would be extremely valuable. One possible means of doing this would be through the use of a dynamic analytical model and a numerical integration scheme.

This three-dimensional problem can be reduced to two dimensions by assuming the wave front to be plane rather than the true arc of a circle. This assumption contributes little error unless the weapon yield is small or the area being investigated is close to "ground zero". In these cases the straight line wave front deviates from the circle seriously.

It is obvious, however, that a solution of this type would be extremely difficult without some knowledge of the behavior of one-dimensional dynamic models. Therefore, the purpose of this report is to develop a satisfactory model for the one-dimensional case. This study could then serve as a first step in the development of a two-dimensional model. Several dynamic models are examined, and a new model, designated as the Newmark model, as shown in Fig. 1(c), is selected for use in this report. This model is of a visco-elastic nature, i.e., stresses are transmitted by viscous elements (dashpots) as well as elastic elements (springs). The model is characterized by a comparative simplicity of computation and by a great amount of flexibility in use. By proper choice of parameters it can be made to approximate the well known Voigt, Maxwell, and modified Voigt models. Variations in soil density and/or stiffness with depth are conveniently handled, and a nonlinear stress-strain relationship may be considered by use of a multilinear approximation to the stress-strain cure. Means of handling frictional damping and materials in which the yield strength and ultimate strength depend on the rate of strain are also included.

A step-by-step numerical integration technique, the β-integration method (17)(27)[1], is used to compute the response of the lumped mass system. In this manner the displacements, velocities, accelerations, stresses, and strains are determined at a finite number of points for each time interval. Thus, the transmission and accompanying attenuation of these quantities can be traced as the wave passes through the soil mass.

A method is developed to prevent reflections from the fixed end of the model, and thus it is possible to consider an infinitely long soil column.

---

1. Numbers in parentheses refer to the Bibliography.

Although in most of the numerical work physical parameters similar to those that might be found in a vertical soil column have been used, the materials which may be considered are in no way limited to soils or to soil-like materials. It is felt that stress wave propagation in any material may be studied in the manner presented.

It must be emphasized that this report is not a solution to the general problem of blast wave attenuation in soils. Two effects are present in the actual problem, the one-dimensional attenuation considered here, and a spatial dispersion occurring in three dimensions. This spatial dispersion is considered in the Appendix for an elastic, homogeneous, isotropic, and massless half space loaded with a plane wave. A possibility exists that the two solutions could be combined in some manner to give an approximate solution for the combined effects. The method of superposition is unknown, and any such method would undoubtedly be highly approximate.

The one-dimensional solution is more appropriate when the point being investigated lies directly under an atomic air blast. The entire ground surface beneath the blast is loaded virtually simultaneously. Since the loading is approximately equal everywhere in the region of importance, the major effects in the soil will occur in the vertical direction only. In addition, there are many other stress propagation problems which are essentially one-dimensional and which can be solved in this manner, e.g., stress waves in any bar of material in which the long dimension is much larger than the lateral dimensions.[2]

---

2. For certain restrictions to this statement see Section 2.1.

1.2 Brief Summary of Important Previous Work

It would be impossible to mention more than a small percentage of the previous studies dealing with waves in one-dimensional media. Interest in this general field of wave propagation dates from the 17th Century when Newton attempted an explicit mathematical solution to the problem of sound wave propagation, a solution finally completed by Lord Rayleigh in the 19th Century (22, p. 148). For an excellent summary of wave propagation studies prior to 1953 consult Kolsky's Stress Waves in Solids (11). This reference contains a bibliography of more than 100 entries.

The theory of propagation of longitudinal waves in an elastic prismatic bar is presented in a number of references. Among those which present the theory in a concise and easily understood manner are L. H. Donnell (6) and Timoshenko and Goodier (26). Credit for the development of this theory is shared by several authors, primarily in the 19th Century. The solution for this case can be said to be virtually complete if the assumption is accepted that the inertia forces corresponding to lateral expansion or contraction are negligible. The resulting error is not significant if the wave length of the wave is long compared with the lateral dimensions of the bar. Pochhammer (1876) solved the problem considering lateral inertia for a cylindrical bar only (11, p. 54). Davies (1948) also considered lateral inertia in arriving at a more useful solution for this effect. He summarized his work and the work of others in this line in an excellent presentation with another very complete bibliography in the Sir G. I. Taylor commemorative volume (5). Mindlin (1951) simplified these solutions in his studies (15).

A considerable amount of study has also been given to linear viscoelastic materials. Kolsky (11) is again an excellent summary in this field.

He presents the standard models of visco-elasticity developed by Maxwell (1890) and Voigt (1892) as well as more complex models of three and four parameters. Brown University studies have recently greatly advanced the study of linear visco-elasticity. Kolsky and Shi compared results obtained experimentally for high polymers over a wide frequency range with the results obtained from two and three parameter models (12). J. A. Morrison, also at Brown, has developed a mathematical solution for the propagation of a step pulse in both a Voigt model and several three parameter models (16).

A valuable method using a modified means of superposition valid for nonlinear materials was developed by L. H. Donnell in 1930 (6). The complete theory of plastic wave propagation was developed only recently during the Second World War. Classified reports written by T. Von Karman, by Le Van Griffis and M. P. White, and by G. I. Taylor were developed independently at this time, and publications summarizing these developments were issued after the war in unclassified form (29)(30)(23). Experiments at the California Institute of Technology directed by P. E. Duwez and others have qualitatively verified this theory (7)(8)(9)(10). L. E. Malvern extended this theory in 1951 to a bar of material which exhibits a strain rate effect (13).

A numerical integration of the wave equation using a method quite similar to this thesis was developed by E. A. Smith (19)(20). The purpose of this method was to analyze the action of a pile while being driven into the ground. Smith considered a purely elastic spring response with no damping and stated plans to include frictional damping along the sides of the pile in later calculations.

Almost all of the studies mentioned here and elsewhere have used methods of a rather limited scope. Most have considered uniform density and

stiffness of the material. Where viscosity was considered, a nonlinear response could not be considered, and vice versa. Classical mathematical solutions become very difficult when considering problems of a more general nature. Thus, there was no technique which considered more than just a few of the factors. For this reason a new technique was desired.

1.3 Notation

Each symbol used in the text is fully explained when it is first introduced. However, a summary of the notation is presented for the convenience of the reader.

- A = Amplitude of vibration of m_L in highest mode of vibration
- B = Amplitude of vibration of m_s in highest mode of vibration
- b_o = Point on surface of ground directly under blast wave front (Appendix)
- b_n = Point on surface of ground n integration intervals behind blast wave front (Appendix)
- C = Viscosity of relative dashpot
- C_a = Viscosity of absolute dashpot
- C' = Distributed capacitance of electrical analog
- E = Young's modulus
- E_1 = Young's modulus for spring with no parallel dashpot
- E_2 = Young's modulus for spring with parallel dashpot
- F = Total Coulomb force on one complete Newmark model
- F_L = Concentrated Coulomb damping force on m_L
- F_s = Concentrated Coulomb damping force on m_s
- f = Distributed Coulomb damping force
- g = Unit of acceleration, 32.2 ft/sec^2
- h = Increment of time for β-integration method
- I_H = Influence coefficient for horizontal stress (Appendix)
- I_V = Influence coefficient for vertical stress (Appendix)

i (subscript)	=	i^{th} mass
j (subscript)	=	j^{th} time interval
K	=	Spring stiffness for one complete Newmark element
K_1	=	Spring stiffness of spring with no parallel dashpot
K_2	=	Spring stiffness of spring with parallel dashpot
k_o	=	Coefficient of earth pressure at rest
L	=	Distributed inductance of electrical analog
ℓ	=	Length of sample
M	=	Mass of impact mass
m	=	Total mass of one complete Newmark element
m_L	=	Larger mass within element
m_s	=	Smaller mass within element
N	=	Integer
n	=	Number of masses in main thesis
n	=	Number of integration interval being considered, in Appendix only
P	=	Line Load (Appendix)
P(t)	=	Applied force (on end mass only)
p	=	Undamped natural frequency
p_s	=	Instantaneous value of overpressure (Appendix)
p_{so}	=	Maximum value of overpressure (Appendix)
r	=	Percentage of critical damping in single-degree-of-freedom system
Q	=	Internal forces (springs and dashpots)
S_1, S_2, S_3	=	Amplitude of incident, reflected, and refracted waves, respectively
T_s	=	Shortest period of vibration

t = Time

t_o = Time at which strain reaches ϵ_o

u = Displacement of mass

$\dot{u}$ = Velocity of mass, $\partial u/\partial t$

$\ddot{u}$ = Acceleration of mass, $\partial^2 u/\partial t^2$

$\dddot{u}$ = $\partial^3 u/\partial t^3$

V = Instantaneous velocity of impact mass

V_o = Impact velocity of impact mass

v = Velocity of propagation in elastic model

v_f = Fast velocity of propagation

v_s = Slow velocity of propagation

W = Yield of atomic weapon in kilotons (Appendix)

w = Displacement of mass

x = Longitudinal coordinate (in direction of u)

Z = Surge impedance of electrical analog

z = Depth (Appendix)

α = Ratio of spring stiffnesses, K_2/K_1

β = Parameter in β-integration method

γ = Parameter used to study convergence, $\gamma = ph$

ϵ = Strain

ϵ_o = Strain at which time strain rate effect computation begins

η = Ratio of masses, m_s/m_L

λ = Distance between masses

ρ = Density

σ = Stress

σ_o = Stress at beginning of impact

σ_H = Horizontal stress (Appendix)

σ_v = Vertical stress (Appendix)

τ = Relaxation time for Maxwell model only

τ = Retardation time, C/K_2, for other models

τ_{cr} = Critical retardation time

φ = Dimensionless distance, distance/z (Appendix)

ψ = Ratio of impact mass to mass of bar

II. GENERAL METHOD OF ANALYSIS

2.1 Basic Assumptions and Methods

The first step is to consider a column of material, the length of which is assumed very long with respect to the diameter. This means that transverse waves can be neglected, and only longitudinal dilatational (irrotational) waves considered. The continuous mass of the column is lumped into finite masses with generally equal distances between each mass. The masses are connected by springs and/or dashpots in order to represent the elasticity and viscosity of the system. The force, or pressure pulse, can then be placed on the first mass and the response of the system computed by a numerical integration technique.

The assumption that the kinetic energy of the transverse waves can be neglected is the most restrictive and basic assumption made. It is valid for two general classes of problems. One type is the wave propagation in a very large mass of material in which the entire surface is loaded uniformly. The second type is a bar of material in which the longitudinal dimension and the wave lengths are much greater than the lateral dimensions. In the first case lateral strains cannot occur due to the restraining action of the adjacent material. The assumption is certainly valid for this case; if lateral strains are restricted, lateral kinetic energy cannot develop. In the second case the lateral inertia does modify the wave front, but this effect can be often safely neglected, as verified by both theory and experimental results (11, Chapter III). However, when the wave lengths and lateral dimensions are of the same order of magnitude, serious errors may result as shown in the experiments reported in Sections 7.3 and 7.4.

It is further assumed that the applied force is applied equally over the end of the bar and that plane sections throughout the length of the bar remain plane. The stress at each section is assumed to be uniformly distributed over the section.

2.2 General Description of Models Used in Various Parts of the Investigation

This investigation of one-dimensional wave propagation can be divided into three general areas. The first area, or preliminary phase, deals with a study of wave propagation in a purely elastic medium. For this phase a simple perfectly elastic model is used. The purpose of this phase is to examine the effect of certain very fundamental characteristics of the numerical technique. The preliminary phase is reported in Chapter III. A more complex model, designated as the Newmark model, is then used for the bulk of the study. This model contains dissipative elements and is of a visco-elastic nature. The primary purpose of this phase of the work is to study the behavior of the model when certain model parameters are varied. This phase is reported in Chapters IV and VI. Finally, in Chapter VII an attempt is made to compare experimental results with the response of models. In comparing the results of experiments with copper wire no viscous elements are used, but trilinear stress-strain relations are introduced into a model otherwise similar to the model used in the preliminary studies. In the case of tests on Ottawa sand specimens a Newmark model with nonlinear springs is used.

2.3 β-Integration Method

The technique chosen for integration of the model response is the β-integration method developed by N. M. Newmark. For a complete description and derivation of this method see Reference (17).

The generalized form of the β/integration equations follows:

$$\ddot{u}_{j+1} = \frac{P(t) - Q}{m} \tag{2.1}$$

$$\dot{u}_{j+1} = \dot{u}_j + \frac{h}{2}(\ddot{u}_j + \ddot{u}_{j+1}) \tag{2.2}$$

$$u_{j+1} = u_j + h\dot{u}_j + h^2 (1/2-\beta)\ddot{u}_j + h^2 \beta \ddot{u}_{j+1} \tag{2.3}$$

where u = Deflection of mass

$\dot{u}$ = Velocity of mass

$\ddot{u}$ = Acceleration of mass

j = j^{th} time interval

$P(t)$ = External loads

Q = Internal loads

m = Mass

h = Increment of time

β = Parameter of β-method

The quantities above all refer to one mass, the i^{th} mass, but those subscripts are omitted to avoid confusion.

This method of integration is a successive approximation type. At each time interval the following steps are taken:

1) Assume $\ddot{u}_{j+1}$ for each mass.

2) Compute $\dot{u}_{j+1}$ for each mass from equation (2.2).

3) Compute u_{j+1} for each mass from equation (2.3).

4) Compute $\ddot{u}_{j+1}$ for each mass from equation (2.1).

5) Compare $\ddot{u}_{j+1}$ from step 4) with 1). Use step 4) value for assumed $\ddot{u}$ in next cycle and repeat until the desired accuracy is obtained.

The choice of a particular value of β can be associated with the shape of the acceleration-time curve in the integration interval. For example,

$\beta = 1/4$ assumes a uniform acceleration with a value equal to the average of the acceleration at each end of the time interval. $\beta = 1/6$ assumes a linear variation in acceleration. $\beta = 0$ assumes a concentrated acceleration pulse at each interval, which in turn causes an instantaneous jump in velocity at the beginning of each interval. The classical wave theory assumes the velocity at any given point equals zero until the wave reaches that point, at which time the velocity jumps instantaneously to its maximum value (for an initially peaked pulse only). Thus, it would seem probable that $\beta = 0$ would give the closest agreement with theory, and for this reason should not be eliminated from consideration, even though $\beta = 0$ is very seldom used in structural problems.

III. PRELIMINARY STUDIES

3.1 Choice of Simple Elastic Model

Since the purpose of the preliminary studies is to investigate the effect of certain very basic parameters on model response, it is very desirable to pick the simplest possible model. The model selected is represented in Fig. 1(a) and is a purely elastic model.

Consider a prismatic elastic bar of material whose length is large compared with its lateral dimensions. The bar is divided into n sections, each section of equal length. The mass of each section is then divided in half and concentrated at the end of each section.[3] The result is n + 1 masses, the masses concentrated at the ends of the bar having one-half the value of the interior masses. These masses are connected by elastic weightless springs. For convenience the mass, m, and spring stiffness, K, are considered equal to one. The number of masses are always large enough to prevent reflections from the end of the model.

3.2 Differential Equation and Method of Solution

Consider again a long, prismatic, and elastic bar of unit cross-sectional area with a simple tension or compression wave traveling in the longitudinal direction. Extracting a small element of length dx and density ρ, in which the axial deformation is u, the unit strain on one side of the element is $\frac{\partial u}{\partial x}$ and on the other side is $\frac{\partial u}{\partial x} + \frac{\partial^2 u}{\partial x^2} dx$. The stress on either side will be the product of the modulus of elasticity, E, and the unit strain. Summing forces

3. Several problems were computed concentrating the masses at the midpoint of each section, making n masses of equal weight. Results were not as satisfactory as with the method described.

on the element in the longitudinal direction and using Newton's equation of motion,

$$E\left[\frac{\partial u}{\partial x} + \frac{\partial^2 u}{\partial x^2}\,dx\right] - E\,\frac{\partial u}{\partial x} = \rho\,\frac{\partial^2 u}{\partial t^2}\,dx$$

or

$$E\,\frac{\partial^2 u}{\partial x^2} = \rho\,\frac{\partial^2 u}{\partial t^2}\,, \tag{3.1}$$

where t refers to time.

This equation is the well known wave equation.

Using a three point finite difference expression with interval λ to expand $\frac{\partial^2 u}{\partial x^2}$ yields

$$\frac{E}{\lambda^2}\,(u_{-\lambda} - 2u_o + u_\lambda) = \rho\,\frac{\partial^2 u}{\partial t^2}\,.$$

The lumped constants K and m are related to E and ρ by

$$K = \frac{E}{\lambda} \text{ and } m = \rho\,.\,\lambda\,. \tag{3.2}$$

If u_o is considered to be the displacement of the l^{th} mass and (3.2) is used,

$$K\,(u_{l-1} - 2u_l + u_{l+1}) = m\ddot{u}\,. \tag{3.3}$$

This equation could also be derived directly by summing forces on a mass in the model shown in Fig. 1(a) and is presented in this manner to show that the model solution is actually identical to a mathematical solution in which the finite difference expression is used to expand the wave equation when the bar is prismatic. If the bar is nonprismatic, the finite difference expression cannot be used; the governing equations are instead derived directly from the model.

The University of Illinois high-speed electronic digital computer (Illiac) was used to compute the numerical results for the model using an existing code. Although this code was originally written for solution of multi-degree-of-freedom shear beams, it is applicable since it integrates n differential equations of the type of Equation (3.3) using the β-integration method.

3.3 Convergence Limit

The shortest period of vibration for this system may be determined when the masses are vibrating as indicated in Fig. 1(a) and when $x_{i-1} = -x_i = x_{i+1} = u$. A summation of the forces acting on the mass m_i gives the following:

$$K \cdot 2u + K \cdot 2u = m\, p^2 u$$

$$\text{or} \qquad 4\,\frac{K}{m} = p^2$$

$$\text{or} \qquad p = 2\left(\frac{K}{m}\right)^{1/2} = \text{undamped natural frequency}$$

Since $T = \frac{2\pi}{p}$,

$$T_s = \text{shortest period} = \pi\left(\frac{m}{K}\right)^{1/2} \tag{3.4}$$

For $\beta = 0$ the stability limit is T_s/π. This value, T_s/π, is also the convergence limit for $\beta = 1/4$. Furthermore, this value represents the most severe restriction on h, the time interval, in regard to convergence and stability for all the useful choices of β (17). Therefore

$$\left(\frac{m}{K}\right)^{1/2} = \text{convergence and stability limit.}$$

Using equations (3.2),

$$m = \rho \lambda \; ; \; K = E \lambda \quad . \tag{3.2}$$

Then $$\left(\frac{m}{K}\right)^{1/2} = \left(\frac{\rho\lambda^2}{E}\right)^{1/2} \quad .$$

But $$\left(\frac{E}{\rho}\right)^{1/2} = v = \text{velocity of propagation.}$$

Therefore $$\left(\frac{m}{K}\right)^{1/2} = \frac{\lambda}{v} = \text{Transit time between masses.} \tag{3.5}$$

Thus, the time required for the wave to propagate from one mass to the next is identically equal to the stability and convergence limit.

3.4 Results of Parameter Variation

3.4.1 Variation of Rise Time

The influence of rise time is the most important factor in determining the degree of accuracy of the preliminary model. For normal choices of h, the step pulse (no rise time) is severely distorted. In fact, for any rise time less than $\pi\left(\frac{m}{K}\right)^{1/2} = T_s$ the wave is propagated with an increased rise time and some oscillation. When the rise time is equal or greater than T_s, excellent reproduction of the wave shape is obtained for all β values. In fact, for rise times equaling $2\left(\frac{m}{K}\right)^{1/2}$ the distortion is slight and the solution quite satisfactory. See Fig. 2 for a comparison of problems with various rise times.

Owing to a peculiarity of the $\beta = 0$ method, a step pulse will propagate exactly if $h = \left(\frac{m}{K}\right)^{1/2}$ and the end mass has a value of m/2. This type of solution is of very limited value, since either the use of any other value of β or any time interval other than the transit time between masses, or the addition of damping will very severely distort the step pulse.

The inability of models of this type to propagate accurately a step pulse (no rise time) has previously been considered a serious defect. In actuality, although step pulses are often very attractive theoretically, few experimental pulses even approach this condition. If, however, the actual rise time is very small, by taking a large number of masses this model can be made to propagate a wave with a reasonably small rise time.

Further analysis of Fig. 2 will show the spreading action which occurs with this model and all other lumped mass models. The numerical integration technique used tends to spread the wave form slightly, both ahead and behind the theoretical shape. This is an inherent error in this method of analysis.

3.4.2 Variation of Integration Constant β

As mentioned in Section 2.3, the choice of a given value for β is associated with the shape of the acceleration-time curve within a given time interval. Normally β values of 1/6 or 1/4 are felt to give the best approximation to this shape for structural problems, and since a β value of 0 assumes a discontinuous acceleration-time curve, it is not usually considered as an acceptable value. However, since the $\beta = 0$ assumption is closest to the classical wave theory, it is tested along with $\beta = 1/4$ and $\beta = 1/6$. Because the time interval for convergence is small, the difference in these assumptions is also small, and there is little to choose between the three with regard to the degree of agreement with the theoretical solution. In fact, for rise times equaling $\pi(\frac{m}{K})^{1/2}$ the three solutions plot almost as one line. For smaller rise times the agreement is not as good, but for every comparison $\beta = 0$ gives the best solution, with average errors about two-thirds that of the $\beta = 1/4$ and $\beta = 1/6$ solutions.

$\beta = 0$ has other advantages. The β-integration equations are somewhat simplified for this case and the method becomes noniterative without damping. With damping, especially when the amount of damping is small, convergence is more rapid when $\beta = 0$. On the other hand, stability is more critical for $\beta = 0$.

3.4.3 Choice of Integration Time Interval

A time interval of $h \leq \frac{1}{2} T_s$ gives excellent results if the rise time is sufficiently long. If, however, the rise time is too short, the rise time effects camouflage any improvement that might be gained by decreasing h.

A second exact solution was discovered when theoretically examining values of h. This exact solution occurs only when the following conditions are met exactly:

1) $\beta = 0$
2) $h = \frac{\lambda}{v} = \left(\frac{m}{K}\right)^{1/2}$
3) Forcing function is a series of straight lines. The intersection of any two of these straight lines must occur at times equal to $N \cdot \left(\frac{m}{K}\right)^{1/2}$, where N is an integer.
4) First mass = m, not m/2.

This solution is also actually of little practical value since very poor results will occur if there is any variation in spring stiffness or mass size or if any damping is introduced. Therefore, for good results, h should not exceed $1/2 \left(\frac{m}{K}\right)^{1/2}$.

3.5 Impact of a Rigid Mass on the End of a Bar Whose Other End Is Fixed

The problem of a rigid mass striking the end of a perfectly elastic bar has long been a classical wave propagation problem. A complete mathematical solution to this problem was given by J. Boussinesq (1883) and numerical values calculated by Saint Venant (1883). The classical theory is discussed by Timoshenko and Goodier (26, Chapter 15), but a more

complete report of Saint Venant's numerical results is presented in Handbuch der Physik (18). L. H. Donnell (6) also discusses the problem.

It can be shown that the stress and particle velocity for a forward traveling wave are related by the following expression (26, p. 441):

$$\sigma = V (E\rho)^{1/2}, \tag{3.6}$$

where V = particle velocity or instantaneous impact velocity of the rigid body

Therefore, the initial velocity of the rigid body and the initial impact stress are related by the expression

$$\sigma_o = V_o (E\rho)^{1/2}. \tag{3.7}$$

As the rigid mass is slowed down by the bar, the value of the stress wave being imparted to the bar by the mass also decreases. Thus, a compression stress wave with front σ_o and with a monotonically decreasing stress behind the front travels down the bar. When it reaches the fixed end it is reflected as a compression wave, doubling the stress at the fixed end. When the reflected wave returns to the "free" end (actually now a fixed end since the velocity of the impacting mass cannot change abruptly), a second compression wave reflection occurs. Thus, by equations (3.6) and (3.7), the instantaneous value of the stress at the free end will now be

$$\sigma = 2\sigma_o + V (E\rho)^{1/2}, \tag{3.8}$$

The stress-time curve at the free end will therefore be comprised of curves with decaying amplitude, but with instantaneous jumps of $2\sigma_o$ every $2\ell/v$ time units, in which ℓ is the length of the bar.

This problem is solved by the use of the elastic model. The bar is divided into 25 sections with half masses on the ends. The impact mass is rigidly attached to the half mass at the free end and is given an initial velocity V_o. This case of an instantaneously applied impact velocity is the same as the step pulse, and for the normal choice of model parameters the step pulse will be propagated with a definite rise time and oscillatory error. However, if the parameters chosen are those of the special case discussed in 3.4.1, i.e., $\beta = 0$ and $h = \left(\frac{m}{K}\right)^{1/2}$, the wave front will be propagated exactly.

Therefore, in the first set of problems this special case is considered. Two factors should cause the solution to deviate slightly from St. Venant's exact solution. One, the β method assumes the velocity-time curve for the rigid mass to be similar to a series of stair steps rather than the true smooth curve. Since the time scale is divided into from 75 to 350 intervals, depending on the total duration of the impact, it is felt that this error is not too serious. Two, although the stresses at the extreme ends of the bar are desired, the stresses in the first and last springs are not exactly at the ends, but rather a distance of $\ell/50$ from the ends. To overcome this disadvantage a parabola was mathematically fitted to the plot of the appropriate stresses of the last three springs on both ends and then extrapolated to the end of the bar. The extrapolation reduces the small error between the last spring and St. Venant's solution by about 50 percent.

A total of five problems with this special method were computed for various values of ψ. If M is the mass of the rigid body,

$$\psi = \frac{\rho \ell}{M} \tag{3.9}$$

or ψ is the ratio of the mass of the bar to the mass of the rigid body. Figures 3 and 4 show part of the results of these problems and also show the results of St. Venant's calculations in parentheses. The end of impact is defined as the time at which the stress at the impact end first equals zero. The exact time that this occurs is also determined by means of a parabolic extrapolation.

The agreement in Fig. 3 is thought to be excellent with the exception of one point, i.e., at a time of $4\frac{vt}{\ell}$ for $\psi = 1/2$. The value reported in both Timoshenko and Goodier (26, p. 450) and Handbuch der Physik (18, p. 541) is in error for this value. The basic theory indicates that the value of the stress jump at this time must be $2\sigma_o$ rather than the σ_o shown in these references, and the correct value must therefore be either 2.135 or 2.136 rather than 1.135. Since the duration of impact of 4.709 checks exactly with the value determined in this numerical integration, the error is probably one of transposition from Saint Venant's original work. In Fig. 4 Saint Venant's curve for the maximum reaction end stress versus $1/\psi$ is plotted and the points from the five problems also shown. It is impossible to show any difference in the values for the two theories on this figure.

The special case described above is really a trick method since it will not work for any case besides the prismatic elastic bar considered. The purpose of this thesis is to develop a more general method applicable to a wide range of problems of a nonuniform and/or nonlinear nature. Although the normal selection of $h \leq \frac{1}{2}\left(\frac{m}{K}\right)^{1/2}$ will obviously result in some oscillation and flattening of the wave front, three problems were computed using a value of $h = 0.4\left(\frac{m}{K}\right)^{1/2}$. No extrapolation technique is used; the stress in the last spring is plotted directly since it is approximately the same as at the extreme end. This also results in an increase in the apparent rise time

of 0.04 time units. The results of these problems are shown in Fig. 5 along with replotted curves from Fig. 3. Reasonably good agreement is obtained. The large discrepancy for $\psi = 1/4$ at the end of the impact is easily explained. In the first solution the stress became zero prior to the third return of the front of the compressive wave. In the second case, due to a slight error in duration, the front of the wave arrived prior to the end of impact and the stress increased considerably at this point. It is felt that the second solution, although it deviates more from the exact theory, is of more value since it is applicable to a wider range of problems. The agreement with the theoretical solution would be greatly improved if the impact velocity had any appreciable rise time.

IV. DEVELOPMENT OF NEWMARK MODEL FOR VISCO-ELASTIC MATERIALS

4.1 Time Effects to be Considered

The behavior of many materials under dynamic loads has often been found to be very dependent on the rate of deformation. This effect has never been fully explained theoretically. One method of considering these time effects is by the use of viscous elements in the dynamic model. In this manner part of the stress wave is transmitted by "viscous action". The relative size of this viscously transmitted part will be determined by the rate of straining of the system. To accomplish this result dashpots of the Newtonian type, in which the stress is proportional to the difference between the velocity on each side of the element, will be included in the couplings between masses. This type of inter-mass viscosity is referred to as relative damping. Absolute damping, in which the dashpot is attached from a moving mass to a fixed reaction, is very commonly used in structural dynamics, but it is less useful in this case since there is no stationary reference within a moving mass of material to act as a reaction for absolute dashpots. The resulting visco-elastic action of such models has often been considered as applicable to high polymers of rubber and plastics, and it is felt that this general type of model is applicable to soils.

The effect of the addition of viscous elements depends on the model chosen and is described more completely in the discussion of each model. Generally it permits the more rapid propagation of rapidly applied strains and causes a decrease of the maximum stress propagated along with a change in the wave form, but it does not fully or satisfactorily explain all the time effects in the case of the dynamic models considered. The partial propagation of the stress wave by the viscous elements will result in a steeper stress-strain

curve in any viscous model since the dashpot stress is additive to the spring stress. However, when the elements unload, they will not retrace their original path, but will recover along a curve below the original stress-strain curve, since the viscous action is now subtracting stress from the spring stress. A hysteresis loop results, and the area enclosed by the loop represents a loss in the mechanical energy. In the majority of the work done in this thesis the internal friction of the material is assumed to be caused solely by this phenomenon.

A second type of time effect will be considered in an attempt to consider more correctly the phenomena of increased yield stress under rapid loading. This concept is designated as "Strain Rate Effect" and is divorced from viscous action. A more complete discussion of strain rate effect is presented in Section 4.6.

4.2 Choice of Dynamic Model

A number of possible dynamic models are considered, each one basically the same type of lumped mass system as in the preliminary model, but with more involved couplings between the masses. These models were each analyzed with respect to their degree of accomplishment of the following items:

1) Consideration of viscous time effects
2) Transmission of static stress
3) Wide range of attenuation of maximum stress and change of wave form.
4) Equations of simple form
5) Upper limit to velocity of propagation
6) Consideration of nonlinear stress-strain relationships possible
7) Numerical integration technique readily available

8) Sufficient number of variable parameters to enable model to fit test data.

None of the models considered fit these requirements completely, but it is felt that the Newmark model came closer than any other model considered. In the following sections the major deficiencies and strong points in the eight items above are discussed for the models considered.

4.2.1 Maxwell Model

This model consists of a spring and dashpot connected in series. As shown by Kolsky (11, p. 107), the differential equation relating stress, σ, and strain, ϵ, for this model is

$$\frac{d\sigma}{dt} = E\frac{d\epsilon}{dt} - \frac{\sigma}{\tau} \quad , \tag{4.1}$$

where τ is the relaxation time of the solid. Consider a load applied at a constant rate. The response will be the same as an elastic solid at first.[4] As the stress increases, the solid behaves more and more like a viscous fluid with viscosity $E\tau$ until, when the duration is long compared to τ, the solid is almost completely viscous.

Whereas this model might be of some value in creep or similar studies, it cannot be considered further since it will not offer resistance to a static load. This observation is valid whenever a dashpot is used without a spring in parallel with it.

---

4. For an elastic solid $\sigma = E \cdot \epsilon$

Differentiating; $\frac{d\sigma}{dt} = E \cdot \frac{d\epsilon}{dt}$.

4.2.2 Voigt Model

The Voigt model consists of a spring and dashpot in parallel. Since the differential equation of motion for the Newmark model is very similar to that of the Voigt model, the Voigt model equation is derived. Consider a prismatic bar of Voigt material. The stress in each element is the sum of the stress in the dashpot and in the spring.

Therefore, $$\sigma = E \cdot \frac{\partial u}{\partial x} + (C\lambda) \frac{\partial^2 u}{\partial x \partial t} \quad ,$$

where $C\lambda$ is the distributed viscosity of the material. Differentiating with respect to x,

$$\frac{\partial \sigma}{\partial x} = E \frac{\partial^2 u}{\partial x^2} + (C\lambda) \frac{\partial^3 u}{\partial x^2 \partial t} \tag{4.2}$$

The wave equation (3.1) can be written in a more general form for a material in which the stress is not directly proportional to the strains, i.e.,

$$\frac{\partial \sigma}{\partial x} = \rho \frac{\partial^2 u}{\partial t^2} \quad . \tag{4.3}$$

Substituting (4.3) in (4.2),

$$\rho \frac{\partial^2 u}{\partial t^2} = E \cdot \frac{\partial^2 u}{\partial x^2} + (C\lambda) \frac{\partial^3 u}{\partial x^2 \partial t} \quad . \tag{4.4}$$

Using three point finite difference expansions on the right-hand side of equation (4.4) and substituting

$$m = \rho\lambda \qquad \text{and} \qquad K = \frac{E}{\lambda} \tag{3.2}$$

$$m \ddot{u} = K (u_{i-1} - 2u_i + u_{i+1}) + C (\dot{u}_{i-1} - 2\dot{u}_i + \dot{u}_{i+1}) \tag{4.5}$$

in which $C = C\lambda \div \lambda$ = viscosity of dashpot.

This expression is identical to that obtained by summing forces on a single mass of the model.

The Voigt model is somewhat more attractive than the Maxwell model since it will transmit an elastic static stress. However, stresses are propagated much more rapidly than the theoretical elastic velocity of propagation. There is actually no upper bound to the Voigt model velocity of propagation; a small stress will reach the end of any finite length model instantaneously. This feature was considered a serious flaw. Elasto-plastic resistances[5] to static loads are not correctly handled by a Voigt model. Whenever the yield resistances of the springs are exceeded, the masses will deflect at increasing velocities until the entire excess stress is transmitted by the dashpots. Thus, a statically applied stress which is considerably above the yield point will be transmitted without attenuation. Furthermore, other studies have shown that two parameter models are very inadequate in attempts to fit their response to experimental data.

4.2.3 Standard Linear Model

The modified Voigt model, or standard linear model, adds a spring in series with the Voigt element as shown in Fig. 1(b). This model is mathematically equivalent to a Maxwell model with a spring added in parallel.

The differential equation governing the motion of a modified Voigt material is derived by summing strains across one complete element (11, p. 115), resulting in

$$\frac{(C\lambda)\rho}{E_1+E_2}\frac{\partial^3 u}{\partial t^3}+\rho\frac{\partial^2 u}{\partial t^2}=\frac{E_1E_2}{E_1+E_2}\frac{\partial^2 u}{\partial x^2}+\frac{(C\lambda)E_1}{E_1+E_2}\frac{\partial^3 u}{\partial x^2\partial t}\quad . \tag{4.6}$$

5. An elasto-plastic resistance is a bilinear stress-strain relationship in which the second slope is zero.

The subscript 1 refers to the spring with no parallel dashpot; the subscript 2 to the spring with a parallel dashpot.

Again using a three point finite difference approximation to expand the derivatives with respect to x, and using the equations (3.2), we obtain the following:

$$\frac{Cm}{K_1+K_2}\ddot{u} + m\ddot{u} = \frac{K_1K_2}{K_1+K_2}(u_{i-1} - 2u_i + u_{i+1})$$

$$+ \frac{CK_1}{K_1+K_2}(\dot{u}_{i-1} - 2\dot{u}_i + \dot{u}_{i+1}) \qquad (4.7)$$

This third order differential equation now contains only one variable and could be integrated numerically by a number of methods, e.g., by an extension of the β-integration method. Such a scheme was developed and some calculations made on a desk calculator. However, the time consumed is much greater than for a second order equation. Furthermore, there have been no convergence or stability studies for an integration of this type.

The standard linear model has all the advantages of the Voigt model except for the simplicity of the equations and availability of tested integration techniques. In addition, it has a definite upper limit for the velocity of propagation, and has one more parameter to increase the possibility of getting a better fit to test data. The case of elasto-plastic resistance can be correctly considered. The only reason that the Newmark model (actually a very slight modification of the standard linear model) is used in preference to this model is that it possesses all the attributes of the standard linear model plus the Voigt model advantage of simplicity.

4.2.4 Four and Five Parameter Models

There are a number of possible four or five parameter models which could be considered, e.g., two Voigt elements in series, two Maxwell elements in parallel, or either of the above with a third spring in series or parallel. None of these models nor other more complex models were considered in this investigation. It is felt that the additional flexibility in the choice of parameters does not warrant the adoption of a more complex and time consuming numerical technique.

4.2.5 Newmark Model

The Newmark model is obtained by simply introducing a mass between the Voigt element and the series spring K_1 as shown in Fig. 1(c). The actual effect of this mass on the numerical results will be discussed in Section 6.7.4, but the major advantageous effect is the reduction of the order of the governing differential equation from three to two. In addition, there are numerous applications of the β-methods to second order equations. The most useful β-method reference considers viscous damping in a single-degree-of-freedom system (27), but since a multi-degree-of-freedom system may be analyzed by superposition of all the modes, it is useful in the Newmark model analysis. A detailed analysis of this model is presented in the rest of this chapter.

4.3 Differential Equations for Newmark Model

The Newmark model may be thought of as a Voigt model with every other dashpot missing. Therefore, the equations (4.2) through (4.5) discussed for the Voigt model are somewhat applicable to a Newmark model. However, since for the Newmark model the spring stiffness and viscosity of adjacent elements are not necessarily equal, the finite difference equation (4.5) must be altered. It is therefore best to sum the forces on any mass in the lumped

mass model and to derive the differential equation for the model directly. The resulting general expression is

$$m_i \ddot{u}_i = P(t)_i + \left[u_{i-1} - u_i\right] K_{i-1} + \left[u_{i+1} - u_i\right] K_i + \left[\dot{u}_{i-1} - \dot{u}_i\right] C_{i-1} + \left[\dot{u}_{i+1} - \dot{u}_i\right] C_i \quad . \tag{4.8}$$

In the actual coding of this equation several additional terms are included (see Section 4.7). One of the C values will always be zero and P(t) will act only on the end mass. If $K_{i-1} = K_i$ and $C_{i-1} = C_i$, it can be noted that equation (4.8) can be rewritten and becomes identically equal to equation (4.5).

With only a few exceptions $\beta = 0$ was used for the Newmark model calculations. For this case the β-integration equations (2.2) and (2.3) become

$$\dot{u}_{j+1} = \dot{u}_j + \frac{h}{2} (\ddot{u}_j + \ddot{u}_{j+1}) \tag{4.9}$$

$$u_{j+1} = u_j + h\, \dot{u}_j + \frac{1}{2} h^2 \ddot{u}_j \quad . \tag{4.10}$$

Although $\beta = 0$ is noniterative where there is no damping, it is iterative for this case since the trial value of $\ddot{u}_{j+1}$ affects $\dot{u}_{j+1}$, which in turn affects the new computed $\ddot{u}_{j+1}$. Equations (4.8) through (4.10) are thus the basic equations used in Newmark model computations.

4.4 Description of Parameters α, η, v_s, and v_f.

In order to keep the total mass and elasticity of one complete Newmark model element constant, the sum of two adjacent masses, $m_s + m_L$, will be designated as m, and the combined elasticity of K_1 and K_2 in series as K. These subscript designations are shown on Fig. 1(c).

Let $$m_s = \eta\, m_L \; ; \; K_2 = \alpha\, K_1 \quad . \tag{4.11}$$

Then $$m = m_L + m_s = (1 + \eta)\, m_L \quad .$$

Therefore $$m_L = \frac{m}{1+\eta} \; ; \; m_s = \frac{\eta}{1+\eta} \cdot m \quad , \tag{4.12}$$

and $$\frac{1}{K} = \frac{1}{K_1} + \frac{1}{K_2} \; ; \; \frac{1}{K} = \frac{\alpha+1}{\alpha K_1} \quad .$$

Therefore $$K_1 = \frac{(\alpha+1)}{\alpha} K \; ; \; K_2 = (\alpha+1)\, K \quad . \tag{4.13}$$

For this model the maximum, or fast, velocity of stress propagation, v_f, for a high frequency wave can be differentiated from the minimum or slow velocity of propagation, v_s, for a slow frequency wave. For a very rapid movement of the masses the dashpots "lock in" and the system acts as if the springs k_1 represent the only elasticity in the system. Therefore, $v_f = (\frac{K_1}{m})^{1/2}$. On the other hand, when a load is applied very slowly the system acts as if the dashpots were not present and the slow velocity is $v_s = (\frac{K}{m})^{1/2}$, where K is the combined stiffness of the two springs in series. v_f may be thought of as due to an increased Young's modulus for rapid strain rates. If $v_f >> v_s$ (when $K_1 >> K_2$) the various speed components tend to spread out over a wide range, greatly increasing the attenuation. If, however, $v_f \approx v_s$ (when $K_2 >> K_1$), no spreading will occur, and attenuation will be small. It would therefore appear that the parameter α will be a very effective parameter in causing a variation in the amount of attenuation.

4.5 Convergence and Critical Damping

One advantage of the Newmark model is that a coefficient of critical damping can be computed for the lowest period of vibration. Since previous

studies have shown that the convergence limit of undamped multi-degree-of-freedom systems is the shortest period, T_s, divided by π, the determination of T_s will also be of value.

If the system is vibrating in its highest frequency the masses will be moving as shown in Fig. 1(c).

Let u = deflection of masses m_L

Let w = deflection of masses m_s

Since the vibration will be harmonic, let

$$u = A \sin pt \; ; \; w = B \sin pt$$

Therefore

$$\dot{u} = pA \cos pt \; ; \; \dot{w} = pB \cos pt$$

$$\ddot{u} = -p^2 A \sin pt \; ; \; \ddot{w} = -p^2 B \sin pt$$

Therefore

$$w = B/A \; u$$

$$\dot{w} = B/A \; \dot{u} \tag{4.14}$$

$$\ddot{w} = B/A \; \ddot{u}$$

By summing forces on masses m_L and m_s,

$$\begin{aligned} m_L \ddot{u} + K_1 (u + w) + K_2 (u + w) + C (\dot{u} + \dot{w}) &= 0 \\ m_s \ddot{w} + K_1 (u + w) + K_2 (u + w) + C (\dot{u} + \dot{w}) &= 0 \end{aligned} \tag{4.15}$$

Therefore

$$m_L \ddot{u} = m_s \ddot{w}$$

or

$$\ddot{w} = \frac{m_L}{m_s} \ddot{u} \tag{4.16}$$

Using (4.14),

$$\dot{w} = \frac{m_L}{m_s} \dot{u}$$

$$w = \frac{m_L}{m_s} u$$

Replacing $\frac{m_L}{m_s}$ by $\frac{1}{\eta}$ from (4.11) and substituting the above into the second of (4.15) yields

$$m_L \ddot{u} + (K_1 + K_2)\left(u + \frac{u}{\eta}\right) + C\left(\dot{u} + \frac{\dot{u}}{\eta}\right) = 0$$

or

$$\ddot{u} + \left(\frac{K_1+K_2}{m_L}\right)(u)\left(\frac{\eta+1}{\eta}\right) + \frac{c\dot{u}}{m_L}\left(\frac{\eta+1}{\eta}\right) = 0$$

Using relations (4.12) and (4.13) and simplifying,

$$\ddot{u} + \frac{K}{m} \cdot \frac{(\alpha+1)^2(\eta+1)^2}{\alpha\eta} \cdot u + \frac{C}{m}\frac{(\eta+1)^2}{\eta} \cdot \dot{u} = 0 \qquad (4.17)$$

The equation has now been reduced to a single-degree-of-freedom equation of the well known form:

$$\ddot{u} + 2r\,p\,\dot{u} + p^2 u = 0 \qquad (4.18)$$

where r = percentage of critical damping.

Solving for T_s using (4.17) and (4.18),

$$p^2 = \frac{K}{m}\frac{(\alpha+1)^2(\eta+1)^2}{\alpha\eta}$$

$$p = \left(\frac{K}{m}\right)^{1/2} \frac{(\alpha+1)(\eta+1)}{(\alpha\,\eta)^{1/2}} \qquad (4.19)$$

$$T_s = 2\pi \left(\frac{m}{K}\right)^{1/2} \frac{(\alpha\eta)^{1/2}}{(\alpha+1)(\eta+1)} \qquad (4.20)$$

If the h/T requirement for stability and convergence for a single-degree-of-freedom system is met by h/T_s in a multi-degree-of-freedom system, the chosen value of h will of necessity insure stability and convergence of all the modes of vibration. Therefore, the requirements for h/T in the one mass system will be applied to the highest mode of vibration of the Newmark model.

This is done by analysis of the results of T. P. Tung and N. M. Newmark for a damped single-degree-of-freedom system (27). The following analysis is from their work:

If $$\gamma^2 = \frac{p^2h^2}{1 + \beta p^2h^2}$$

then in the case of $\beta = 0$

$$\gamma^2 = p^2h^2 \tag{4.21}$$

If γ^2 exceeds four, the solution will always diverge. Therefore, from (4.21),

$$\text{Convergence Limit} = \frac{2}{p} = \frac{T_s}{\pi} \tag{4.22}$$

However, when $4 > \gamma^2 > 2$ the solution may oscillate seriously. The lower limit therefore sets up an absolute safe limit for h, or for ph.

Thus, $$\text{maximum ph} = (2)^{1/2} = 1.414 \tag{4.23}$$

The problems of Tung and Newmark had values for r of 1, 1.5, and 2.0. If in the Newmark model critical damping occurs when $\tau/\tau_{cr} = 1$, r and τ/τ_{cr} may be related directly. A conservative empirical formula obtained from Tung and Newmark's numerical results relating r, p, and h which will insure good results in the range $2 \geq r \geq 1$ is

$$rph \leq 0.5 \tag{4.24}$$

Since the use of this formula gives increasingly conservative results when r is increasing, it is felt that it is applicable whenever $r \geq 1$. Further analysis of the trends indicates that when r = 0.5 a ph of 1.0 will give satisfactory results.[6] However, it is arbitrarily stated that 1.0 will be the

---

6. When r = 1.0, the choice of ph = 1.0 gave results with satisfactory amplitudes, but with some error in time. With r = 0.5 the results must be improved.

maximum value for ph even with no damping, thus insuring that equation (4.23) will not be violated. For the range $1 \geq r \geq 0$ the following formula is therefore arbitrarily and conservatively chosen:

$$ph = \frac{1}{1+r} \tag{4.25a}$$

Equations (4.24a) and (4.25a) can be rewritten in terms of T_s and τ/τ_{cr}.

$$\frac{h}{T_s} = \frac{1}{4\pi \cdot \tau/\tau_{cr}} \qquad \tau/\tau_{cr} \geq 1.0 \tag{4.24b}$$

$$\frac{h}{T_s} = \frac{1}{2\pi(1 + \tau/\tau_{cr})} \qquad 1 \geq \tau/\tau_{cr} \geq 0 \tag{4.25b}$$

This pair of formulas in conjunction with (4.20) will determine the time interval which will give satisfactory results with a minimum of wasted computation time. If the model parameters vary with length, the element which gives the shortest h must be used. Since these equations are based in part on extrapolations of other results, they were checked by numerical calculations. Scaling difficulties in the Illiac prevented checking these expressions completely, but the results shown in 6.7.1 do verify them satisfactorily.

Although the term τ/τ_{cr} has been used in the convergence analysis, the meaning of critical damping is now fully discussed. Using (4.17) and (4.18),

$$2\ rp = \frac{C}{m}\frac{(\eta+1)^2}{\eta}$$

or

$$C = 2\ rpm\ \frac{\eta}{(\eta+1)^2}$$

Since r critical = 1

$$C_{cr} = 2\ pm\ \frac{\eta}{(\eta+1)^2}$$

Substituting (4.19) for p,

$$C_{cr} = 2\left(\frac{K}{m}\right)^{1/2} \frac{(\alpha+1)(\eta+1)}{(\alpha\eta)^{1/2}} \cdot m \cdot \frac{\eta}{(\eta+1)^2}$$

or
$$C_{cr} = 2\,(Km)^{1/2} \left(\frac{\alpha+1}{\eta+1}\right) \cdot \left(\frac{\eta}{\alpha}\right)^{1/2} \qquad (4.26)$$

The concept of "retardation time", τ, used by Kolsky (11, p. 120) is useful.

Let $\tau = c/K_2$ (in units of time)

Using (4.13),

$$\tau = \frac{c}{(\alpha+1)K}$$

Substituting C_{cr} from (4.26),

$$\tau_{cr} = 2\,(Km)^{1/2} \left(\frac{\alpha+1}{\eta+1}\right)\left(\frac{\eta}{\alpha}\right)^{1/2} \cdot \frac{1}{(\alpha+1)K}$$

Therefore,

$$\tau_{cr} = 2\left(\frac{m}{K}\right)^{1/2} \left(\frac{\eta}{\alpha}\right)^{1/2} \cdot \frac{1}{\eta+1} \qquad (4.27)$$

When

$$\alpha = \eta = 1\ ,\ \tau_{cr} = \left(\frac{m}{K}\right)^{1/2}\ ,$$

or is identically equal to the slow transit time across one complete element.

The concept of critical retardation time applies only to the highest mode of vibration. It therefore does not exactly predict the actual degree of damping, but it will be used, nevertheless, throughout the thesis to compare the relative amounts of damping in the various problems.

4.6 Method for Considering Strain Rate Effect

As mentioned in Section 4.1, the response of the visco-elastic models does not fully explain all the time effects observed in experimental work. The major difficulty occurs when nonlinear stress-strain curves are considered, especially in the elasto-plastic case.

Much investigation concerning the changes in the stress-strain curves for dynamic loadings has occurred at the University of Illinois and elsewhere in recent years (13)(14)[7]. The investigations reported in Massard's summary of dynamic testing (14) indicate that the major effect in mild steel is an increase in the yield stress with increasing strain rate. This type of behavior with an assumed static elasto-plastic resistance cannot be properly considered with the visco-elastic models previously discussed. The discrepancy discussed in 4.2.2 for the Voigt model, in which the dashpots carry the full amount of the applied stress in excess of the spring yield point for a static load, is present whenever a model has an uninterrupted dashpot connection between masses. However, if this connection is interrupted, as in the case of the standard linear or Newmark models, the elasto-plastic resistance of the spring K_1 determines the maximum stress transmitted through this element regardless of the strain rate.

To overcome this difficulty an approximate method is used to increase the yield stress in the spring elements when the strain rate is more rapid than the "static test" strain rate. The cause of this type of strain rate effect is beyond the scope of this thesis, but it is arbitrarily assumed to be independent of viscous action. Actually, as far as this method is concerned, the important fact is that some materials do act approximately in this fashion.

---

7. See list of references in these publications for other investigations.

Thus, two types of time effects can be considered. The first is a viscous type action which acts as a dissipative force in attenuating the maximum stress and in changing the wave form. The second effect is more apropos to materials such as steel or copper and permits an increased yield point or a propagation of stress at reduced strain in the case of materials with no definite yield point. The two effects may be considered separately or jointly.

In most of the available experimental work an "average strain rate" has been used in the calculation of the strain rate effect. Since the strain rate usually was not constant, an averaging scheme normally was used to determine the average strain rate. To be consistent with the test data to be used, the average strain rate was used here. The question as to the extent of the portion of the loading history which affects the yield point of a material is complex. Does the material possess a "long memory" and therefore does the initial strain rate influence the yield point as much as the strain rate immediately prior to yielding, or is the only important part of the strain rate history that part near the actual yield point? In the method developed an arbitrary strain level, ϵ_o, may be picked, for example, 50 percent of the static yield strain, and the strain-rate history occurring prior to that strain is not considered in computing the strain rate.

In the utilization of this method a bilinear or trilinear approximation is made to the static stress strain curve.[8] As the applied force is applied to the Newmark model, a stress wave propagates through the bar of material. The actual average strain rate, $\dot{\epsilon}$, in each spring is computed by means of the following equation:

$$\dot{\epsilon} = \frac{\epsilon - \epsilon_o}{t - t_o} \tag{4.28}$$

8. The choice of only two or three lines is strictly a matter of convenience in coding for the Illiac. More lines could be handled with an appropriate code modification.

ϵ_o is the value of strain discussed in the previous paragraph. Subsequent to the arrival of time, t_o, when ϵ_o is first reached, the average strain rate is computed for each mass at each time interval. An experimental curve of strain rate versus increase in yield stress (or strain) is then entered with the computed strain rate. The yield strain is increased by the amount determined from this curve. The process is continued for each time interval, the yield stress and strain being continuously adjusted to agree with the computed average strain rate. Once this yield stress is reached in a particular spring element, the yield point is frozen at that level and the response is based on this final computed stress-strain curve. For an example of the actual use of this method refer to Section 6.9.

This scheme for considering strain rate effect cannot be defended as being rigorous. It is admittedly only intended as an approximate solution. However, since variations in the strain rate of one order of magnitude cause little variation in the yield stress chosen, differences in the average strain rate are not significant. As more experimental and theoretical information concerning time effects in materials becomes available, more precise approximations will be warranted.

4.7 Programming for Illiac

To solve the differential equations (4.8) through (4.10) the University of Illinois Digital Computer (Illiac) was used. A code, 1108T, was written to solve not only the problem as stated previously in this presentation, but also to include several other factors designed to make the code more general, and thus make it more applicable to other types of problems.

The major additions to the previously stated problem were the addition of two other forms of damping, absolute damping and frictional, or

Coulomb, damping. Two terms are therefore added to equation (4.8), resulting in

$$m_i \ddot{u}_i = P(t)_i + \left[u_{i-1} - u_i\right] K_{i-1} + \left[\dot{u}_{i+1} - \dot{u}_i\right] K_i$$

$$+ \left[\dot{u}_{i-1} - \dot{u}_i\right] C_{i-1} + \left[\dot{u}_{i+1} - \dot{u}_i\right] C_i - \dot{u}_i \ (C_a)_i \pm F_i \qquad (4.29)$$

where $(C_a)_i$ refers to the coefficient of absolute damping on mass i and F_i refers to the frictional force acting on mass i. F_i is shown with both plus and minus signs since its direction depends on the velocity of the mass. It is necessary to have the sign of F_i depend on the velocity of mass i at the previous time interval (j) rather than at the present time interval (j+1) for which computations are being made. When the sign of F_i was allowed to vary with the velocity at interval j+1, on several occasions the problem entered a never ending cycle in which the reversal of the sign of F_i introduced a large enough change in the force acting on a mass to cause the velocity to change its sign again in the next iteration. This would then change the sign of the frictional force and cause the nonconvergent cycle. The method of handling the sign of F_i introduced a small, but necessary error -- this error always occurring well after the maximum response had been reached.

A resistance-deflection subroutine was written to handle purely elastic, bilinear, or trilinear stress-strain curves. In all cases recovery is assumed to be elastic, i.e., parallel to the first slope.

Either an applied stress pulse or impact velocity may be applied to the end mass by approximating the stress or velocity versus time curves with a series of up to ten straight lines. The strain rate versus yield strain curves were straight line approximations with up to thirteen straight lines.

Except for the details already mentioned, the problem solved by this code is the one described in the previous sections. When the strain rate effect modification is used, the springs must all have the same stiffness,[9] but otherwise complete flexibility is possible. Spring stiffnesses, mass sizes, yield strains, and the viscous parameters α and τ may be varied in any desired manner. The maximum number of masses, n, is twenty-five.

It is anticipated that this code may be utilized for purposes other than those discussed in this thesis. Other wave propagation problems such as the pile driving problem discussed by E. A. Smith (20), wave propagation in railroad trains, and a variety of structural dynamics problems in which the shear beam technique is used could be handled. It is felt that the relative damping considered in this thesis might be superior to the absolute type in the analysis of a multi-story shear beam structure. Sliding problems in which Coulomb damping is present may also be solved with 1108T.

The numerical results of this Illiac code have been checked by desk calculator results for a number of cases including elastic models, linear visco-elastic models, models with bilinear and trilinear springs, models with Coulomb damping, models with absolute damping and models using the strain rate effect modification. Although these solutions on the desk calculator were not carried very far in accuracy or duration, it is felt that the correctness of the Illiac solution has been established without a doubt.

---

9. This restriction could easily be removed by rewriting a portion of Code 1108T.

V. LINE TERMINATION

5.1 Purpose of Line Termination Device

For wave propagation in bars of a finite length there is no problem with regard to termination of the model. The end of the model can be considered as either free or fixed. Either case is very easily handled, the fixed end by considering the half mass at the end as never deflecting, and the free end by adding a spring with no resistance to the end of the model. However, it is sometimes desired to study the stress wave propagation in a finite length of an infinitely long bar. For example, it might be desired to find the attenuation in the top 200 ft. of an infinitely deep soil column. Any model must have a definite length with a specified end condition. If this end condition is specified as fixed, the reflected wave has the same sign as the incident wave, and the stress is doubled. If it is considered free, the reflected wave is of the opposite sign and the net stress is zero.

It is possible to eliminate reflections by considering a column of soil so long that the reflections do not return to the area considered until after the entire original wave has passed the region of interest. However, since n has a maximum value of 25, for any but the shortest durations of loading, λ must be taken very large. This results in numerical values being obtained in only the first few springs representing stresses at widely separated points. In addition, the results are less accurate in these first few elements, and the rise time requirement becomes quite restrictive.

For these reasons a line termination device is developed to enable a finite length model to approximate an infinitely long bar of material.

5.2 Electrical Analog Line Termination

Since this problem is similar to the problem of transmission line termination, a solution is derived from the electrical analog. The mechanical elements of the Newmark model are transformed into the electrical analog by using the transformations used by Von Karman and Biot (28, p. 372). This transformation is shown in Fig. 6. If a transmission line is terminated with a resistance in ohms equal to the "surge impedance", or "characteristic impedance", of the line, no reflection will occur. For a "perfect line", analogous to the elastic model, Bewley shows that the surge impedance,

$$Z = \left(\frac{L}{C'}\right)^{1/2} \tag{5.1}$$

where C' is the distributed capacitance and L the distributed inductance (1, p. 54). For a dissipative line, unfortunately, the surge impedance is a complex quantity which varies widely with time. Also complicating this concept is the fact that the line may have varying constants along its length and may be nonlinear. Nonetheless, using the equation (5.1) is the key to determining a satisfactory termination.

An extensive study was made in attempting to design complex terminations which would give no reflections, some of which had resistances which varied with time. However, the simple termination described in the following section proved to be the most effective.

5.3 Application of Electrical Termination to Mechanical Model

The design of the termination is most easily visualized by the description of an illustrative example. Suppose that the analysis of the stress wave propagation in the top 220 ft. of an infinitely deep homogeneous soil deposit is desired. Six complete Newmark models will be needed for this

computation if λ is taken as 20 ft. It was found that connecting a single terminating dashpot to the end of these six elements did not give acceptable results. Instead, a somewhat more elaborate termination is used. Two additional identical elements are added to the system as "buffers". The "buffers" are followed by a perfect element consisting of two equal springs in series (no dashpots, $\alpha = \eta = 1$). This element has its total stiffness and mass equal to that of the previous elements, and since $\alpha = \eta = 1$, from equations (4.12) and (4.13), $m_{end} = 0.5m$ and $K_{end} = 2\ K$. Finally the system is terminated to a fixed end by an absolute dashpot with $C_a = (Km)^{1/2}$, the equivalent mechanical element for the terminal resistance described by equation (5.1).

At the junction of the "buffers" and the perfect element a reflection will occur since the impedances are not perfectly matched. However, the effect of this reflection on the original system is remarkably small. Since the impedance of the terminating dashpot is identical to that of the perfect system, no reflection occurs at the fixed end.

In the "buffer zone" the effect of the reflection is somewhat larger, but the resulting stresses are still reasonably valid.

Figure 7 shows the remarkable efficiency of this termination as compared with two systems without a proper termination. Code 1108T was modified to allow a 29 mass system (problem A-79) to be solved. Seven of these half-elements represented the termination. In this problem it would take 0.23 seconds for the small reflections from the perfect elements to reach the sixth element. There would be no major reflections, even if these perfect elements were fixed ends, up to almost 0.4 sec. Therefore it is reasonably valid to consider the long model used in A-78 as infinite as far as the results in element six are concerned. Problem A-98 was only a thirteen mass system, seven masses of which were also line termination. The stresses in the

sixth element from the loaded end, the last element before the "buffers", were compared for the two problems. If severe reflections were occurring, the 13 mass model length is short enough and the time duration long enough to allow these reflections to modify the stresses in all elements. Nevertheless, the results are in very close accord. Results for other choices of model parameters also show this close agreement.

Problems A-99 and A-101 show the very large reflection errors introduced when the terminating resistance is omitted. The oscillations in these problems are caused by multiple reflections which occur as the reflected wave bounces back and forth between the free and fixed ends.

At the present time Code 1108T will consider only linear dashpot resistances. Line terminations for models with bilinear or trilinear springs must have terminations of the same shape. The existing code must be modified if infinite length systems with nonlinear resistances are considered.

VI. NUMERICAL RESULTS WITH NEWMARK MODEL

6.1 Physical Problem Considered

In keeping with the original desire to examine wave propagation in soils, in this part of the thesis parameters which might fit a hypothetical soil were used. Although the velocities of propagation are roughly those which have been observed in Nevada soils at the Atomic Energy Testing Grounds, no real attempt is made to relate the model parameters to those found in any particular soil, nor is there any attempt to fit the results of this investigation to measured stresses observed in the field. Even if such comparisons were made, they would not be valid, since for all measured data the effects of spatial dispersion would have to be separated from the one-dimensional attenuation.

Uniform soils with velocities of propagation of 1000 and 2000 ft. per sec. are analyzed. Stratified soils and a soil whose stiffness increases gradually with depth are also considered. Linear visco-elasticity was assumed. This assumption is at least approximately valid, since very little plastic deformation has been shown to occur in field tests at this pressure level. Strain rate effect in soils is considered. Table I shows a list of all the problems discussed in this chapter. Other problems whose results appear more as background information are not listed.

The question of the increase of stiffness with depth is not easy to answer. An empirical relation between the horizontal pressure and the modulus of elasticity may be determined by triaxial tests. However, the determination of the horizontal pressure is not elementary. The portion of the horizontal pressure due to the static loading of the soil itself is equal to the product of the coefficient of earth pressure at rest, k_o, and the vertical weight of a soil column of unit area. Actual data concerning reliable values for k_o are

almost nonexistent (24, pp. 139 and 323). The dynamic loading of the soil causes a horizontal pressure which decreases with depth. The horizontal pressure attenuation with depth due to spatial dispersion in a homogeneous soil is greater than the corresponding vertical pressure attenuation (see Appendix). Therefore, this effect may more than counteract the increased static pressure with depth. For example, if a soil weighs 100 lb. per cu. ft. and $k_o = 0.5$, the static horizontal pressure at 100 ft. is about 35 psi. As shown in the Appendix, the difference in maximum horizontal pressure for a 40 Kt weapon between 10 ft. and 100 ft. might easily be 40 psi considering spatial dispersion only. Furthermore, the stiffness variation with depth actually changes with time. These effects must be more precisely handled in any two dimensional solution to this problem. Work being accomplished by M. R. Mehta at the University of Illinois concerning stresses in layered systems may be of some help in formulating a solution to this problem. For the present, however, the assumption of a uniform stiffness with depth may not be as badly in error as a casual observation might indicate.

The solutions presented here could have been equally well presented in dimensionless form. If the shape of the applied force remains constant, the time scale and length scale may be scaled equally and results obtained for wave propagation in bars of much less length for forces of correspondingly shorter duration. Thus, the results of these calculations can be applied qualitatively to other problems as long as the applied force shape is not markedly different.

6.2 Choice of Model Parameters

Since the primary purpose of this investigation is to analyze the effect on the model response when certain model parameters are varied, most

parameters were varied over a wide range. The effects of variation of these parameters are discussed in Section 6.7. However, the value of certain of the parameters remained constant for most problems. The reasons for the constant values selected for these parameters are given below.

The ratio of the masses, η, was taken as unity for most of the problems, since computation time greatly increases if η is taken too small. For one representative problem, in comparison with the computation time when $\eta = 1$, taking $\eta = 1/9$ doubles the computation time, and if $\eta = 1/25$ the time is 8 times as long. As shown in Section 6.7.4, the choice of η does not affect the numerical results greatly. If η is taken quite small, the response of the model should approach that of the standard linear model.

The choice of λ, the distance between each mass, is influenced by four factors.

1) Since the time interval for convergence is directly proportional to the transit time between masses, i.e., $\frac{2\lambda}{v_s}$, increasing λ decreases computation time.

2) Increasing the total number of subdivisions in a bar of material by decreasing λ, increases the accuracy of the results by giving values of the stress at more points along the bar and also by virtue of the fact that finite difference expressions are more accurate with decreasing interval length.

3) Rise time studies (see Section 3.4.1) indicate that the rise time must be at least $\frac{2}{\pi} T_s$. Since for the Newmark model m and k refer to one complete element of length 2λ, the minimum rise time requirement for the Newmark model is $(\frac{m}{k})^{1/2}$, or $\frac{2\lambda}{v_s}$, if both α and $\eta = 1$. If a relatively short rise time is required, this factor will dictate a maximum λ.

4) The depths at which reliable stresses are desired must not be too close to either end of the model. That is, if the model is 19 masses in length

(3 of which represent line termination not including "buffers"), the stresses in springs 3 through 12 exhibit less spurious effects than the springs 1, 2, and 13 through 16. Thus, if the stress is desired at both 50 ft. and 200 ft., a very narrow range of λ will place both 50 ft. and 200 ft. within springs 3 to 12. For this example this range would be 17.4 ft. to 20 ft.

In this phase the number of masses was normally taken as 19. as a compromise between greater accuracy and smaller computational time. $\lambda = 20$ ft. was found to be the most satisfactory compromise between the four factors mentioned and was used throughout this phase. However, the use of $\lambda = 20$ ft. meant that rise times of 40 ms. were used for most problems, 80 ms. being required for one.

Values for the slow velocity of propagation were arbitrarily taken as 2000 ft. per sec. for most problems. This corresponds to a static modulus of elasticity of approximately 85,000 psi if the density is 100 lb. per cu. ft. Other values of 1000 and 4,000 ft. per sec., used in several problems, represent moduli of 21,500 psi and 345,000 psi. If these values seem high, it must be considered that a very high lateral pressure exists and that lateral strains are prevented. In fact, these values represent average values determined from observations of acoustic velocities of soils in place.

6.3 Applied Forces

The applied stress wave on the ground surface is considered to be caused by the ground surface detonation of atomic weapons. The maximum pressure is assumed to be 100 psi and is also assumed to be caused by either a 40 Kiloton or 5 Megaton weapon. Brode's curves (2) are used to determine the shape of the pressure-time curves. Only the positive phase of the blast wave was considered, and its duration was obtained from the Atomic Energy Commission's 1957 handbook (25). The rise times were chosen by the criteria established in the preliminary

studies in order to prevent spurious oscillations. A rise time of 40 milliseconds was generally used. Straight line approximations were made to Brode's curves so as to keep the areas under the curves relatively constant. Since the same requirements as for rise time are valid concerning changes in slope of the applied forces, no straight lines are used with a projection on the time axis of less than 40 milliseconds. Figure 8 shows both Brode's curve and one of the straight line approximations for the 40 Kt weapon. Brode's curve for the 5 Mt weapon has the identical shape, but the duration is increased to 2.38 sec. The straight line approximation is much better for the 5 Mt weapon, since the 40 ms. restriction does not introduce as much error.

6.4 Method of Presentation of Results

Most of the figures used in the presentation of the results for this phase fall into one of three categories.

1) Stress or acceleration versus time. In this type of plot the stress or acceleration in a given element with respect to time is shown. These plots would be most valuable in the design of underground structures. If several plots are shown on one figure for one problem, an idea as to the change in wave form can be indirectly visualized. Similarly, the effect of parameter variation on the wave form can be deduced when several problems at the same depth are plotted on one figure. These plots should be shown as smooth curves; however, most of them have been drawn as a series of straight lines.

2) Stress versus depth at a given time. These stress distribution curves show the stress in every element at one specific time. The change in shape of a wave as it passes through the soil is directly obvious. This type would normally be more valuable than type 1) in studying wave distortion, but unfortunately the wave is so spread out along the depth axis that for any

given time only a portion of the wave is within the model, and the entire wave shape cannot be shown.

3) Maximum stress or acceleration versus depth. These plots are actually summary curves in which the maximum value of stress or acceleration reached in each element is plotted. They show the attenuation of the maximum values conveniently. For accelerations they are the only really worthwhile way of plotting the results.

The effect of lumping a half mass at the ground surface causes a large error in the computed ground surface acceleration. If λ were decreased, a smaller surface mass would be used, and the accelerations would be larger. For this reason it is felt that the numerical values of accelerations are not valid. On the other hand, it is felt that the percentage attenuation of the acceleration with depth is of value, and, except for Fig. 9, all acceleration data are presented in relation to the acceleration of the mass concentrated at the ground surface. The points on these acceleration curves tend to fall on two smooth curves that are practically parallel. When a mass is preceded by a Voigt element, the stress is transmitted more rapidly, resulting in a higher acceleration than is experienced if the mass were preceded by a simple spring. A smooth compromise curve is therefore drawn between these two curves.

In the normal case of $\eta = 1$ the stress in any given model element is said to represent the stress midway between the masses, or at the center of the sections into which the original bar was subdivided. However, when $\eta < 1$, the inertia force of m_s is correspondingly smaller, and therefore the stress in the elements on each side of m_s are more nearly equal. When $\eta = 0$, as in the standard linear model, the stress in the spring K_1 and in the Voigt element are identical. In the latter case it would seem more reasonable to assume that this stress is the stress midway between the large masses. Similarly, when

$1 > \eta > 0$, the stress is assumed to represent the stress at a point closer to m_s than m_L, the distance from m_s being $\frac{m_s}{m_s + m_L} \cdot \lambda$. When this slight difference in location is considered, the results of any one problem plotted as type 2) or 3) above fall on a smoother curve.

6.5 Basic Uniform Soil with 40 Kiloton Weapon Loading (Problem A-48)

Problem A-48 is considered as the basis for comparison of most of the following results. A soil of constant stiffness and v_s = 2000 ft. per sec. is loaded with a 40 Kt applied force as shown in Fig. 8. The ratio of spring stiffnesses, α, and the ratio of the masses, η, were taken equal to one, and the retardation time, τ, was one-half τ_{cr}.

Results of Problem A-48 are included in Figs. 9 through 21, excepting Fig. 18, but only Figs. 9 through 11 relate solely to this problem. Figure 9 shows the stress versus time at four depths. The stress wave front flattens, and the maximum stress attenuates. The law of conservation of momentum applies, and since the area under the stress-time curve is proportional to the momentum, the areas under these curves are all equal. In Fig. 10 the accelerations of three masses are shown. As stated previously, the numerical values of acceleration are less than would be expected in actual tests. The stress distribution or wave shape as it passes through the soil is shown in Fig. 11 for a number of various times. The spreading effect on the wave form is obvious.

The other figures containing data from Problem A-48 will be discussed in the following sections.

6.6 Comparison of Problem A-48 with Voigt Model

One problem was computed using the Voigt model to point out the disadvantage of the high velocity of stress propagation. This problem, A-73, used the same model parameters as A-48, the only difference being the extra dashpot used in A-73. The two solutions are compared in Fig. 12. As expected,

the Voigt model attenuates the wave much more rapidly by sending a large portion of the wave energy ahead in high velocity components. This extremely high velocity propagation of small strains is one feature of the Voigt model which makes it less desirable than the Newmark model.

Also shown on this figure is the theoretical solution for an elastic medium. It can be noted that the Newmark model also sends high velocity stress components ahead of v_s but none more rapid than v_f. Since some test results indicate a more rapid propagation of small strains than elastic theories predict, a small effect of this type is desired. The maximum stress is propagated at approximately the v_s speed for both problems.

6.7 Effect of Parameter Variation

A complete investigation of the effect of each model parameter was accomplished by varying each of the parameters while the others remained constant. The effect of each parameter can be measured by plotting the results versus some standard, usually Problem A-48. In order to fit the model response to experimental results, a knowledge of the results which occur when these parameters are varied must be known.

6.7.1 Variation of Time Interval

In Section 4.5 expressions (4.20), (4.24b), and (4.25b) were derived in order to insure stability and convergence of the numerical method as well as a satisfactory degree of accuracy. The purpose of this section is to verify the usefulness of these expressions. In writing the Code 1108T, scaling factors were used in such a manner as to attempt to prevent the accidental use of much larger time intervals than specified by these equations. In doing this, it made it impossible to pick time intervals that would cause instability or a lack of convergence. In Table 1 the theoretical h from the equations is shown as well

as the h actually used. In most cases the h chosen was the value closest to the theoretical h which allowed the use of convenient scaling factors; therefore the h values fall on both sides of the theoretical. Since almost all the problems reported had very little undesirable oscillation, it is felt that the expressions are verified as being somewhat conservative yet not overly wasteful of computing time. The few problems that did oscillate considerably, e.g., A-105, had time intervals that were certainly small enough, and the oscillations were probably due to other causes. Several problems were checked with smaller h values than shown in Table I with little change in the numerical solution.

6.7.2 Variation of Percentage of Critical Damping

With all other quantities remaining the same as Problem A-48, the retardation time, τ, was varied from 0.1 τ_{cr} to 5.0 τ_{cr}, where

$$\tau_{cr} = 2 \left(\frac{m}{K}\right)^{1/2} \cdot \frac{1}{\eta+1} \cdot \left(\frac{\eta}{\alpha}\right)^{1/2} \qquad (4.27)$$

The results of the variation are shown in Figs. 13 and 14. In Fig. 13 the change in shape of the wave is shown.

The area inclosed within the hysteresis loop formed by the dynamic stress-strain curve gets progressively larger with increasing τ, and the dissipation of energy associated with this loop is therefore larger for large τ values. Increasing τ also tends to propagate more of the stress wave at velocities between v_s and v_f. When τ gets very large, the bulk of the wave is transmitted at velocities near v_f. This variation of the velocity of propagation tends to decrease the maximum stress by spreading the wave. However, when τ exceeds a certain value, the velocity effect tends to concentrate the wave front near the v_f speed and increases the maximum stress, even though the total energy of the wave has been decreased.

Figure 14 is a summary figure in which the maximum stresses at selected depths are shown for 18 problems. The solid curves show the maximums obtained from the series similar to A-48. The maximum attenuation seems to occur in the vicinity of τ_{cr}, although the value of τ which causes the maximum attenuation seems to increase with depth.

A series of problems with the ratio of spring stiffness, α, not equal one was also run. The effects of α variation are discussed in 6.7.3, but, as far as τ variation is concerned, at a constant α the above remarks apply equally well. These curves for $\alpha < 1$, however, must be treated as possibly slightly suspect. An oscillation developed in some of these problems making the maximum value for the stress somewhat in doubt. For this reason it is felt that the values at $\tau = \tau_{cr}$ for $\alpha = 1/10$ are too high, especially the value at 90 ft.

No figure is presented for accelerations, but the maximum attenuation for depths greater than 100 ft. occurs near τ_{cr} for $\alpha = 1$. However, the variation with depth is opposite that for stress, and at 60 ft. for $\alpha = 1$ the minimum acceleration has not yet been reached when $\tau = 5.0\ \tau_{cr}$.

6.7.3 Variation of Ratio of Spring Stiffnesses

Decreasing the ratio of k_2 to k_1, α, increases v_f. When this occurs, the spreading effect of the wave increases, more energy being sent ahead of the main part of the wave. This effect is easily seen in both Figs. 15 and 16, where results of problems with α values of 1, 1/3, and 1/10 are presented. Note that τ remained constant in these problems. Since τ_{cr} is a function of α, from (4.27) the τ/τ_{cr} values for A-48, A-65, and A-67 are 0.5, 0.289, and 0.158 respectively. If the ratio of τ/τ_{cr} had been held constant while τ varied, there would be even more difference in the three curves. To compare attenuation at constant τ/τ_{cr} refer to Fig. 14.

The maximum accelerations as shown in Fig. 17(a) are much less for the two $\alpha < 1$ problems than they are for the $\alpha = 1$ problem. However, $\alpha = 1/10$ plots above $\alpha = 1/3$. This seeming inconsistency may be due to spurious oscillations. On the other hand, since the theoretical accelerations are proportional to the rate of change of the stress, and since these maximum accelerations occur fairly early in a problem, it is possible that the more rapid rate of change of the stress for $\alpha = 1/10$ in the early stages of the problem might cause $\alpha = 1/10$ to plot above $\alpha = 1/3$.

Figure 17(b) shows the maximum stress versus depth. As expected, decreasing α causes a decrease in the maximum value of stress propagated. Had τ/τ_{cr} remained constant this decrease would have been larger.

The hysteresis loop produced by rapidly loading a Newmark model is an excellent measure of the mechanical energy which is dissipated by viscous damping. Figure 18 shows the dynamic stress strain curves for two problems. The average stress in one complete Newmark element is plotted versus the strain in the same element. Problem A-58 shows relatively little dissipation occurring when $\alpha = 1$ and $\tau = 0.5\ \tau_{cr}$. For A-78 the damping is slightly increased to $0.72\ \tau_{cr}$, but $\alpha = 1/3$. This change in α greatly increases the area within the hysteresis loop. The greatly increased dissipation, however, has not reduced the maximum stress markedly since the duration of loading is so long (see section 6.7.6).

Spurious oscillations occurred in a number of the problems in this set. It is felt that the time interval was sufficiently short, but the oscillations might be due to a rise time difficulty across the soft springs (k_2) caused by the rapid stress transmittal through the adjacent stiff springs (k_1). If additional problems with $\alpha < 1$ are computed, this difficulty should be investigated further. In these problems $\eta = 1$. It might be happenstance, but in

subsequent problems when $\alpha < 1$, η was less than one also, and the oscillations were not present. Actually, the effect is not important in most cases. It is most noticeable here when attempting to perform a study on the effect of parameter variation. An error of five percent can cause a curve to break at the wrong point or plot incorrectly in another manner. These oscillations usually cause artificially high maximum stresses to be stored and are therefore conservative. In no other section of the thesis were these oscillations bothersome.

6.7.4 Variation of Ratio of Masses

In this section it will be seen that the value of the ratio of the masses, η, has no major effect on the numerical results. The parameter η was normally taken as one to speed convergence as in Problem A-48. The stress-time curves in the 8th element for problems in which η is 1/4, 1/9, and 1/19 are compared to the similar curve for Problem A-48. As shown in Fig. 19, the results are very similar. In fact, when $\eta = 1/9$, the curve agreed so closely with the $\eta = 1/19$ curve that both curves could not be shown on the figure. The maximum stresses for these two problems were 73.97 psi versus 74.08 psi respectively. Due to the closeness of the plotted curves the points at which the stresses are known are not shown. The print interval for A-48 was 0.015 sec. and for A-74 and A-76 0.01 sec.

Despite the great difference in the mass sizes the accelerations agree remarkably well. For the 8th mass (140 ft.) the maximum accelerations for $\eta = 1$, 1/4, 1/9, and 1/19 are 1.50, 1.38, 1.30, and 1.26 g's respectively.

It may be noted on Fig. 19 that the depths shown are not the same for all problems. This is because η varies. If this difference in depth is considered, the agreement is even better.

Based on these problems, the assumption that the Newmark model behaves much like the standard linear model seems acceptable, even when $\eta = 1$.

It seems reasonable to assume that the results obtained when $\eta \leq 1/4$ will agree very closely with the standard linear model results. These conclusions are of course based on the further assumption that the $\eta = 1/19$ model is virtually a standard linear model. Since the change between $\eta = 1/9$ and $\eta = 1/19$ is negligible, this assumption seems warranted.

The fact that the very close agreement in these problems occurred when the value of τ remained constant is of interest since τ_{cr} is a function of η, the value of τ/τ_{cr} ranged from 0.5 for $\eta = 1$ to 1.15 for $\eta = 1/19$. This fact adds weight to the statement that the ratio τ/τ_{cr} does not completely describe the amount of damping within the system but only the percentage for the highest mode of vibration. Even though the results of these problems in this section are practically identical, due to the different values of η the amount that any particular mode is excited probably varies considerably from problem to problem. For these reasons it may sometimes be of more value to compare results at a constant τ rather than a constant τ/τ_{cr}.

6.7.5 Variation of the Amount of Coulomb Damping

Frictional, or Coulomb, damping is added to the column of material as a force, f, in psi per ft. of length. This unusual choice of units was selected so that the total frictional force acting in one complete element could be readily determined by multiplying f by 2λ, since λ is given in feet in this section. The resulting coulomb force, F, was then applied to the two masses within one element in proportion to their mass.

A number of problems with Coulomb damping were worked, and the results for three problems are shown in Figs. 20 and 21. It should be noticed that the shape of the stress-time curve in Fig. 20 remains unchanged but is lowered everywhere by an amount which increases slowly with time. In Problem B-3 the stress abruptly levels off at about 20 psi. Since the frictional force

acting on each mass is 5 psi, the stress in each element will not decay to zero but will instead reach an equilibrium when the unbalanced force in the elements on each mass equals 5 psi. It is also in this region that the small numerical errors occur due to the reversal of the direction of the frictional force one time interval after the change in the direction of the velocity.

In Fig. 21 the wave form is essentially the same for all problems, but the amount of the stress decrease gets larger with increasing depth, since more and more Coulomb forces are encountered by the stress wave.

Both figures show that the propagation of wave energy near v_f is retarded since the static frictional force (assumed to be equal to the dynamic frictional force) must be overcome before movement occurs.

If a plot of stress-time curves, similar to Fig. 9, were drawn for one of these problems, the area under the curves would no longer be equal, since momentum is removed from the system with the frictional forces.

6.7.6 Variation of Duration of Loading

The response of this model to a pulse of much longer duration is examined by loading with a pressure pulse produced by a 5 Mt weapon at the 100 psi level. The duration of the pulse is five times that of the 40 Kt weapon.

Figures 22 through 24 deal with the 5 Mt loading on the same model as Problem A-48. The stress attenuation is considerably less for the longer duration loading. However, by comparing Figs. 17(a) and 24 it can be seen that the acceleration attenuation for the 5 Mt problem and A-48 are almost identical. Furthermore, the numerical values of acceleration in g's compare equally well. This shows that the accelerations are more a function of the rise time than of weapon yield. This is true because the maximum acceleration occurs usually in the early part of the problem, e.g., for the eighth element at 0.087 sec. for

both problems. As can be seen in Fig. 22, this is before the longer duration of the 5 Mt weapon is even felt by this element. Since the duration does have a slight effect on the slope of the stress-time curve at the lower depths, a very slight trend towards higher accelerations can be detected for the larger weapon at the lower depths.

The variation of model parameters has little effect on the results for large durations of loading. This can best be understood by reference to the 5 Mt problems discussed in Sections 6.7.3 and 6.7.7.

6.7.7 Variation of Acoustic Velocity

In Fig. 25 two acoustic velocities, v_s, are considered with a 40 Kt weapon, and in Fig. 26 three acoustic velocities are considered with a 5 Mt weapon. By looking at the two figures separately two entirely different concepts of the effect of the choice of v_s could be obtained.

In Problem B-50 of Fig. 25 the attenuation is relatively high due mainly to the short duration of loading. Therefore, decreasing v_s from 2000 to 1000 ft. per sec. greatly increases the attenuation. Furthermore, the value of τ/τ_{cr} remained constant, thus the numerical value of τ for v_s = 1000 ft. per sec. is twice that for v_s = 2000 ft. per sec.

In the problems of Fig. 26 the attenuation is small due to the long duration loading. Therefore, changes in v_s, α, τ, or any other variable do not show up markedly. Also, in these problems τ remained constant. This meant that for v_s = 4000 ft. per sec., $\tau = 1.0\ \tau_{cr}$, whereas for v_s = 1000 ft. per sec., $\tau = 0.25\ \tau_{cr}$. This further reduced any variation expected in the three problems. The only really noticeable differences are therefore the movement along the time axis and a slight decrease in the maximum stress. The decrease in initial slope for v_s = 1000 ft. per sec. is mainly due to the fact that an 80 ms. rise time was used for this case to prevent spurious oscillations.

Only a slight difference in slope occurs between the v_s = 4000 ft. per sec. and v_s = 2000 ft. per sec. problems.

Since the stiffness of the soils with a slower v_s is less, the applied forces cause much larger accelerations at the ground surface. However, if the attenuation of stress is high, as in B-51, the maximum stress and slope of the stress-time curve decrease more rapidly than for the stiffer soil. This results in smaller accelerations at large depths. For example, the accelerations of the mass at the surface and at 220 ft. are 1.92 g's and 0.82 g's respectively for B-50 with v_s = 2000 ft. per sec., whereas for B-51 with v_s = 1000 ft. per sec. the corresponding accelerations are 3.51 g's and 0.63 g's. The accelerations for the 5 Mt problems are higher for the softer soils at all depths.

6.7.8 Variation of Integration Constant β

In order to further establish β = 0 as a valid choice for the β-integration technique, a series of problems with β = 0 (A-48), 1/12, 1/8, 1/6, and 1/4 is computed. It is impossible to plot the results because the largest spread was only 0.641 psi, i.e., all β values gave virtually the same answer. If plotted on an expanded scale the β = 0 and β = 1/4 solutions would form an envelope which contains the other results.

β = 0 converged somewhat more rapidly, since its new computed values are more dependent on the previous time interval than are those for any other β value. β = 1/4 was the slowest, since it depends equally on the past and present values. However, the difference is of very little importance. For the problem considered, β = 0 took an average of 8.00 trials per interval and β = 1/4 an average of 8.54 trials per interval.

6.8 Stress Wave Propagation in Soils Whose Stiffness Varies with Depth

In any soil in which the stiffness or density changes either abruptly or gradually, reflections and refractions of the incident wave occur. An increase in stiffness will cause an increase in stress above and below the interface, and a decrease in stiffness will cause an opposite effect. It is sometimes hard to visualize a reflection of this first type causing a stress increase in the refracted wave if part of the energy is reflected. Therefore, an explanation of the theory is presented along with an example.

In a perfectly elastic medium the following equations govern the reflection at a plane interface (11, p. 34):

$$S_2 = \frac{S_1 (\rho_2 v_2 - \rho_1 v_1)}{\rho_2 v_2 + \rho_1 v_1} \qquad (6.1)$$

$$S_3 = \frac{S_1 (2 \rho_1 v_1)}{\rho_2 v_2 + \rho_1 v_1}$$

where S_1, S_2, and S_3 are the amplitudes of the incident, reflected, and refracted waves.

Consider a step function stress wave of stress σ_o and amplitude S_1 striking an interface at which the velocity of propagation increases by a factor of two and the density does not change. According to (6.1) the reflected wave would have an amplitude of $S_1/3$, increasing the stress in the top layer to $1.33\ \sigma_o$. In the lower layer the refracted wave would have an amplitude of $2S_1/3$. Since the modulus of elasticity is four times as large, despite the decrease in amplitude of the wave the stress propagated is $2.67\ \sigma_o$. In a visco-elastic material the relations indicated above are not valid, but the qualitative reasoning applies.

The first soil with variable stiffness to be considered is one in which the acoustic velocity is assumed to vary linearly with depth from

1000 ft. per sec. at the ground surface to 4000 ft. per sec. at 200 ft. The problem is handled by stratifying the soil into 40 ft. layers, so that each layer is represented by one complete element of the model. The springs K_1 and K_2 within each layer are given the stiffness corresponding to the average acoustic velocity within the layer. τ remains constant with depth, and since K_2 increases with depth, the coefficient of damping, C, increases with depth. Since the transit time decreases with depth, τ_{cr} also decreases with depth; the ratio of τ/τ_{cr} is 0.25 at the surface and 1.0 at 200 ft.

Figures 27 through 29 show the results of this problem. As predicted, reflections occur at each interface. The effect of these reflections is greater than the attenuation between layers, and the stress therefore increases with depth as shown in Figs. 27 and 28. On the other hand, the acceleration versus depth plot of Fig. 29 shows the much more rapid acceleration attenuation in a soil of this type.

The series of problems designated as "Stratified Soils I" compares the results of three 2-layer systems and one 3-layer system with a problem in which the soil column is prismatic. The upper layer for these problems always has a v_s of 1000 ft. per sec. The soil profiles are shown in Fig. 30 and the maximum stress versus depth directly below in Fig. 31. Since $\eta = 1/4$ in this model, the stresses obtained in the individual elements are closer to m_s and represent stresses at depths of 16 ft., 24 ft., 56 ft., 64 ft., etc. In plotting it is expedient to average the stresses for two elements and plot the results at 20 ft., 60 ft., etc.

By using Fig. 31 it is possible to determine the effect that an abrupt increase in stiffness would have on the maximum stresses. The maximum

stress, however, does not give the entire picture as to the resulting change in loading that would occur. Figure 32 shows the stress versus time for three of the soils in this group. In the three-layer problem multiple reflections from the two interfaces and the free end occur. The much reduced duration of loading is a result of tension reflections from the free end.

The following three figures, Figs. 33 through 35, deal with "Stratified Soils II". The effects of an underlying soft layer, a thin interbedded soft layer, a thin interbedded hard layer, an infinitely hard base, and an infinitely soft base are all considered. In all cases the upper layer has a v_s of 2000 ft. per sec.

In Fig. 34 both the underlying soft layer and interbedded soft layer show that a substantial decrease in the maximum value of the stress occurs above, in, or below such a layer. Surprisingly, however, the interbedded hard layer did not markedly affect the maximum stress below the hard layer. The fixed end problem might represent a soft clay layer resting on hard rock base. The last plotted stress for this problem is not double that of B-50, since the stress represented is actually 20 ft. from the end of the model. Figure 35 again shows the effect of the multiple reflections. The stress wave at the center of the embedded soft layer (B-47) shows a marked increase in duration.

6.9 Stress Wave Propagation in a Soil Which Exhibits a Strain Rate Effect

The theory and method of handling the strain rate effect concept are discussed in Section 4.6. A number of problems were computed using this concept, and the results of one problem are presented in Figs. 36 through 40.

The static stress-strain curve is not assumed to be linear as in all previous problems, but rather elasto-plastic as shown in Fig. 36(b). The yield

resistance is 50 psi, and the velocity of propagation is 2000 ft. per sec. One problem, B-30, uses the static stress-strain curve. The maximum stress drops immediately to the static yield stress, 50 psi, except for the first few Voigt elements in which the stress slightly exceeds 50 psi. The acceleration also attenuates rapidly in the top 20 ft. In B-31, however, the value of the yield stress is made to vary along with the average strain rate as shown in Fig. 36(b) and (c). A report on the study of dynamic testing of soils at the Massachusetts Institute of Technology presented Fig. 36(c) relating the maximum compressive strength with the rate of strain as compared to the strength at a strain rate of 10^{-2} percent per second (21, p. 46). This chart summarized several series of tests on Boston clay. A summary of this work was presented at the Fourth International Conference on Soil Mechanics (31). The stress-strain curves presented for Boston clay can be very nicely approximated by an elasto-plastic resistance. The arbitrary choice of a v_s of 2000 ft. per sec. and a static yield stress of 50 psi are not necessarily representative of Boston clay. Therefore, the results for B-31 are not the results of wave propagation in Boston clay, but rather for a hypothetical soil whose strain rate effect is the same as that of Boston clay. In fact, it would be an impossibly brittle soil that would have such a high velocity of propagation and yet such a low yield stress. The choice of these values are made simply to be consistent with the previously worked problems.

When strain rate is considered, the stress wave is propagated more rapidly and with considerably less attenuation as shown in Figs. 37 and 38. The acceleration of the ground surface for B-30 is greater than for B-31, since the spring resistance is much less for B-30. However, since the stress is not propagated as rapidly or completely for B-30 as for B-31, the acceleration in B-30 attenuates much more rapidly. Figure 39 shows that the acceleration curves cross before the second mass at 20 ft. depth is reached. In Fig. 40 the fact

that the strain rate decreases with length is shown by observing the decrease in the maximum stress which is also the yield point in this problem for the springs which have yielded. At least the first half dozen springs have yielded.

It has often been suggested in the field atomic tests that the top ten or twenty feet of the soil yield, whereas the remainder of the soil remains elastic. This type of response results in maximum stress versus depth curves which are very similar to the Fig. 40 curves, especially the B-31 curve. The use of elasto-plastic resistances or other bilinear resistances will therefore actually give stress attenuation curves of the same shape as the field data.

VII. COMPARISONS OF MODEL RESPONSE TO EXPERIMENTAL RESULTS

7.1 Description of Plastic Wave Propagation Tests in Copper Wire

During the Second World War a series of tests under P. E. Duwez at the California Institute of Technology was conducted in order to verify the theory of plastic wave propagation developed by Von Karman (29). These tests on 40 to 80 in. copper and aluminum wires, 8 and 11 in. bars of copper and aluminum, and later in steel and lead specimens are comprehensively reported in National Defense Research Committee Reports which have been declassified since the end of the war (8)(9)(10). The tests are summarized by Duwez and Clark in a more readily obtainable Reference (7). Only computations based on the copper wire are included in this thesis. It is felt that the other materials could have been equally conveniently handled had time permitted.

The copper wire was carefully annealed and stretched to a diameter of 0.100 in. and then scratched at 1-in. intervals prior to testing so that the permanent strains could be easily detected. The static stress-strain curve is presented in Fig. 41. The impact testing machine can be described as a sling-shot machine in which an impact hammer is accelerated by means of large rubber bands until it strikes the tup at a certain impact velocity. The tup, to which the wire is attached, and hammer then move together at constant velocity, since the rubber bands continue to exert force on the hammer. When the tup strikes the anvil, the loading is stopped, after which time the wire is free to continue its motion until the kinetic energy of motion is converted into strain energy in the wire. The durations of loading were chosen in the 80-in. specimens so that the plastic wave front would have progressed from 10 to 20 in. along the wire at the time the force was removed. In the two 80-in. cases

considered this duration was 1.7 ms. For the 50-in. wire the duration was longer, 2.77 ms in the case considered, in order to study the effect of reflection.

The results of the tests are presented primarily as plots of the permanent strains in the wire versus distance from the impact end after the completion of the tests. The results are then compared to Von Karman's theory. In the first report (9) the agreement is not too good, since the effect of reflections and of the unloading wave produced by the release of the deforming force were not considered. In other words, the theoretical solution froze the strains at the values which occurred at the time the load was released. In the latter reports the stopping effect was considered, and the theoretical and experimental curves were in reasonably close agreement (9)(10). Malvern also considered the results of these tests in his theoretical investigation of strain rate effect (13). His theory explained part but not all of the discrepancies still noted between theory and experiment.

7.2 Comparison of Elastic-Plastic Model Response with Copper Wire Tests

A considerable number of problems were solved in an attempt to reproduce the results of Duwez. The agreement for the final models used, which will be described below, is thought to be reasonably good. It is felt, however, that with a closer approximation to the stress-strain curve the results would have been better. The results in Figs. 42 and 43 show the same general shape as Von Karman's theory and Duwez's results. Generally these figures show that a region of relatively constant permanent strain is reached at the impact end, followed by a region of decreasing strain in the center of the bar, and a region of reflection and increased strain at the fixed end.

In Fig. 44, in which the wire is shorter and the duration of impact longer, the strain is practically constant with length. This general

observation is true also for the experimental curve. It should be realized that the stress-strain curve is quite flat in this region, and a very small discrepancy in stress can account for the differences shown in this figure and in the other figures as well. It is further believed that the results in Fig. 44 are within the experimental error.

For these problems the model consists of 20 masses. A modification of the Illiac code allows an impact velocity, which could be varied with time, to be applied at the end of the wire. A true impact on the end of the bar is similar to a step pulse which, as previously noted, will cause oscillations. For that reason both a solution with a true impact velocity and one with an applied velocity with a 0.2 ms. rise time were considered. This hypothetical rise time was actually used by Duwez in an attempt to bring the theory closer to experimental results without much success (9, Appendix) and was also used by Malvern (13). The difference in the results obtained with these two different assumptions was very small, slight decrease in the strains being noted for the 0.2 ms. rise time case. For this reason the original true impact velocity solution is presented.

Since stress-time curves were not presented, it is virtually impossible to determine the best values of the viscous parameters α and τ. Time effects do not show up in a plot of permanent strains. In fact, after an approximation for the stress-strain curve is made, the effect of adding viscous elements does not markedly change the shape of the permanent set curve. This was true for a series of problems in which α varied from 1 to 1/10 and τ/τ_{cr} varied from 0 to 0.5. In addition, the consideration of a strain rate effect of the same magnitude as Habib's results reported by Malvern (13) for copper cylinders did not change the strain at any one point enough to make it worthwhile to include a plot showing the strain rate effect solution. Actually, α

and τ can be so chosen as to give a reasonable approximation of Malvern's assumed dynamic stress-strain curves.

For these reasons, the results presented are for a model very similar to the preliminary model of Fig. 1(a) except that the springs are either bilinear or trilinear approximations to the static stress strain curve as shown in Fig. 41. Whereas the choice of other parameters does not exert a large influence on the solution, the selection of a replacement stress-strain curve is very important. These replacements are chosen by attempting to keep the area under the curves roughly equal for all strains less than the maximum strains expected. Recovery is assumed to be parallel to the first slope of the replacement curve. The discrepancy between solutions for the bilinear and trilinear approximations in Fig. 42 shows the importance of the stress-strain curve. The fact that these two solutions more or less bracket the experimental solution is of some interest, and it is felt that closer agreement could be obtained by the use of better approximations. The choice of a maximum number of three straight lines was used to avoid writing an intricate and space consuming subroutine for the Illiac. A continuous curve or larger number of straight lines could be used if 1108T were suitably modified. Using three straight lines means that the strains are propagated at three different wave velocities. The manner in which these three waves reinforce and partially cancel each other could be considerably different from the manner in which the infinite number of wave velocities act. Certainly a better approximation would show more of an increase in the stress at the fixed end due to reflection than the trilinear approximation does.

7.3 Description of Wave Propagation Tests in Ottawa Sand Specimens

A comprehensive study of the behavior of soils under dynamic loading was accomplished at the Massachusetts Institute of Technology under Taylor and Whitman in 1952 through 1954 for the U. S. Army Corps of Engineers (31)(22).

Whitman presented a summary of these tests in a more readily obtainable reference (30). In these tests the primary objects were investigation of strain rate effect, wave propagation, and dynamic loading of footings.

Strain rate effects for a number of soils were determined.[10] No appreciable strain rate effect was noticed with sands, although viscous time effects were detected. The wave propagation tests were almost exclusively in Ottawa sand with sample lengths ranging from 7 in. to 32 in. In Fig. 45 a triaxial stress-strain curve at a confining pressure of 14 psi is shown (22, Fig. 11.1). Unfortunately, the M.I.T. report presented a curve for an Ottawa sand with void ratio of 0.49 and maximum compressive strength of 32 psi but then used an Ottawa sand with a void ratio of 0.53 and maximum compressive strength estimated at 28 psi. Therefore, in obtaining Fig. 45 all ordinates were scaled by a factor of 28/32.

The wave propagation tests were conducted in a "long triaxial machine" under a confining pressure of 14 psi. The 2-in. diameter samples were mounted horizontally and supported by celluloid slings. A spring loaded ram with a 50-lb. mass was released and allowed to strike a lighter pressure gage assembly at the end of the soil sample. Because of its lighter mass the pressure gage assembly separated from the ram, the ram being stopped shortly thereafter by a glass fibre stop. The pressure gage assembly acted as a loading cap and compressed the soil specimen. Impact velocities were those of the pressure gage assembly or loading cap. As the loading cap compresses the soil sample, it loses its momentum, and when the stress at the end becomes zero, the mass rebounds. Thus, this problem is identical to the impact of a rigid mass and elastic bar considered in Section 3.5 except that the bar is now soil instead of an elastic material.

---

10. Part of these results are used in Section 6.9 and Fig. 36(c).

The stress-time records at the impact end and reaction ends were made by using diaphragm type pressure gages and were plotted on one oscilloscope. Some difficulty was reported with nonlinearity of the response of the oscilloscope and with drift of the zero position.

These experiments do not fit into either of the two classes of problems described in Section 2.1, in which the assumption of negligible lateral kinetic energy is valid. Although a lateral pressure exists within the triaxial chamber, lateral strains are definitely not prevented. Furthermore, the length to diameter ratio varies from 3.5 to 16, hardly enough to qualify as the class of problems in which the lateral inertia effect can be safely disregarded. Thus, when the impact velocity is applied to these samples, a serious deviation from the theoretical solution should be expected.

7.4 Comparison of Visco-Elastic-Plastic Model Response with Ottawa Sand Tests

Although the M.I.T. report considered the 20-in. sample results as somewhat inconsistent, this length is selected as the best for this analysis for two reasons. One, the lateral inertia effect is theoretically more significant for smaller length samples. Two, the longer 32-in. samples buckled laterally and could not be accurately analyzed.

These 20-in. samples were divided into 20 elements of 1 in. each, i.e., 10 complete Newmark elements. The impacting mass was rigidly attached to the end half-mass and given an initial velocity. The stresses in the first and last springs were considered to be those of the impact and reaction ends. Various parameters were chosen for the models used, and the best agreement obtained is presented in Figs. 46 through 49. The value of $\eta = 1/4$ is chosen to approximate the standard linear model without appreciably increased computer time. Values of $\alpha = 1$ and $\tau/\tau_{cr} = 0.31$ give arrival times and initial slopes for the

stress waves that agree roughly with the experimental results. Since other errors of more importance occurred in the solutions, the best values of these parameters are still unknown and can be determined only from experimental tests in which the experimental conditions are closer to the assumptions inherent in this numerical method.

The remarks of Section 7.2 concerning the errors caused by the choice of the trilinear stress strain approximation apply equally well to this case.

The main cause of the rather large discrepancies in the experimental and theoretical results in Fig. 46 through 49 is the lateral inertia effect. When a rapidly applied stress pulse propagates into the sample, a certain amount of time elapses before the lateral inertia can be overcome. In this short length of time the sample acts as if lateral strains were prevented, and stresses much higher than the static ultimate strength are attained momentarily. As the soil particles begin to move laterally, this stress decays rapidly to the value which would occur without lateral inertia. This initial stress occurs with very small strains, and the strain, or stress, propagated to the reaction end is delayed considerably.

These theoretical deductions are verified in the experimental results shown in these figures. The initial high impact end stress and delayed rise at the reaction end are shown. The small initial stress at the reaction end is caused by the rapid propagation of the small strains occurring at the impact end during the initial stages of impact. The length of time of the delay is roughly equal to the time associated with the decay of the high impact end stress peak.

The theoretical curves do not show any of the lateral inertia effect, but they usually agree fairly well with what we might assume the experimental shape would be without this effect. These theoretical curves break sharply at 20 psi. This break represents the delay in arrival time between the wave whose

velocity is determined by the initial slope and the wave whose velocity is determined by the second slope of the stress-strain curve. Reflection causes this break to be at a higher stress than indicated by the stress-strain curve, but attenuation and the fact that the stress is not at the extreme end causes this break to be at less than double the stress indicated by the stress-strain curve.

The size of the impact weight used was 8 lbs. In the M.I.T. reports it was stated that the pressure gage assembly weighed 6 lbs. when originally designed. However, in the remarks which followed several modifications were mentioned. Although the final weight of the impact mass was not given, preliminary results from the Illiac using 6 lbs. gave durations which were much too short. Arbitrarily increasing the weight to 8 lbs. resulted in much better agreement; therefore, this size mass is used.

The slightly higher stress obtained by theory in the flat part of the stress-time curves could very probably be due to the assumed perfect reflection which, as suggested in the M.I.T. report, probably did not occur in the experiment. The much higher value for the reaction end shown in Fig. 49 cannot be due to this cause. The most logical explanation for a decrease in stress when the impact velocity has its highest value is that the sample buckled laterally in the same manner as the 32-in. samples.

The discrepancies noted in this section are not discouraging so far as the possibility of theoretically analyzing stress wave propagation in soils. On the contrary, if tests in which the lateral strains are prevented can be successfully conducted, it is felt that the model response could be reasonably well fitted to the results.

VIII. SUMMARY AND CONCLUSIONS

In this thesis the problem of stress wave propagation in a one-dimensional medium has been analyzed by the use of a lumped mass dynamic model and the β-integration method. The purpose is to present a simple and approximate method for handling some of the problems in elastic, elastic-plastic, visco-elastic, and visco-elastic-plastic materials which are either impossible or very time consuming to solve by classical mathematical treatments. This class of problems includes those in which the stiffness or density varies with the length of the material.

The effect of lateral inertia is neglected, and it is shown that this assumption is acceptable for two classes of problems, those in which the lateral strains are prevented and those in which the longitudinal dimension and the wave length of the stress wave are much larger than the lateral dimensions.

This technique may be of interest in studying the two or three dimensional problem of blast wave transmission in soils. This method, however, is not offered as a solution to that problem, except when the loading is such that the entire ground surface in the general vicinity is loaded simultaneously. This situation is approximately reached when a high air burst is detonated directly above the soil column being considered.

In the preliminary studies a perfectly elastic model is considered. A minimum rise time of about $\frac{2}{3} T_s$ is necessary to prevent spurious oscillations. Pulses with rise times shorter than T_s are transmitted with increased rise time. A value of zero for β in the β-integration method is selected as the best value. The convergence and stability limits equal the transit time between masses, and the integration time interval should be equal to or less than half this value to insure good results. A "trick" exact solution exists

for the step pulse with $\beta = 0$ and a time interval equaling the transit time. This "trick" method and the standard choice of time interval are used to solve the classical problem of a rigid mass striking an elastic bar.

A number of dynamic models are examined using selected criteria, and a new model, designated as the Newmark model, is finally selected as the model to be used for visco-elastic materials. The models examined and the principal disqualifying property of each follow:

a) Maxwell model -- does not transmit static stress.

b) Voigt model -- no upper limit to velocity of propagation

c) Standard linear model -- third order equation increases difficulty of solution and no real advantage exists over the Newmark model

d) Four and five parameter models -- equations increasingly complex.

The Newmark model is formed by placing an intermediate mass between the auxiliary spring and Voigt element of the standard linear model. The parameters in the model are discussed, and expressions are derived for the shortest period of vibration, maximum time interval, and critical retardation time for the highest mode of vibration. The various time effects occurring in materials are divided into two classes, viscous action and strain rate effect. Strain rate effect is considered by adjusting the yield stress according to the average rate of strain. The Illiac is used for the solution of the problem, and absolute damping and Coulomb damping are added to the model at this point.

By the use of the electrical analog an efficient line termination is developed which allows stress wave propagation in an infinite bar of material to be considered by a properly terminated finite length model.

In order to obtain numerical values to compare the effect of the variation of parameters, a soil column is loaded with 40 Kt and 5 Mt applied forces. The results of wave propagation in a large variety of hypothetical

soils are presented in figure form. The formulas derived to pick out the time interval are checked by problem results. The amount of stress attenuation can be increased by increasing the relaxation time, τ, or decreasing α, the ratio of the spring stiffnesses. Both measures tend to send a larger part of the stress wave energy ahead of the rest of the wave and to increase the size of the hysteresis loop, thereby spreading the wave out and decreasing the maximum stress. The less powerful of the two means of attenuation, τ, reaches a maximum value for stress attenuation when τ is in the vicinity of τ_{cr}, after which value so much of the wave is being propagated at the higher velocity of propagation that the maximum stress increases. The parameter α, however, continually spreads the wave out and never reaches a maximum effective value. The parameter η, the ratio of the masses, is shown to have very little effect on response, thus showing the close relationship between the Newmark and standard linear models. Coulomb damping decreases the stress propagated without changing the general shape of the stress wave. This effect increases with depth, but at a given depth the effect of Coulomb damping increases only slightly with time. Decreasing the acoustic velocity causes a large increase in stress attenuation for the 40 Kt weapon but has very little effect with the 5 Mt weapon. Very little difference can be detected in the results obtained from various choices of the β parameter in the β-method.

In stratified soils the results are quite interesting. In a soil whose stiffness increases gradually from v_s = 1000 ft. per sec. at the surface to 4000 ft. per sec. at 200 ft. the stresses actually increase with depth, while the opposite is true for accelerations, their attenuation being more rapid than in a uniform soil. The decrease in stress occurring when a hard layer overlies a soft strata is noted, as well as the fact that stiffer layers increase the stress both above, in, and below the stiff layer.

The results of the consideration of strain rate effect in a soil with a static elasto-plastic stress-strain curve are studied. A response of this type is thought to be quite possible in many soils.

Experimental copper wire tests form the basis for a comparison of elastic-plastic model response with a model with bilinear or trilinear springs. The extreme dependence in this type of problem on the stress-strain curve is noted. Yet, even with only a trilinear approximation, the resulting permanent strains are not grossly in error.

The next comparison is between Ottawa sand specimen results and visco-elastic-plastic model response. In this case the agreement is not too satisfactory; the effect of lateral inertia caused large discrepancies in the experimental and theoretical results.

The technique described could be a valuable and simple method of calculating the propagation of stress waves in a wide variety of materials. However, the full utilization of this method is dependent on the accomplishment of carefully instrumented tests on the materials to be considered. For example, tests on soils in which the lateral strains are prevented should be conducted. The main difficulty to be overcome in these tests is the effect of the frictional forces along the sides of the sample. In these tests accurate dynamic and static stress-strain curves must be obtained. These tests should not be carried to failure, but instead should include recovery. In doing this, they would be of value in not only the determination of the static stress-strain approximation to be used, but also in the determination of the viscous parameters α and τ to obtain a good approximation for the hysteresis loop formed by the stress-strain curve at various rates of loading. Once these values are determined for a given material, the wave propagation due to any loading on one-dimensional bars of this material may be predicted. The determination of experimental values for these parameters is beyond the scope of this thesis.

Four drawbacks in the application of this method still exist. One is the computational time required. The average value of h in Chapter 6 was 3 ms. If we are interested in the response of the soil at the 200-ft. depth for a larger weapon of 20 Mt, it may be necessary to run the problem for a total time of at least 0.75 sec. This means 250 iterations, which would be prohibitively time consuming, unless a high speed computer which can handle about 20 such iterations per minute is available. If α or η do not equal 1, the running time will increase. The second objection is the need for a finite rise time. If the actual wave front is nearly vertical, it contains a higher percentage of high frequency components than the sloping front wave. Thus, the actual wave would attenuate more rapidly than would the delayed rise pulse. Furthermore, accelerations do not correspond in magnitude due to the rise time error. The third disadvantage is the stress-strain curve errors. These errors consist of two parts, the use of only three lines to represent a nonlinear function and the fact that recovery in some materials, especially soils, is not necessarily linear. The method could be improved by fitting more complex approximations to new experimental stress-strain curves which show the nature of recovery. The fourth serious drawback has already been discussed and concerns the lack of knowledge concerning reasonable values for the viscous constants α and τ. These last two items are related to each other very closely.

It is felt, however, that only the last drawback stands in the way of extensive use of the model presented. The attempt has been made to simplify the solution of what has previously been a very complex mathematical problem. The assumptions used have not been too restrictive in the hope that this method will be of some value in future wave propagation studies.

BIBLIOGRAPHY

1. Bewley, L. V., Traveling Waves in Transmission Systems, Second Edition, New York: John Wiley and Sons, 1951.

2. Brode, H. L., "Numerical Solutions of Spherical Blast Waves," Journal of Applied Physics, Vol. 26, No. 6, June, 1955, pp. 766-775.

3. Casagrande, A., and Shannon, W. L., "Stress-Deformation and Strength Characteristics of Soils under Dynamic Loads," Proceedings of the Second International Conference on Soil Mechanics and Foundation Engineering, Vol. V, Rotterdam, 1948, pp. 29-34.

4. Casagrande, A., and Wilson, S. D., Effect of Rate of Loading on the Strength of Clays and Shales at Constant Water Content, Publications of the Graduate School of Engineering, Soil Mechanics Series No. 39, Harvard University, 1951.

5. Davies, R. M., "Stress Waves in Solids," Surveys in Mechanics, Edited by Batchelor, G. K., and Davies, R. M., Cambridge University Press, 1956, pp. 64-138.

6. Donnell, L. H., "Longitudinal Wave Transmission and Impact," Transactions, ASME, Vol. 52(1), 1930, APM 52-14, pp. 153-167.

7. Duwez, P. E., and Clark, D. S., "An Experimental Study of the Propagation of Plastic Deformation under Conditions of Longitudinal Impact," Proceedings, ASTM, Vol. 47, 1947, pp. 502-532.

8. Duwez, P. E., Clark, D. S., and Martens, H. E., Behavior of Metals under Dynamic Conditions (NS-109): The Propagation of Plastic Strain in Compression, Progress Report for National Defense Research Committee, OSRD No. 3886, July, 1944.

9. Duwez, P. E., Wood, D. S., and Clark, D. S., The Propagation of Plastic Strain in Tension, Progress Report for National Defense Research Committee, OSRD No. 931, October, 1942.

10. Duwez, P. E., Wood, D. S., Clark, D. S., and Charyk, J. V., The Effect of Stopped Impact and Reflection on the Propagation of Plastic Strain in Tension, Progress Report for National Defense Research Committee, OSRD No. 988, October, 1942.

11. Kolsky, H., Stress Waves in Solids, Oxford: Clarendon Press, 1953.

12. Kolsky, H., and Shi, Y. Y., The Validity of Model Representation for Linear Viscoelastic Behavior, Technical Report No. 5, Contract Nour 562(14) NR-064-421, Division of Engineering, Brown University, January 1958.

13. Malvern, L. E., 'The Propagation of Longitudinal Waves of Plastic Deformation in a Bar of Material Exhibiting a Strain-Rate Effect," Journal of Applied Mechanics, Vol. 18, June, 1951, pp. 203-208.

14. Massard, J. M., Static and Dynamic Tests of Steel Frame Structures into the Inelastic Range of Deformation, Technical Report to the Air Force Special Weapons Center(AFSWC-TR-57-23), Contract AF 33(616)-170, Dept. of Civil Engineering, Univ. of Illinois, May, 1957.

15. Mindlin, R. D., and Herrmann, G., "A One-Dimensional Theory of Compression Waves in an Elastic Rod," Proceedings of the First U. S. National Congress of Applied Mechanics, Chicago, 1951, pp. 187-191.

16. Morrison, J. A., 'Wave Propagation in Rods of Voigt Material and Visco-Elastic Materials with Three-Parameter Models," Quarterly of Applied Mathematics, Vol. 14, July, 1956, pp. 153-169.

17. Newmark, N. M., 'Computation of Dynamic Structural Response in the Range Approaching Failure," Proceedings of the Symposium on Earthquake and Blast Effects on Structures, Earthquake Engineering Research Institute and University of California, Los Angeles, June, 1952, pp. 114-129.

18. Pöschl, T., "Der Längsstoss einer Masse auf das freie Ende eines Zylinders, dessen anderes Ende fesgehalten ist," Handbuch der Physik, Vol 6, pp. 537-543. Berlin: Julius Springer, 1928.

19. Smith, E. A., "Impact and Longitudinal Wave Transmission," Transactions, ASME, Vol. 77, 1955, pp. 963-973.

20. Smith, E. A., 'What Happens When Hammer Hits Pile," Engineering News Record, Vol. 159, No. 10, Sept. 5, 1957, pp. 46-48.

21. Taylor, D. W., and Whitman, R. V., The Behavior of Soils under Dynamic Loadings, 2. Interim Report on Wave Propagation and Strain Rate Effect, Report to Office of the Chief of Engineers (AFSWP-117), Contract DA-49-129-ENG-227, Dept. of Civil and Sanitary Engineering, Mass. Inst. of Technology, July, 1953.

22. Taylor, D. W., and Whitman, R. V., The Behavior of Soils under Dynamic Loadings, 3. Final Report on Laboratory Studies, Report to Office of the Chief of Engineers (AFSWP-117), Contract DA-49-129-ENG-227, Dept. of Civil and Sanitary Engineering, Mass. Inst. of Technology, August, 1954.

23. Taylor, G. I., 'The Testing of Materials at High Rates of Loading," Journal of the Institute of Civil Engineers, Vol. 26, 1946, pp. 486-519.

24. Terzaghi, K., and Peck, R. B., Soils Mechanics in Engineering Practice, New York: John Wiley and Sons, 1948.

25. The Effects of Nuclear Weapons, Department of Defense, Atomic Energy Commission, Washington: Government Printing Office, 1957.

26. Timoshenko, S., and Goodier, J. N., Theory of Elasticity, Second Edition, New York: McGraw-Hill Book Co., 1951.

27. Tung, T. P., and Newmark, N. M., A Review of Numerical Integration Methods for Dynamic Response of Structures, Tech. Report to Office of Naval Research, Contract N6ori-071(06), Univ. of Illinois Civil Engineering Studies, Structural Research Series No. 69, March, 1954.

28. Von Karman, T., and Biot, M. A., Mathematical Methods in Engineering, New York: McGraw-Hill Book Co., 1940.

29. Von Karman, T., and Duwez, P. E., 'The Propagation of Plastic Deformation in Solids," Journal of Applied Physics, Vol. 21, Part 2, No. 10, October, 1950, pp. 987-994.

30. White, M. P., and Griffis, Le Van, 'The Permanent Strain in a Uniform Bar Due to Longitudinal Impact," Journal of Applied Mechanics, Vol. 14, December, 1947, pp. A337-A343.

31. Whitman, R. V., 'The Behaviour of Soils under Transient Loadings," Proceedings of the Fourth Internal Conference on Soil Mechanics and Foundation Engineering, Vol. 1, London: Butterworths Publications, 1957, pp. 207-210.

APPENDIX

SPATIAL DISPERSION OF A BLAST WAVE IN A MASSLESS, ELASTIC, HOMOGENEOUS, AND ISOTROPIC SOIL

1. Introduction

The attenuation of blast waves in solids can be considered as due to two separate causes. The first cause, which is normally the more important of the two causes, is a spatial dispersion. This spatial dispersion is nothing more than a spreading out of a blast wave front over a larger volume, thus reducing the energy at any single point. The spatial dispersion effect is considered in this Appendix. The other effect is the much more complex dissipation of the maximum stress due to damping, nonlinear resistances, and inertia. This effect is treated for the one-dimensional case in the main text of the thesis. It is felt that an approximate solution might be obtained by a judicious combination of the two effects. No method for this combination is presented here.

2. Method of Analysis

The solution adopted is valid only for a homogeneous, elastic, isotropic, semi-infinite medium in which the inertia of the medium is neglected. Since the mass is considered to be zero, the velocity of propagation is therefore infinite because $v = (E/\rho)^{1/2}$.

A blast wave from a ground surface atomic burst is considered to be moving across the ground. Surface waves (Rayleigh and Love waves) are not considered. This blast wave is assumed to have a plane front rather than the arc of a circle with center at ground zero. However, it can be shown that the error involved is small, since in the regions where the ground pressure has a high influence the discrepancy between the arc and straight line is very small.

The error in horizontal pressure will be greater than the error in vertical pressure, but it is felt that this unconservative error is not significant for weapon yields over 20 Kt.

With this assumption the problem becomes two-dimensional, and the solution for stresses in homogeneous semi-infinite platesdue to a line load of infinite lateral extent is applicable (26). Introducing some new nomenclature, the equations for vertical and horizontal stress from Timoshenko and Goodier may be rewritten as

$$\sigma_v = \frac{2P}{\pi Z} \cdot \frac{1}{(1 + \varphi^2)^2}$$

$$\sigma_H = \frac{2P}{\pi Z} \cdot \frac{\varphi^2}{(1 + \varphi^2)^2}$$

where σ_H = horizontal pressure

σ_v = vertical pressure

P = intensity of line load

φ = ratio of horizontal distance of b_n from the underground point to the depth

Z = depth of point being examined

Thus, for a unit line load the influence coefficients for vertical and horizontal stress are

$$I_v = \frac{2}{\pi z} \frac{1}{(1 + \varphi^2)^2}$$

$$I_H = \frac{2}{\pi z} \frac{\varphi^2}{(1 + \varphi^2)^2} \qquad \text{(A.1)}$$

Figure 50 shows the plane wave at one instant of time. The p_{so} versus range curve is a trajectory of the maximum pressure at the front of the wave as it

progresses further away from "ground zero". If the instantaneous value of the pressures at the points designated as b_o, b_1, ..., b_n in Fig. 50 are known, they can be multiplied by the corresponding influence coefficient from equation (A.1). The area under the resultant curve represents the total pressure at the desired depth and is evaluated by Simpson's one-third rule, which assumes a parabolic shape between 3 consecutive points. The wave front is then moved to the right to a new position and the process repeated until sufficient points are located to draw a curve showing the vertical or horizontal pressure versus time.

The job of finding the correct pressures at b_n represents a major part of the problem. Since the problem was designed for computation on the Illiac, the procedure is different from the most efficient desk calculator procedure. The value of the peak overpressure, p_{so}, can be determined by the overpressure-time curve presented in the A.E.C. Handbook (25, Fig. 3.94a). For overpressures greater than 100 psi, p_{so} is assumed to vary as the cube of the range, i.e.,

$$\frac{(P_{so})_1}{(P_{so})_2} = \left(\frac{\text{Range}_2}{\text{Range}_1}\right)^3 \qquad \text{(A.2)}$$

This value is applicable only when the wave front is directly over the b point in question. At any later time the pressure will have decayed from this value. The A.E.C. curve relating arrival time to range (25, Fig. 3.96) is used to get the decay time, i.e., the length of time it took for the wave front to pass from the b point in question to b_o. For ranges near "ground zero" a straight line extrapolation was used, but a better extrapolation would make use of the relation

$$\text{Shock velocity} = 1129\left(1 + \frac{6}{7} \cdot \frac{P_{so}}{P_{\text{atmospheric}}}\right)^{1/2} \qquad \text{(A.3)}$$

The positive phase duration curve from the A.E.C. handbook (25, Fig. 3.96) was also used. For the "close-in" region the duration was arbitrarily chosen as 0.1 sec. at zero range and 0.15 sec. at a range of 0.08 miles for a 1 Kt weapon, and the variation was assumed linear in this region. When the positive phase duration and the decay time are determined, Brode's curves (2, Fig. 29) can be used to find the instantaneous pressure, p_s. The approximate exponential equations given by Brode were used to approximate these curves.

The time factor in the resulting stress-time plots is also computed by the use of the arrival time versus range curve. Due to the erroneous assumption of an infinite velocity of propagation, there will be no real correlation between the various depths and the arrival time of the stress pulse. It is possible, by means of a minor modification, to consider the length of time it takes for a wave to propagate from b_n to the underground point. Although this results in an inconsistent assumption, the solution would undoubtedly be closer to reality. This modification, which is not used here, would result in a somewhat increased maximum pressure and a considerably more abrupt rise time.

A more elaborate analysis of this type will be possible upon the completion of M. R. Mehta's present work mentioned Section 6.1.

3. Results of Numerical Calculations

A series of 24 problems was computed for three weapon sizes: 40 Kt, 1 Mt, and 5 Mt. The integration interval was 0.2z. The pressure versus range curve and time of arrival versus range curve were approximated by 23 straight lines and the duration versus range curve by 8 straight lines.

Table 2 shows a list of these problems and summarizes the maximum vertical and horizontal stresses. Figures 51 and 52 show the decrease in maximum horizontal and vertical pressure with depth for both the 100 and 200 psi

levels. Although an individual problem is required for each depth for one bomb size, once this curve is established the values for other weapon yields, w, can be scaled by the following law:

$$\left(\frac{w_1}{w_2}\right)^{1/3} = \frac{z_1}{z_2} \qquad (A.4)$$

Points from the 1 Mt and 5 Mt yields are scaled to 40 Kt and are shown on Figs. 51 and 52 showing the almost perfect scaling.

Figure 53 shows the variation of vertical stress with time at various depths for the 40 Kt weapon, and Fig. 54 shows the horizontal stress versus time at the same depths. The obvious discrepancy on the time scale which shows the stress reaching the deeper points earlier than the shallow points is a result of the massless soil-infinite velocity of propagation assumption. Making the velocity of propagation finite would translate each curve to the right a time approximately equal to z/v and would also steepen the front and increase the maximums. The percentagewise increase is larger with the smaller yields and greater depths and would be approximately five percent for the 5 Mt weapon at 100 ft.

TABLE 1. LIST OF PROBLEMS REPORTED IN CHAPTER VI

Problem No.	Applied Force	v_s ft/sec	Transit Time @ v_s sec	Theor. h ms.	Actual h ms.	τ sec	τ/τ_{cr}	α	Figs.	Remarks*
A-48	40 Kt	2000	20	3.3	3	0.01	0.5	1	9-21	except 18
A-50	40 Kt	2000	20	2.5	1	0.02	1.0	1	13,14	
A-51	40 Kt	2000	20	4	5	0.005	0.25	1	13,14	
A-52	40 Kt	2000	20	4.6	5	0.002	0.1	1	14	
A-58	5 Mt	2000	20	3.3	3	0.01	0.5	1	22-24,26, 18	
A-63	5 Mt	1000	40	8	10	0.01	0.25	1	26	Rise Time = 80 ms.
A-64	5 Mt	4000	10	1.25	1	0.01	1.0	1	26	
A-65	40 Kt	2000	20	3.4	3	0.01	0.289	1/3	14-17	
A-66	40 Kt	2000	20	3.0	3	0.015	0.433	1/3	14	
A-67	40 Kt	2000	20	2.48	2	0.01	0.158	1/10	14-17	
A-67b	40 Kt	2000	20	2.24	2	0.0182	0.288	1/10	14	
A-68	40 Kt	2000	20	2.51	2	0.0091	0.144	1/10	14	
A-68b	40 Kt	2000	20	2.67	2	0.005	0.079	1/10	14	
A-69	40 Kt	2000	20	0.5	0.5	0.1	5.0	1	14	
A-70	40 Kt	varies	varies	0.42	0.5	0.01	varies	1	27-29	v_s increases w/depth
A-71	40 Kt	2000	20	1.43	1	0.035	1.75	1	14	
A-72	40 Kt	2000	20	0.82	0.67	0.06	3.0	1	14	
A-73	40 Kt	2000	20	----	3	0.01	0.5	1	12	Voigt model
A-74	40 Kt	2000	20	2.33	2	0.01	0.62	1	19	η = 1/4
A-76	40 Kt	2000	20	0.95	1	0.01	1.15	1	19	η = 1/19
A-78	5 Mt	2000	20	1.74	2	0.015	0.72	1	7,18	n = 29, η = 1/9
A-98	5 Mt	2000	20	1.74	2	0.015	0.72	1	7	n = 13, η = 1/9**
A-99	5 Mt	2000	20	1.74	2	0.015	0.72	1	7	n = 12, η = 1/9**
A-101	5 Mt	2000	20	1.74	2	0.015	0.72	1	7	n = 6, η = 1/9**

TABLE 1 (CONTINUED)

Problem No.	Applied Force	v_s ft/sec	Transit Time @ v_s sec	Theor. h ms.	Actual h ms.	τ sec	τ/τ_{cr}	α	Figs.	Remarks*
A-102	40 Kt	2000	20	2.17	1	0.035	1.0	1/3	14	
A-103	40 Kt	2000	20	1.08	1	0.069	2.0	1/3	14	
A-104	40 Kt	2000	20	1.80	1	0.038	0.6	1/10	14	
A-105	40 Kt	2000	20	1.44	1	0.063	1.0	1/10	14	
A-106	40 Kt	2000	20	0.72	1/2	0.126	2.0	1/10	14	
B-3	40 Kt	2000	20	3.3	3	0.01	0.5	1	20,21	f = 0.25 psi/ft
B-6	40 Kt	2000	20	3.3	3	0.01	0.5	1	20,21	f = 0.05 psi/ft
B-7	40 Kt	2000	20	3.3	3	0.01	0.5	1	20,21	f = 0.025 psi/ft
B-30	40 Kt	2000	20	3.3	3	0.01	0.5	1	36-38	Elasto-plastic springs
B-31	40 Kt	2000	20	3.3	3	0.01	0.5	1	36-38	B-30 plus strain rate effect
B-50	40 Kt	2000	20	2.55	2	0.01	0.36	1/3	25,33-35	η = 1/4
B-51	40 Kt	1000	40	5.1	4	0.02	0.36	1/3	25,30-32	η = 1/4
B-52	40 Kt	varies	varies	2.55	2	varies	0.36	1/3	30,31	η = 1/4, 2 layers
B-53	40 Kt	varies	varies	2.55	2	varies	0.36	1/3	30,31	η = 1/4, 2 layers
B-54	40 Kt	varies	varies	1.28	1	varies	0.36	1/3	30-32	η = 1/4, 2 layers
B-55	40 Kt	varies	varies	2.55	2	varies	0.36	1/3	33-35	η = 1/4, 2 layers
B-56	40 Kt	varies	varies	1.28	1	varies	0.36	1/3	30-32	η = 1/4, 3 layers
B-57	40 Kt	varies	varies	2.55	2	varies	0.36	1/3	33-35	η = 1/4, 3 layers
B-58	40 Kt	varies	varies	1.28	1	varies	0.36	1/3	33-35	η = 1/4, 3 layers
B-59	40 Kt	2000	40	2.55	2	0.01	0.36	1/3	33,34	η = 1/4, fixed end, n=8
B-60	40 Kt	2000	40	2.55	2	0.01	0.36	1/3	33,34	η = 1/4, free end, n=9

* n = 19, η = 1, λ = 20 ft, Rise Time = 40 ms., and f = 0 unless noted in Remarks.

** These problems same as A-78 but with various line terminations.

TABLE 2. MAXIMUM VERTICAL AND HORIZONTAL STRESSES IN SPATIAL DISPERSION PROBLEMS

Problem No.	Weapon Size	Pressure Level, psi	Depth ft	σ_v max.	σ_H max.
H-1	40 Kt	100	50	64.4	31.2
H-2	40 Kt	100	100	50.9	22.1
H-3	40 Kt	100	150	42.4	18.2
H-4	40 Kt	200	50	106.0	45.3
H-5	40 Kt	200	100	78.7	29.3
H-6	40 Kt	200	150	63.8	23.8
H-7	1 Mt	100	50	80.5	50.2
H-8	1 Mt	100	100	70.8	37.9
H-9	1 Mt	100	150	63.9	30.6
H-10	1 Mt	200	50	144.9	80.1
H-11	1 Mt	200	100	121.0	56.6
H-12	1 Mt	200	150	104.9	44.5
H-13	5 Mt	100	50	86.2	58.7
H-14	5 Mt	100	100	78.7	47.5
H-15	5 Mt	100	150	73.0	40.3
H-16	5 Mt	200	50	159.7	98.6
H-17	5 Mt	200	100	140.0	74.7
H-18	5 Mt	200	150	125.7	61.0
H-19	40 Kt	100	10	86.2	58.7
H-20	40 Kt	100	20	78.7	47.5
H-21	40 Kt	100	35	70.6	37.5
H-22	40 Kt	200	10	159.7	98.6
H-23	40 Kt	200	20	140.0	74.7
H-24	40 Kt	200	35	119.0	56.1

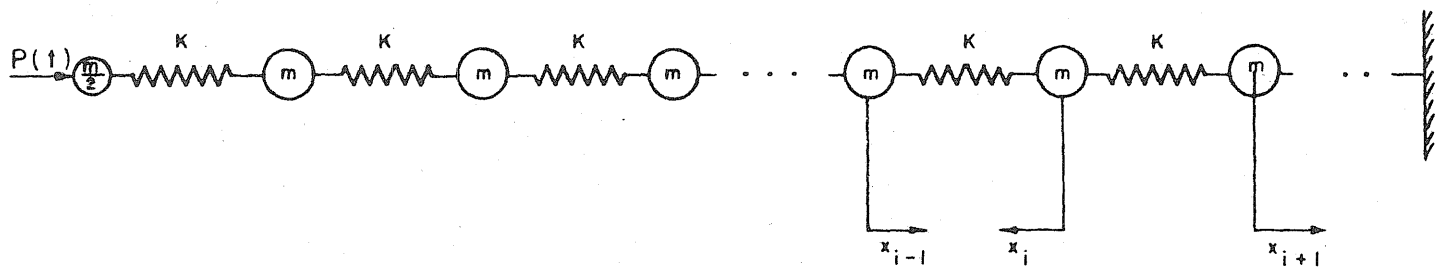

(a) Elastic Model

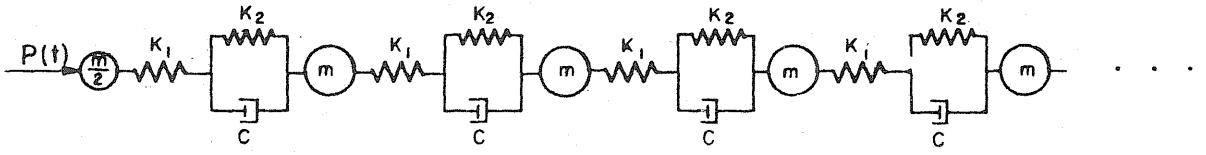

(b) Standard Linear Model

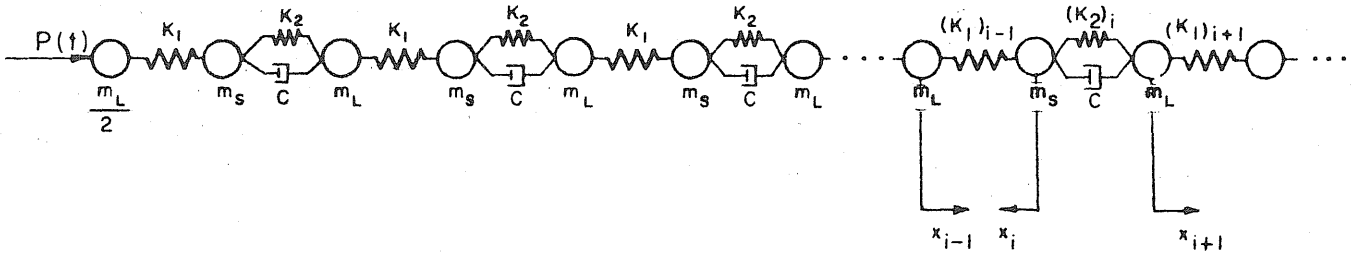

(c) Newmark Model

FIG. 1 MODELS USED IN THE NUMERICAL ANALYSIS

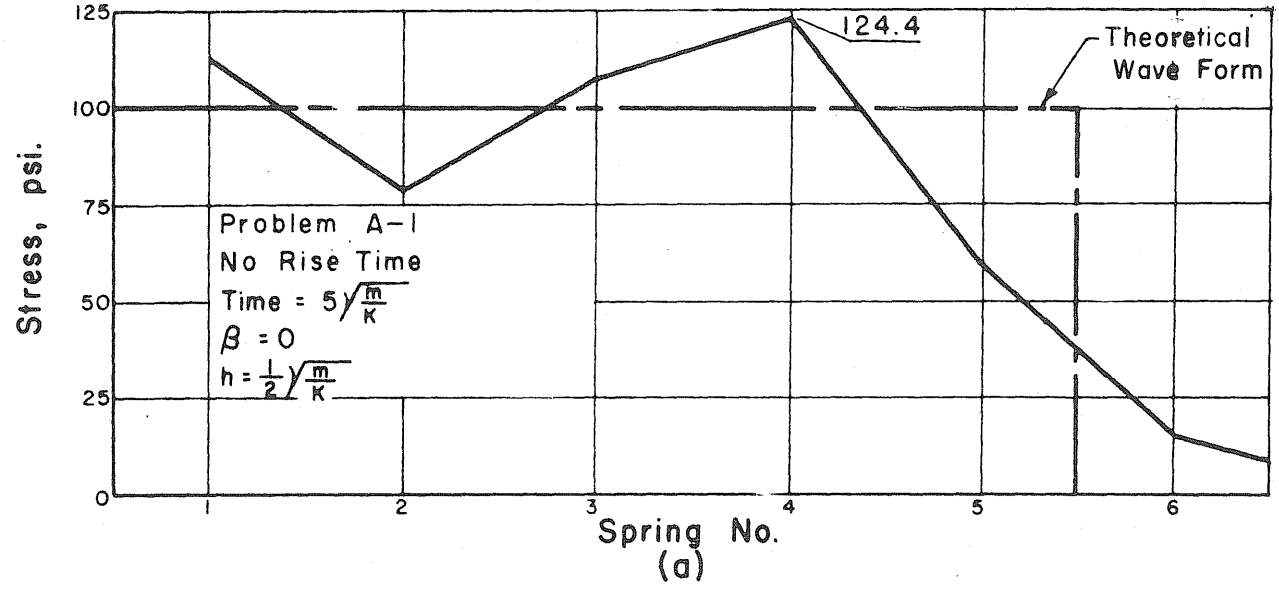

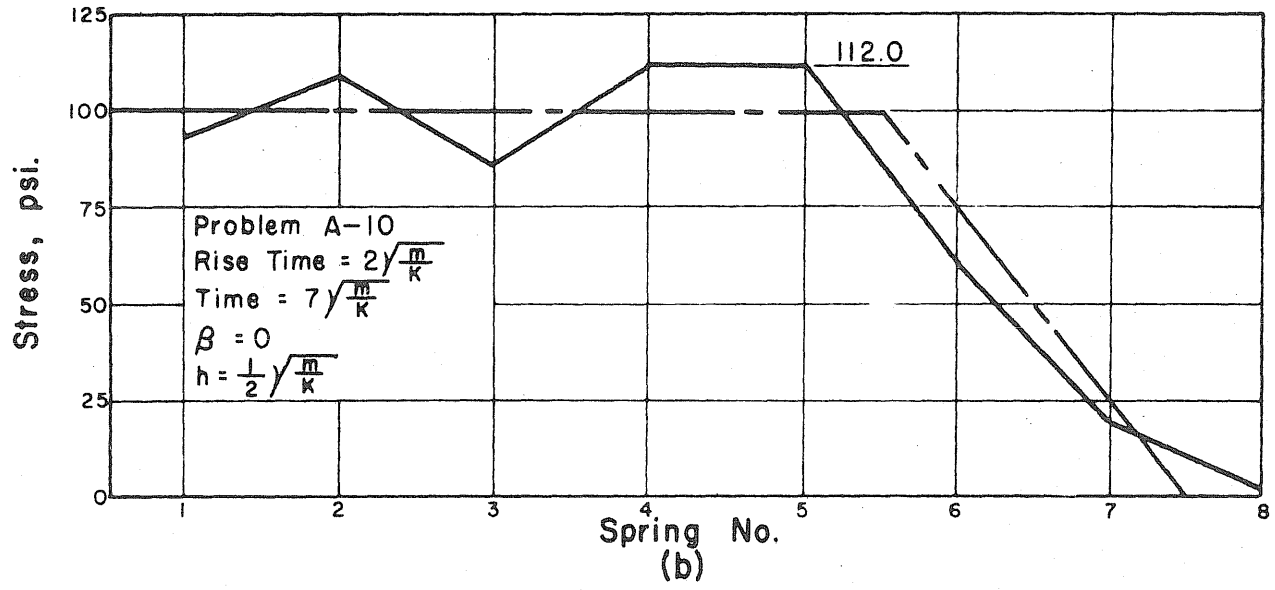

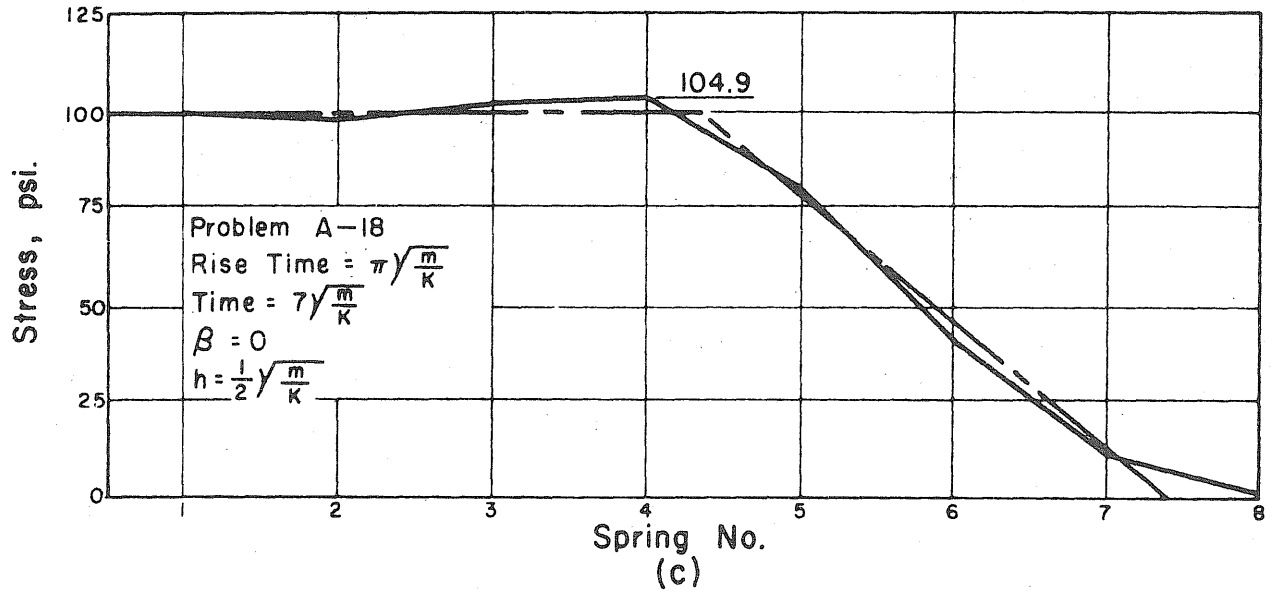

FIG. 2 EFFECT OF RISE TIME ON ELASTIC MODEL

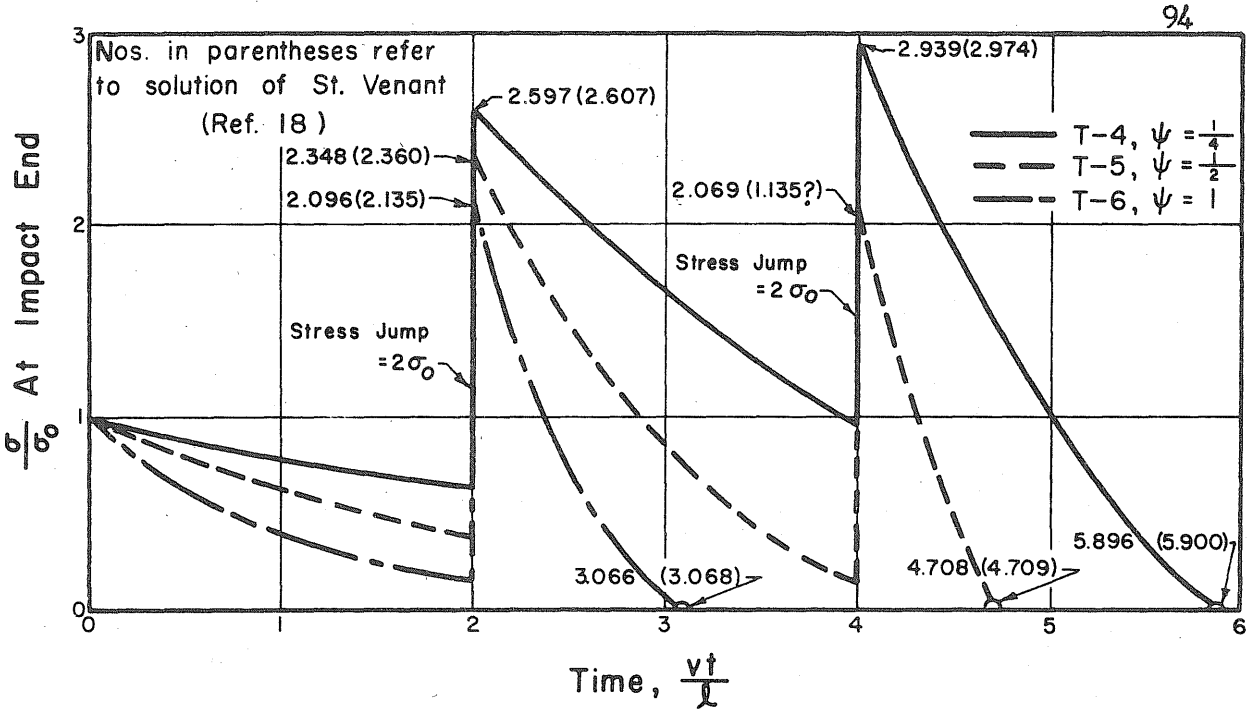

FIG. 3 IMPACT STRESS VERSUS TIME, IMPACT OF RIGID MASS AND ELASTIC BAR

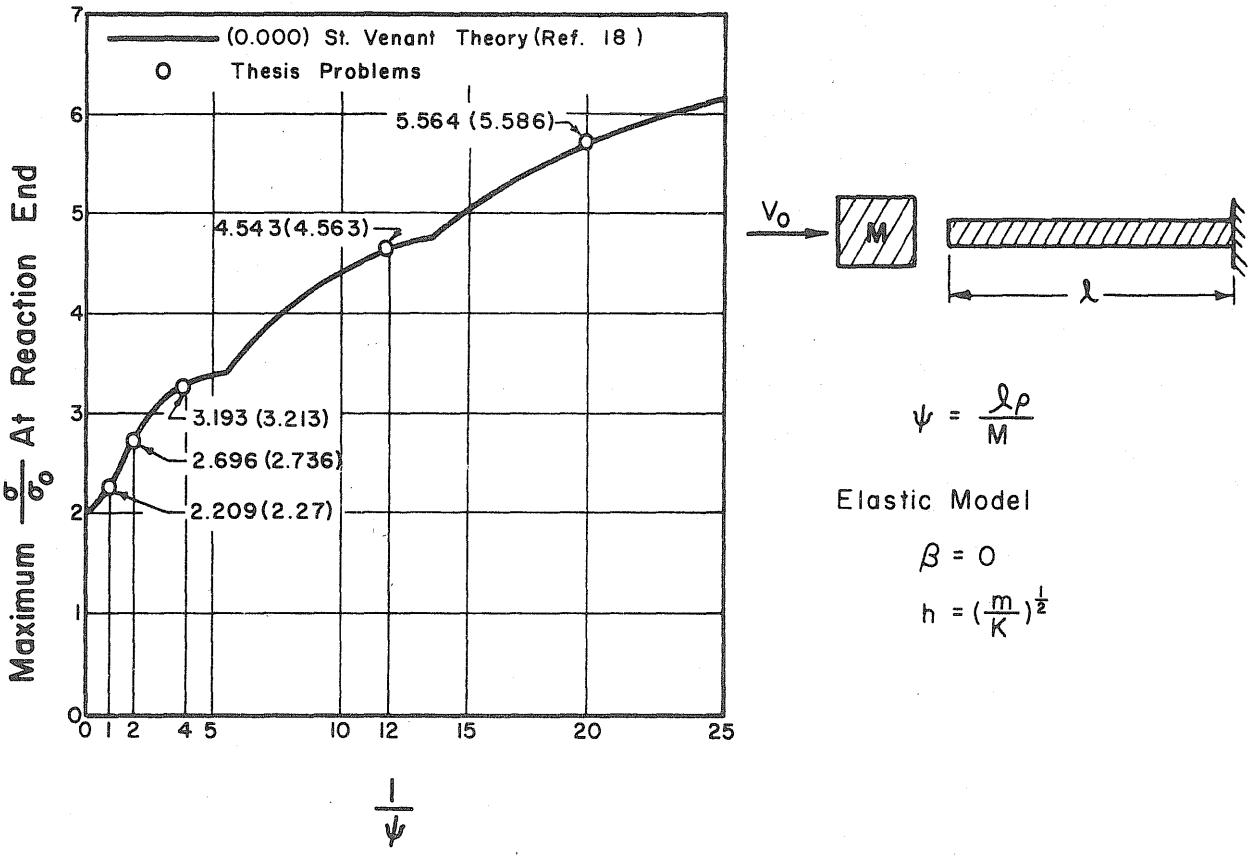

FIG. 4 MAXIMUM STRESS AT FIXED END VERSUS RATIO OF MASSES, IMPACT OF RIGID MASS AND ELASTIC BAR

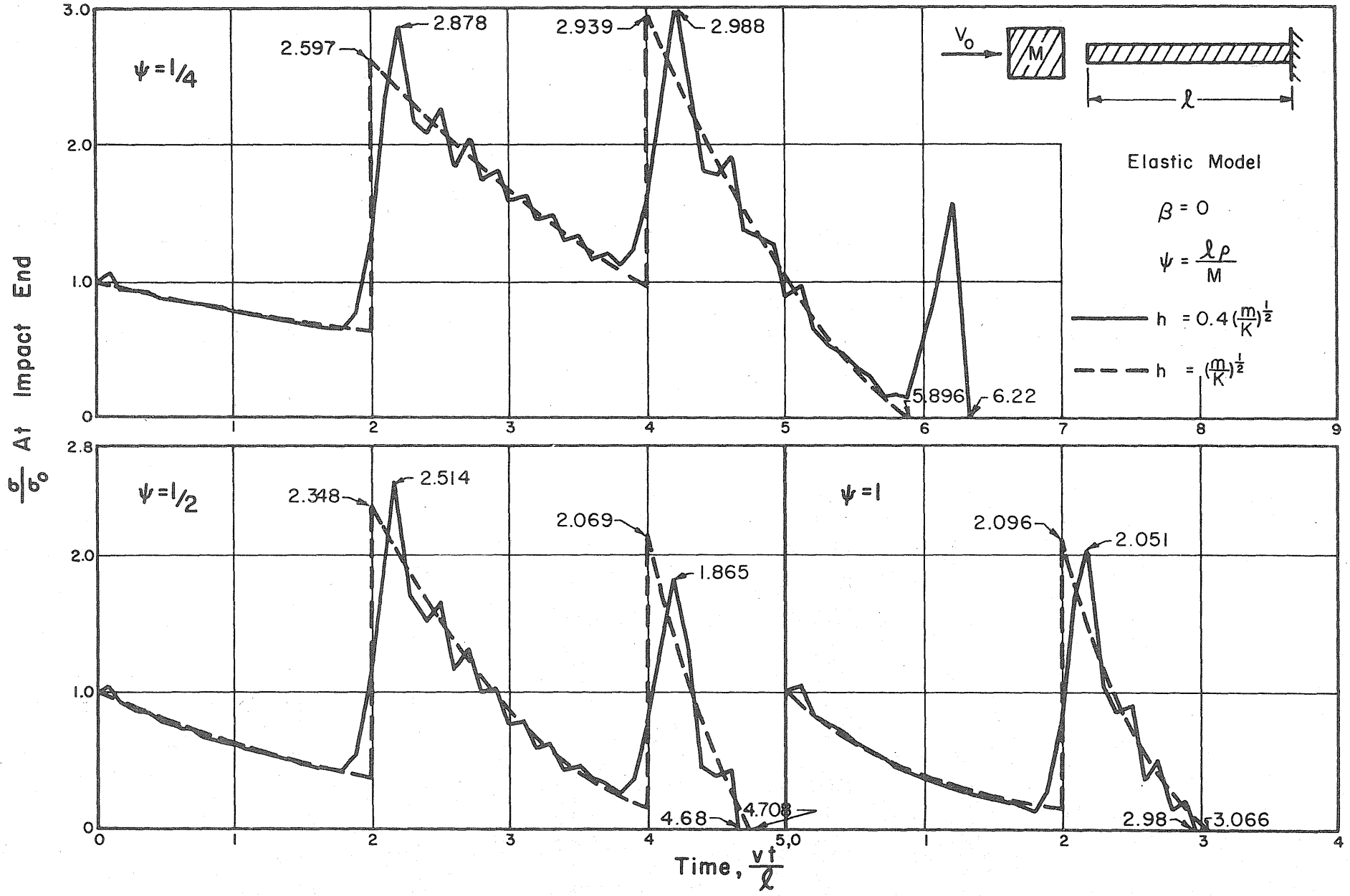

FIG. 5 IMPACT STRESS VERSUS TIME, IMPACT OF RIGID MASS AND ELASTIC BAR

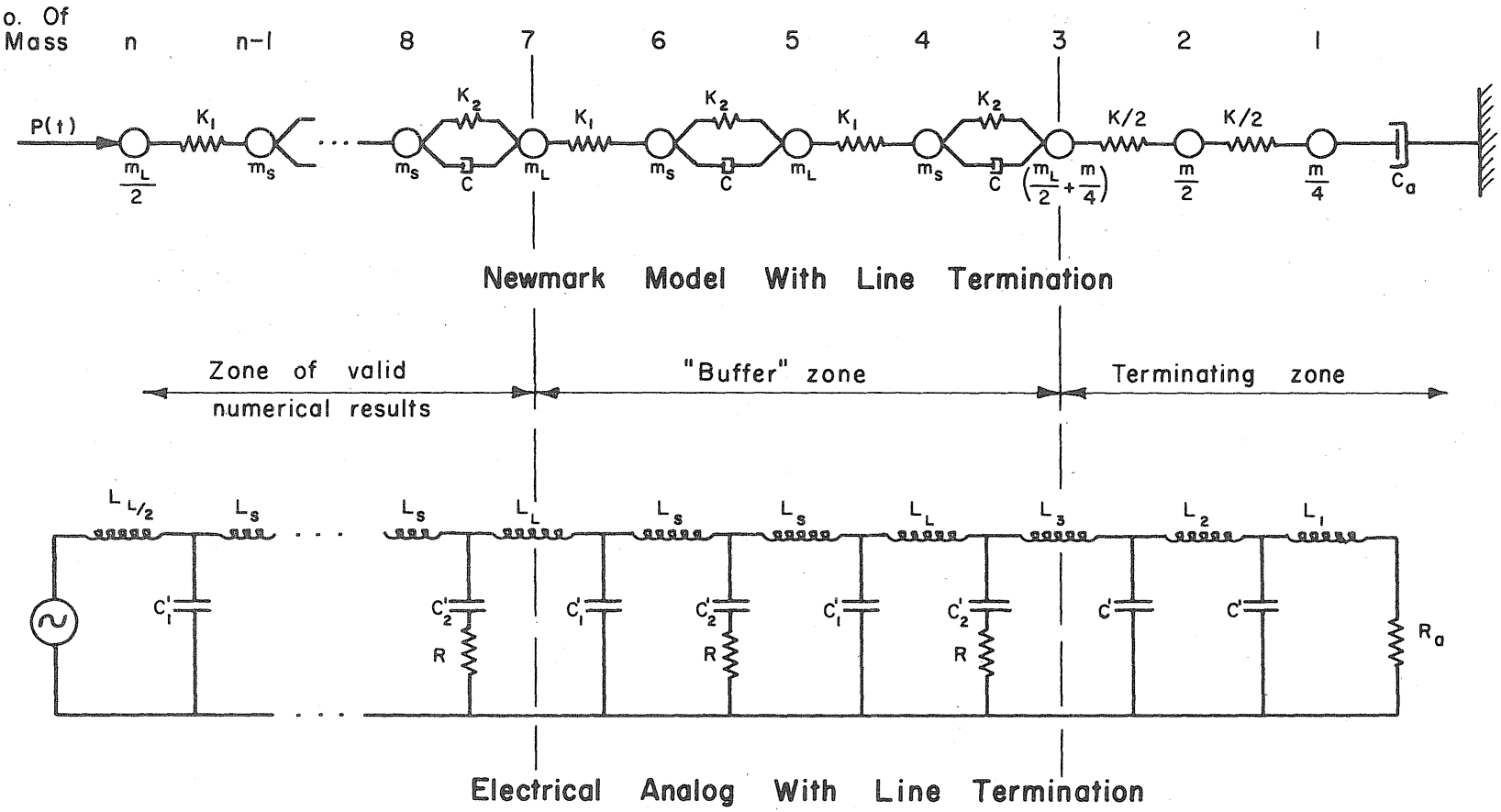

Transformations: For All Elements, $L = m$, $R = C$, $R_a = C_a$, $C' = \frac{1}{K}$

Terminating Resistance, $R_a = \sqrt{\frac{L}{C'}}$; Therefore $C_a = \sqrt{Km}$

FIG. 6 LINE TERMINATION FOR NEWMARK MODEL AND ELECTRICAL ANALOG

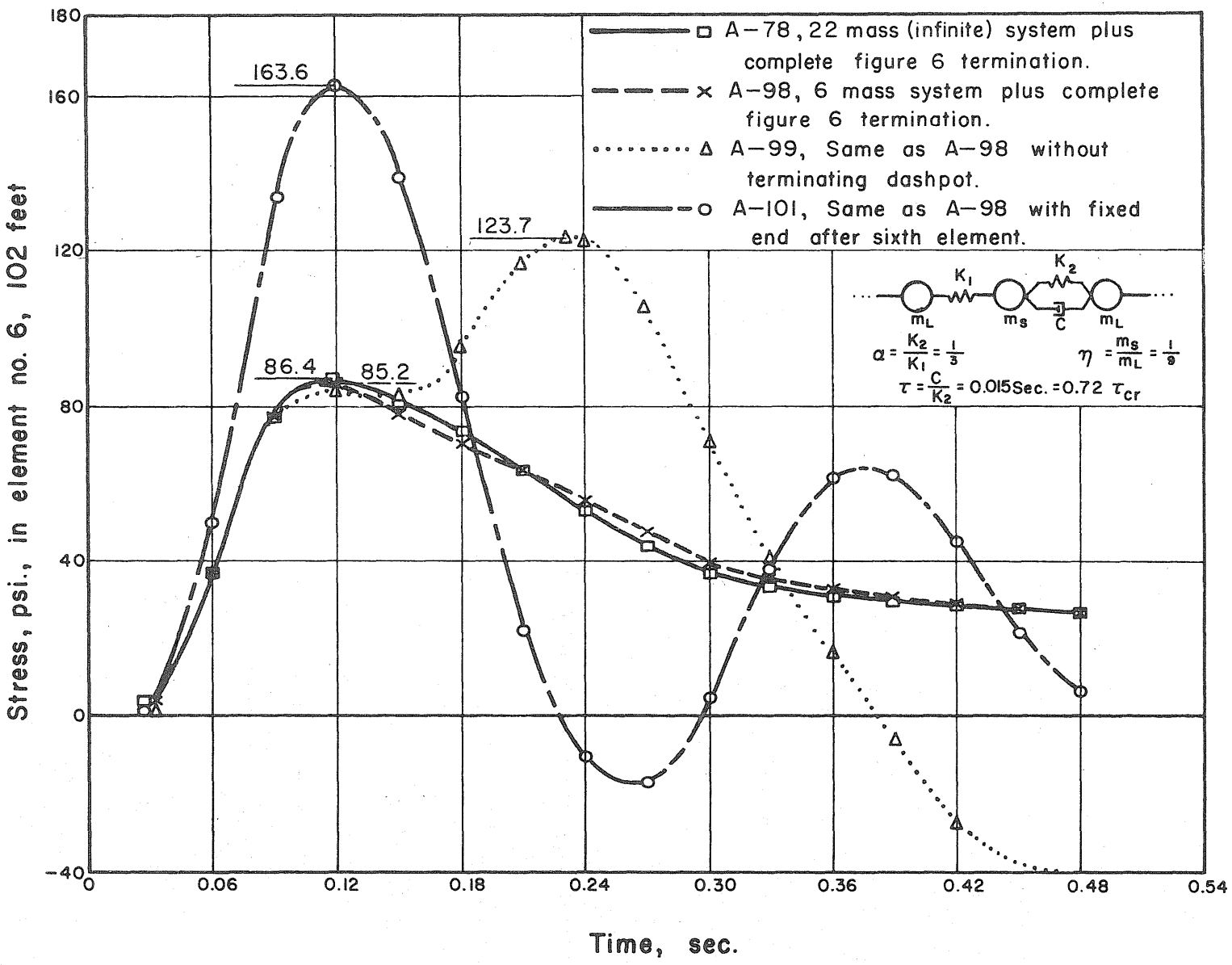

FIG. 7 EFFECT OF LINE TERMINATION ON STRESS-TIME RELATIONSHIP IN SIXTH ELEMENT (102 FEET) – 5 Mt WEAPON

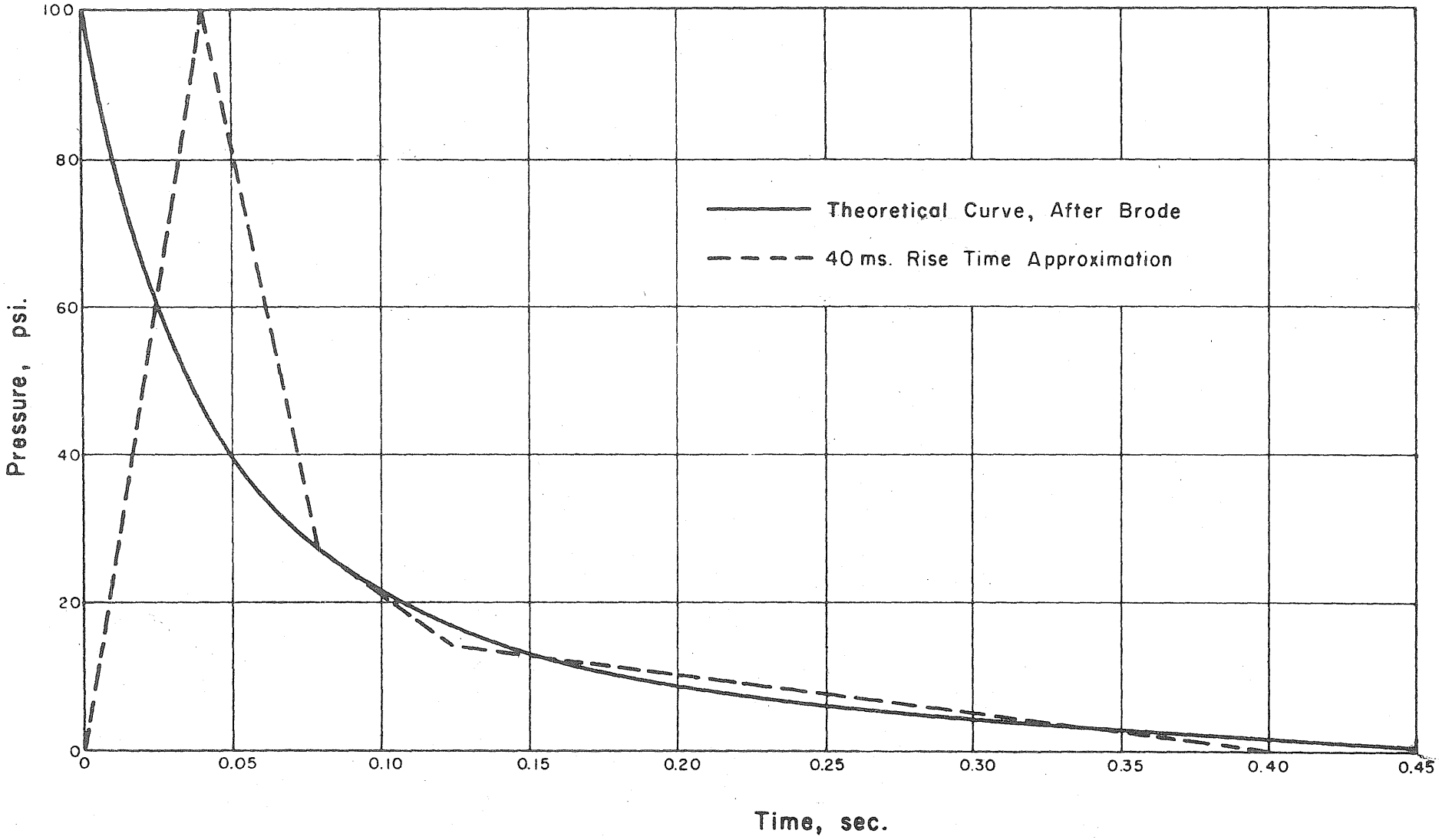

FIG. 8 REPLACEMENT PRESSURE–TIME CURVE
40 Kt WEAPON

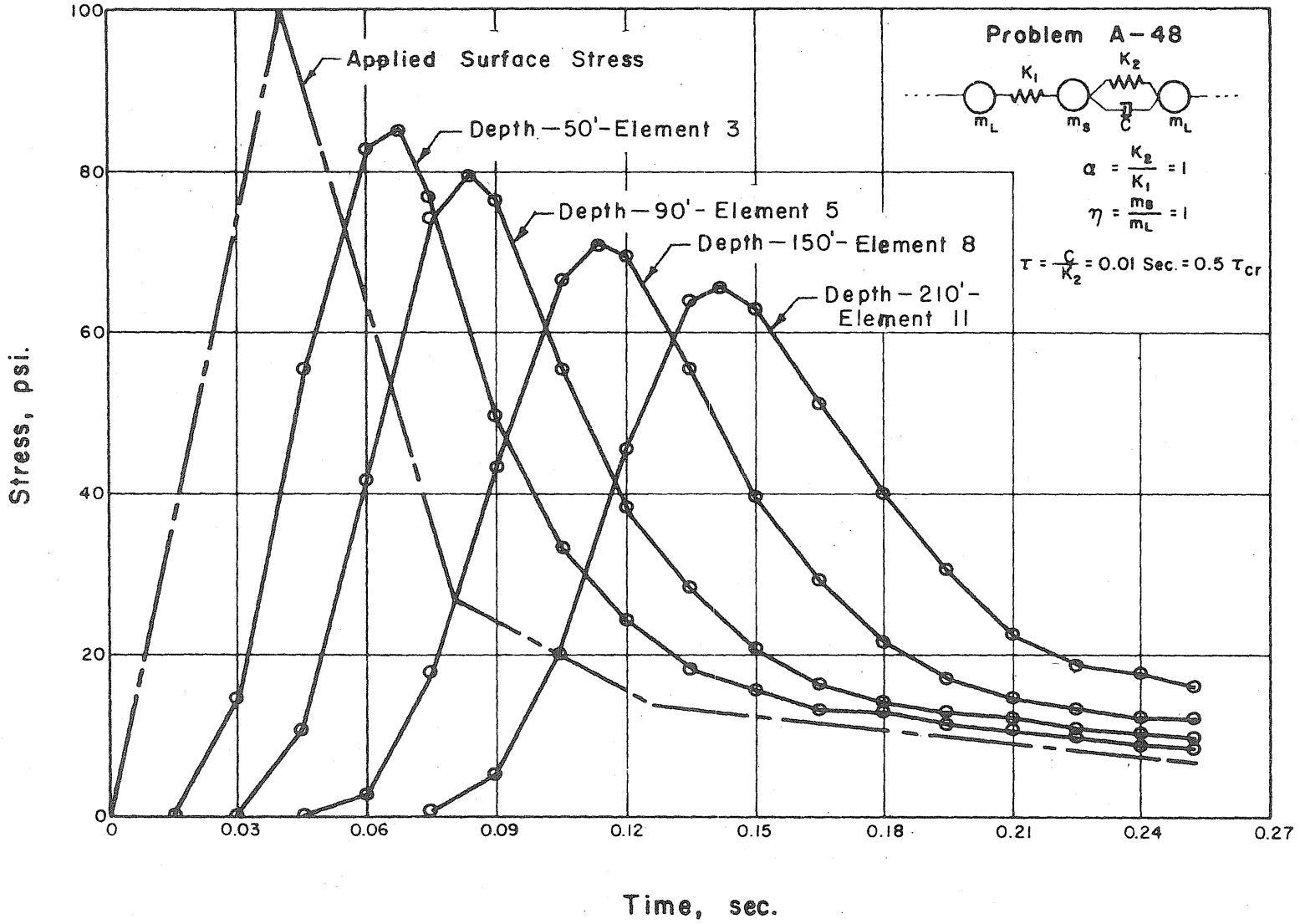

FIG. 9 STRESS VERSUS TIME AT VARIOUS DEPTHS
40 Kt WEAPON

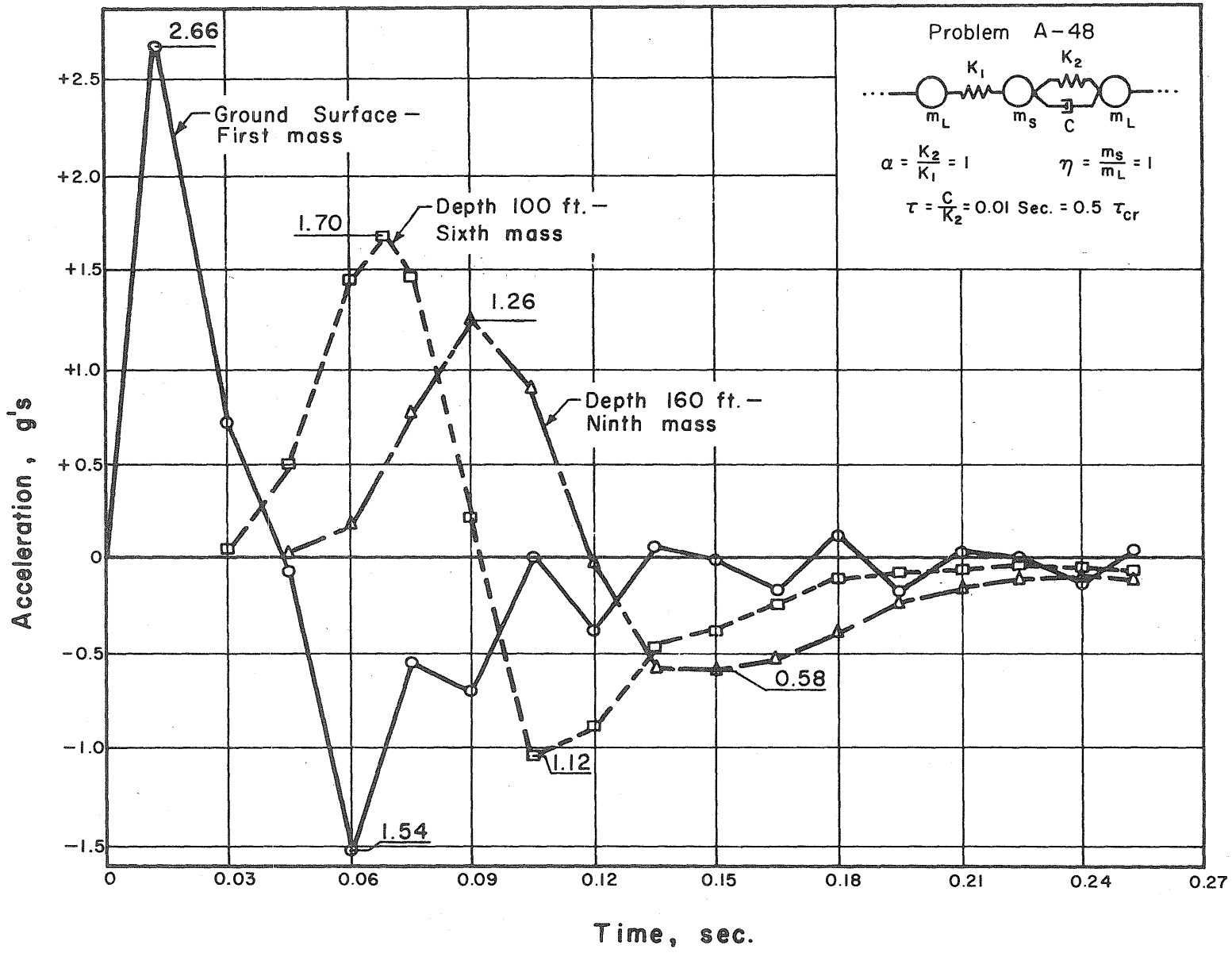

FIG. 10 ACCELERATION VERSUS TIME AT VARIOUS DEPTHS
40 Kt WEAPON (FIG. 8)

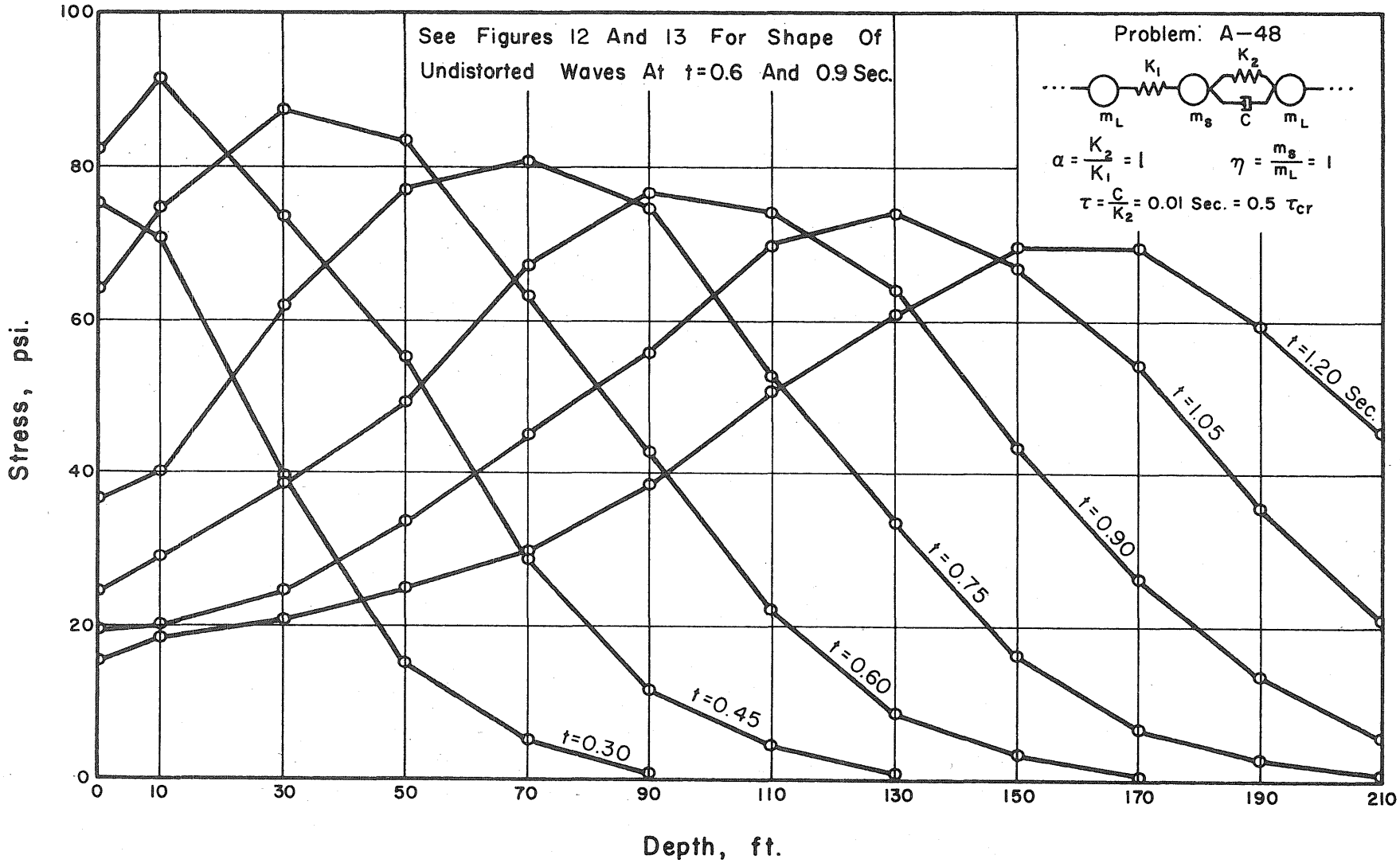

FIG. 11 STRESS DISTRIBUTION AT VARIOUS TIMES
40 Kt WEAPON (FIG. 8)

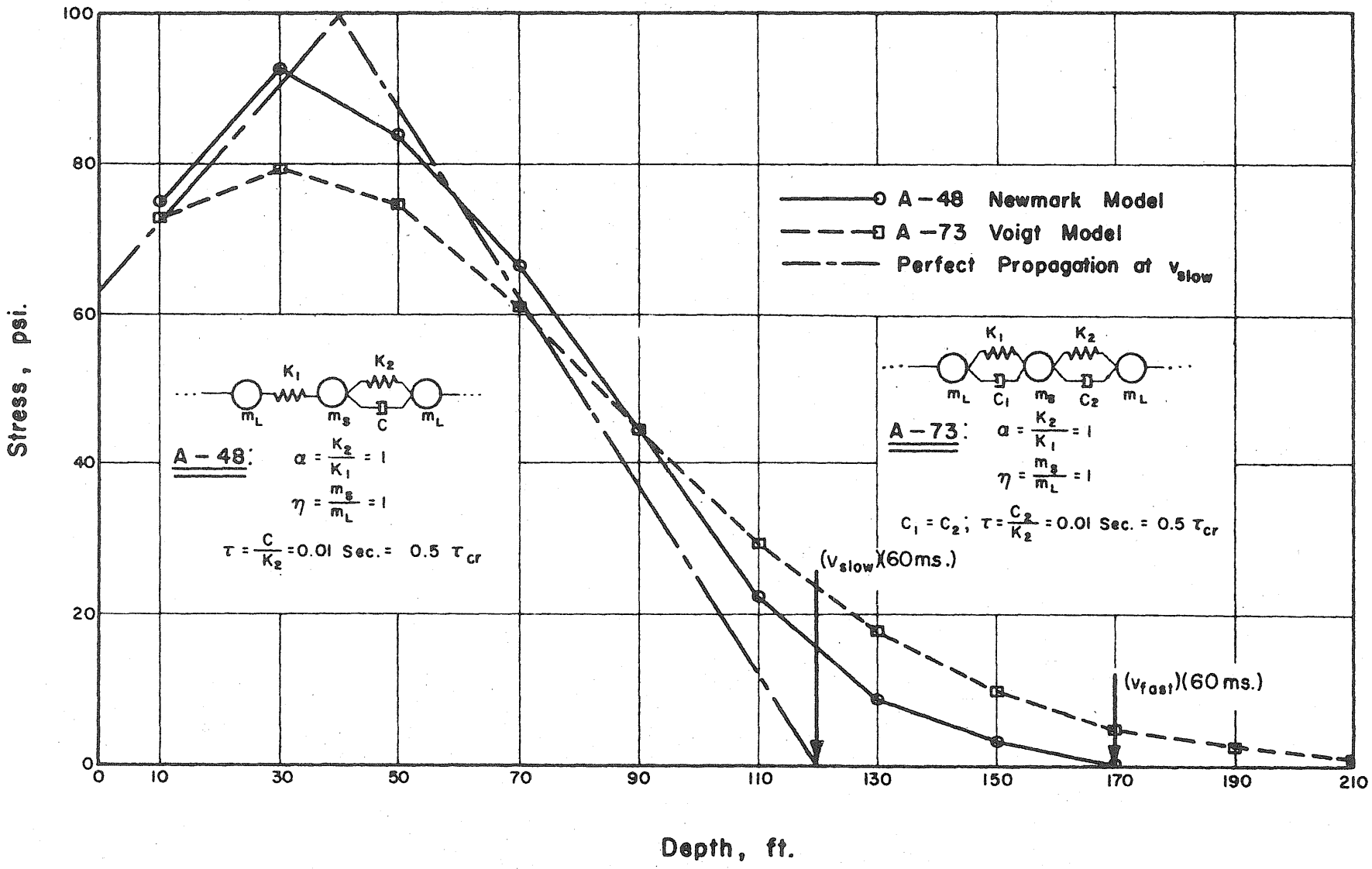

FIG. 12 COMPARISON OF VOIGT AND NEWMARK MODELS AT TIME = 0.06 SEC. 40 Kt WEAPON

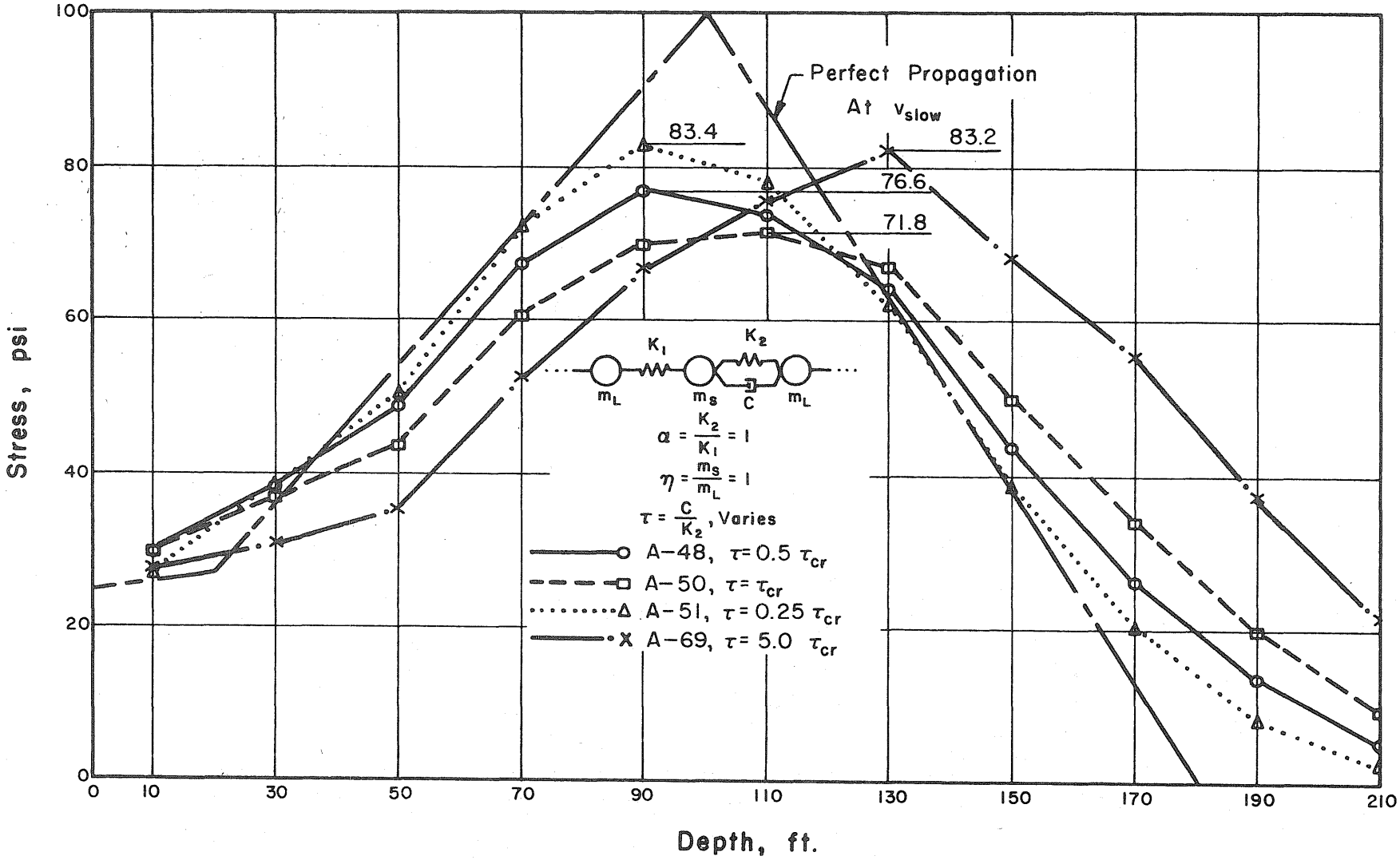

FIG. 13 STRESS DISTRIBUTION AS A FUNCTION OF RETARDATION TIME (τ) AT TIME = 0.09 SECONDS — 40 Kt WEAPON

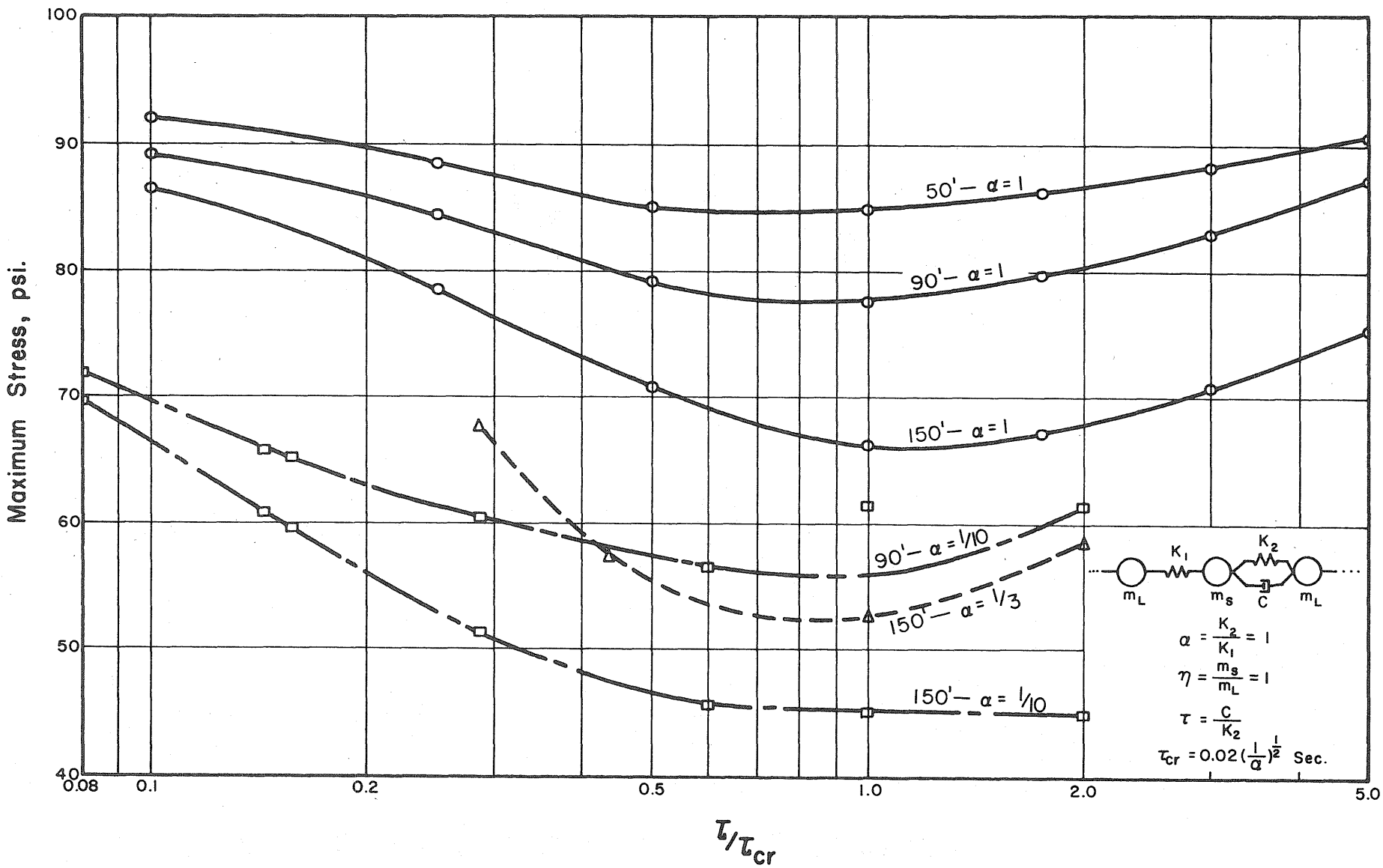

FIG. 14 MAXIMUM STRESS VERSUS RETARDATION TIME (τ)
40 Kt WEAPON

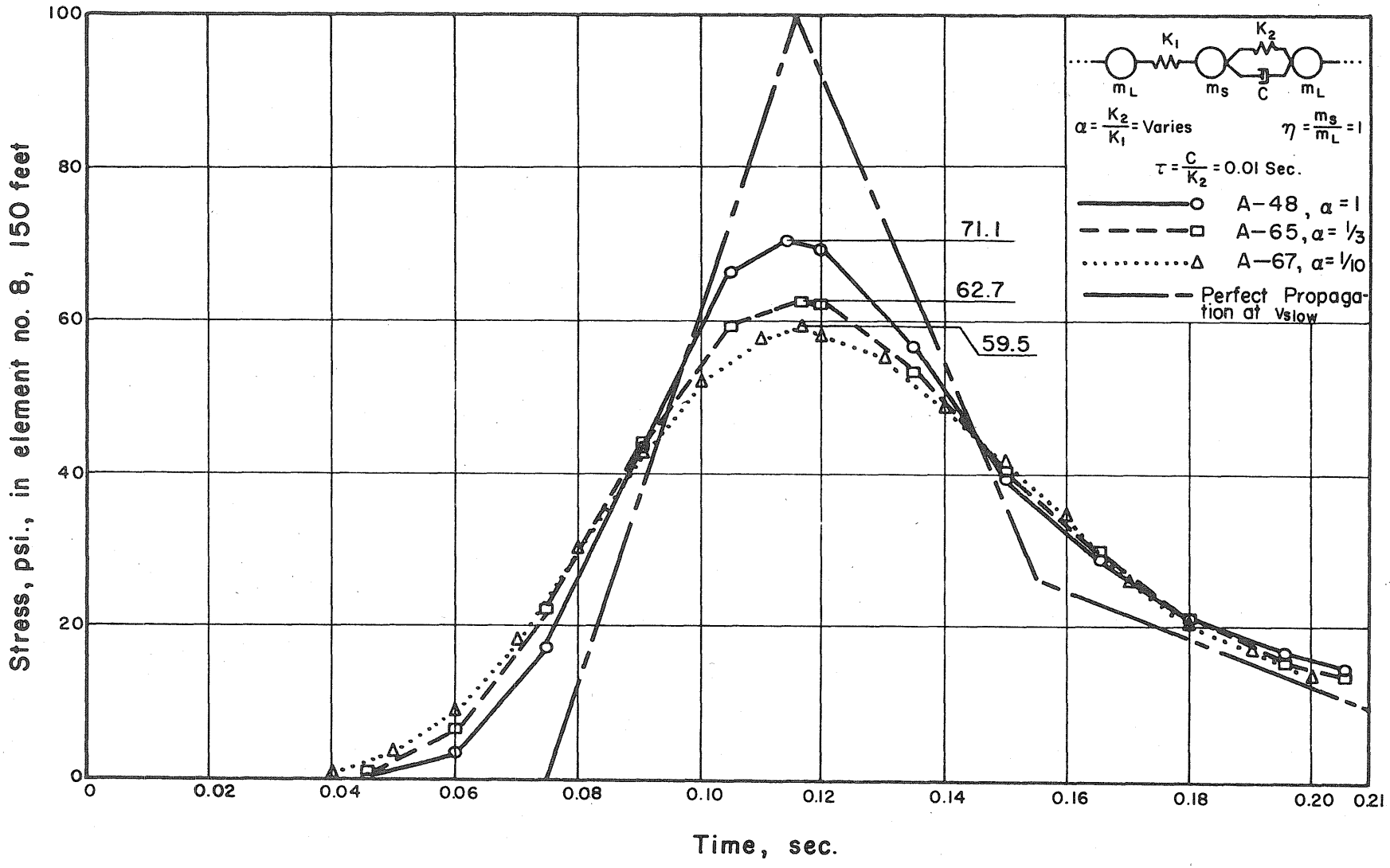

FIG. 15 STRESS VERSUS TIME AT 150 FEET AS A FUNCTION OF RATIO OF SPRING STIFFNESSES (α) - 40 Kt WEAPON

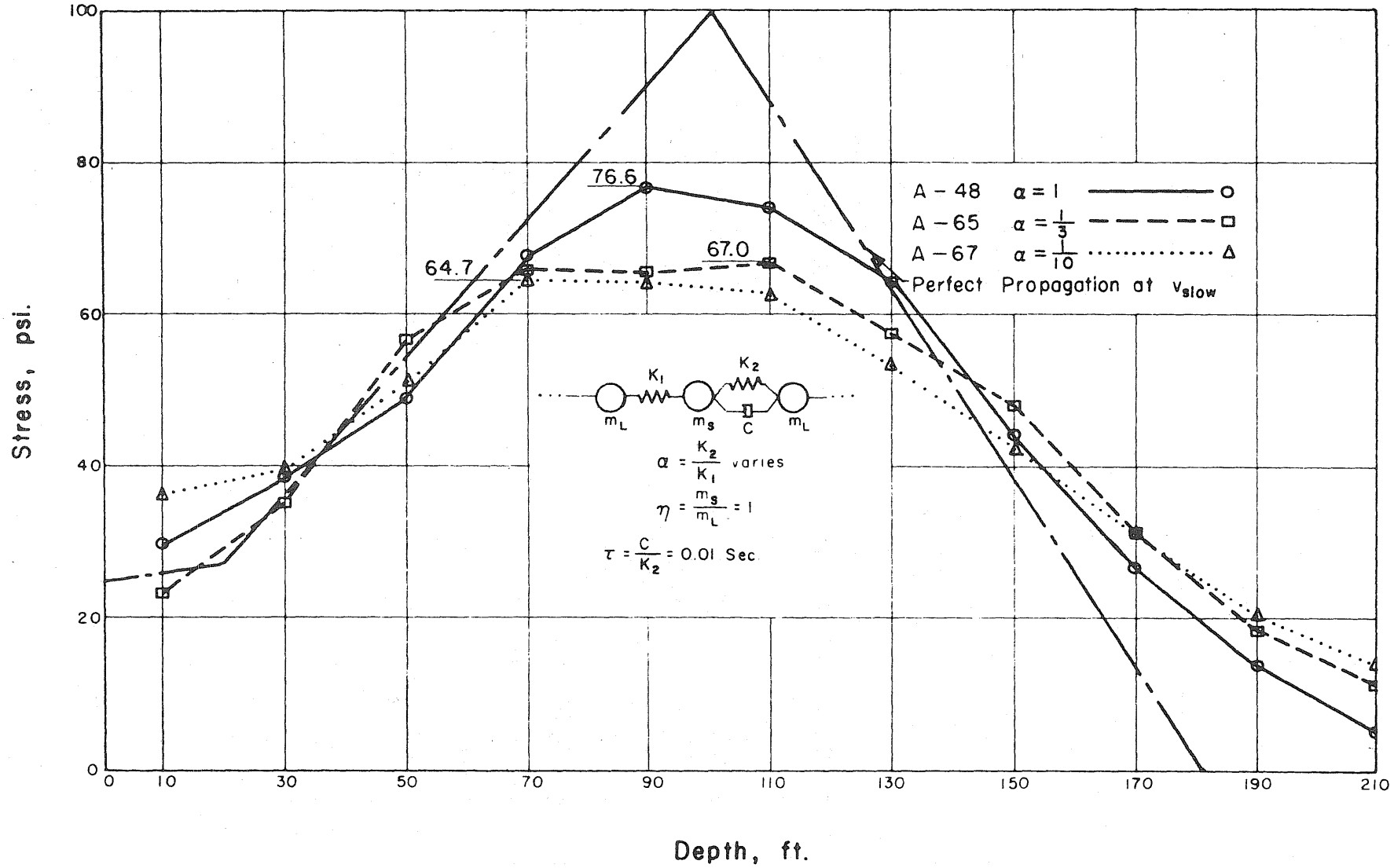

FIG. 16 STRESS DISTRIBUTION AS A FUNCTION OF RATIO OF SPRING STIFFNESSES (α) AT TIME = 0.09 SEC.— 40 Kt WEAPON

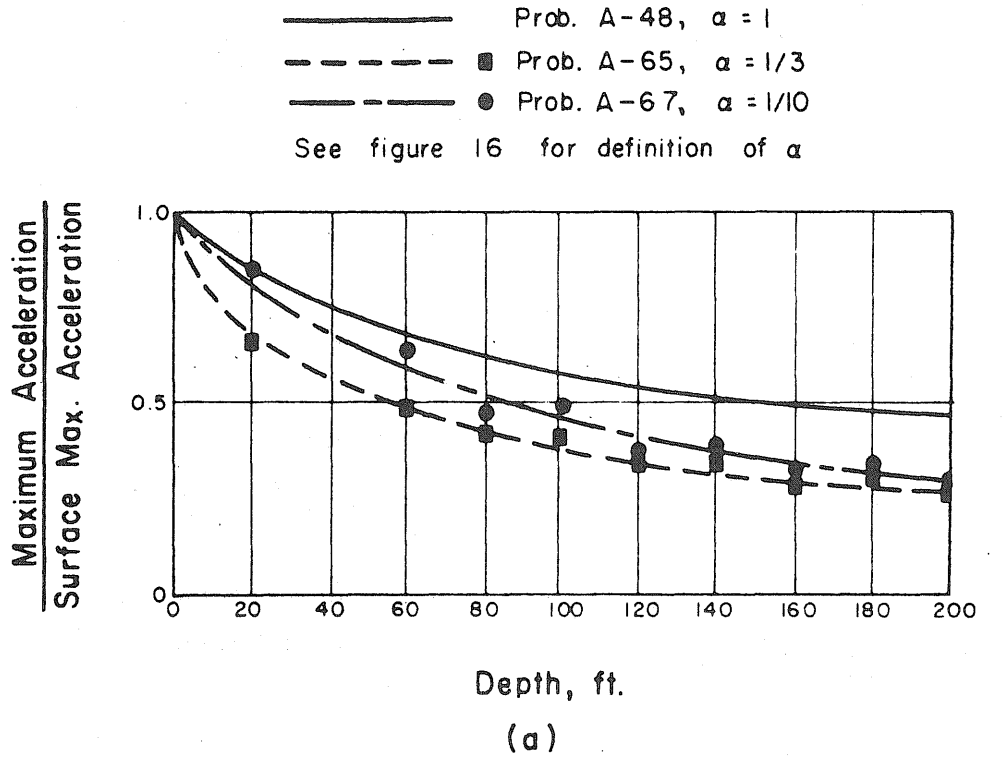

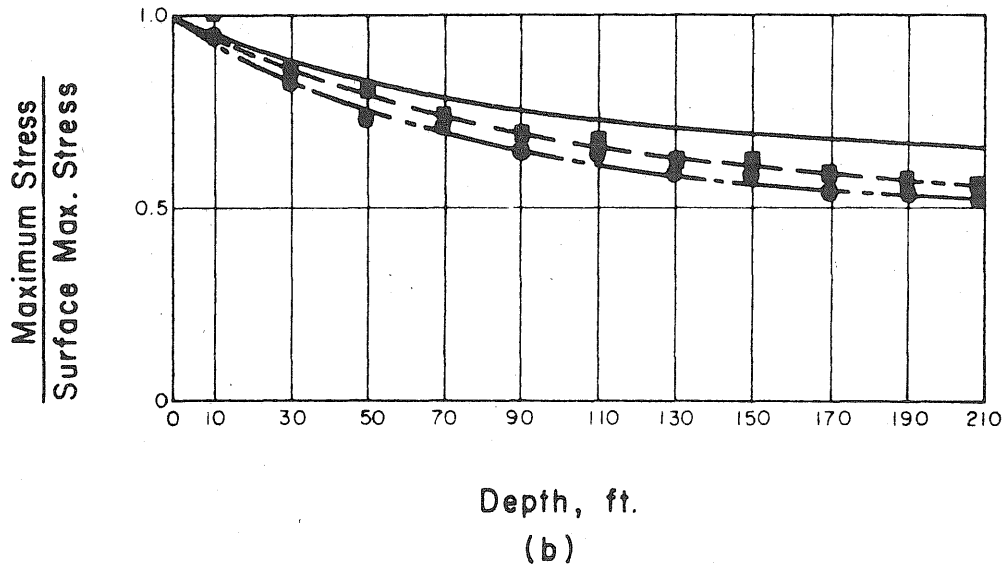

FIG. 17 MAXIMUM ACCELERATION AND STRESS VERSUS DEPTH AS A FUNCTION OF RATIO OF SPRING STIFFNESSES (α) – 40 Kt WEAPON (FIG. 8)

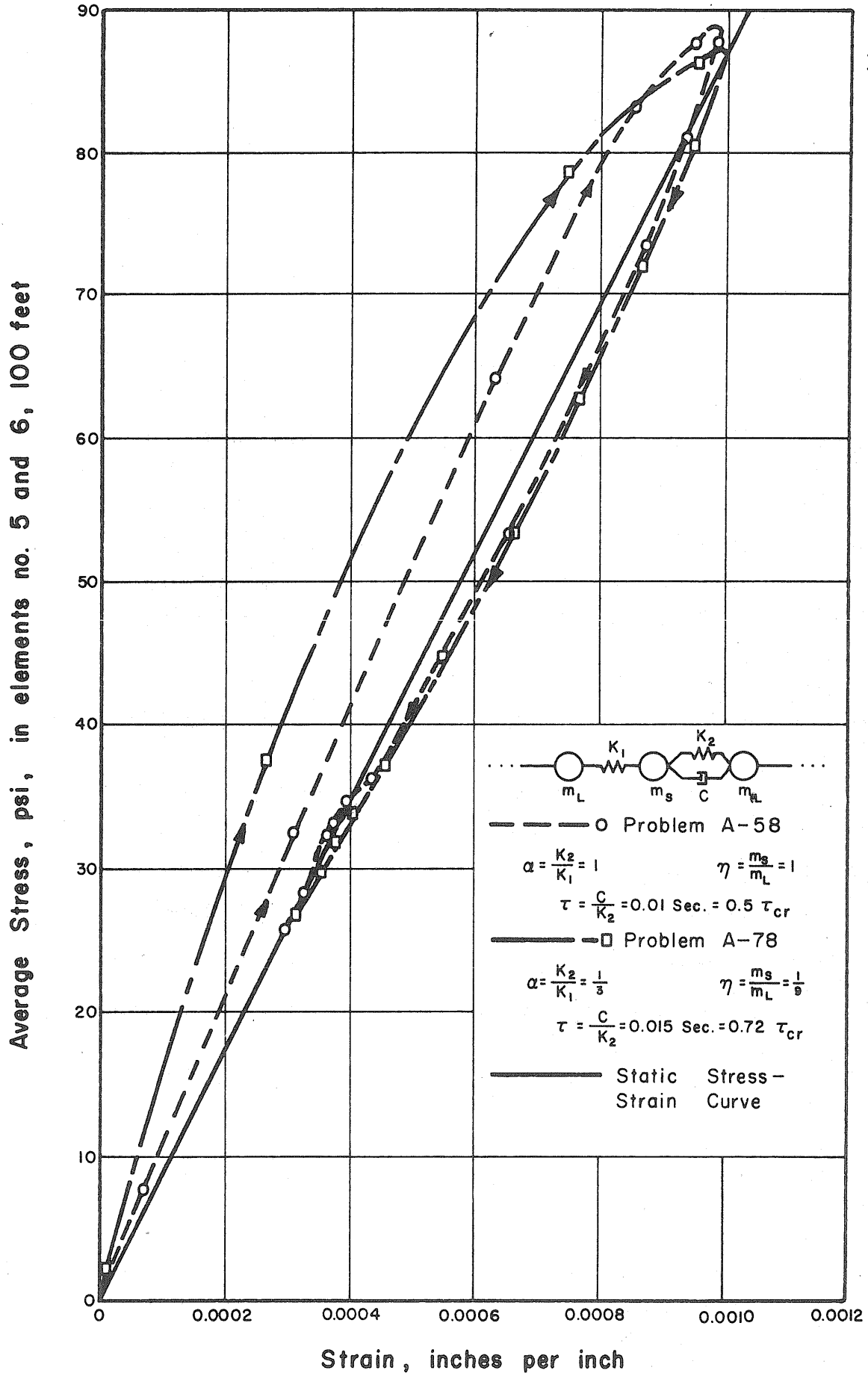

FIG. 18 DYNAMIC STRESS-STRAIN CURVES - 5 Mt WEAPON

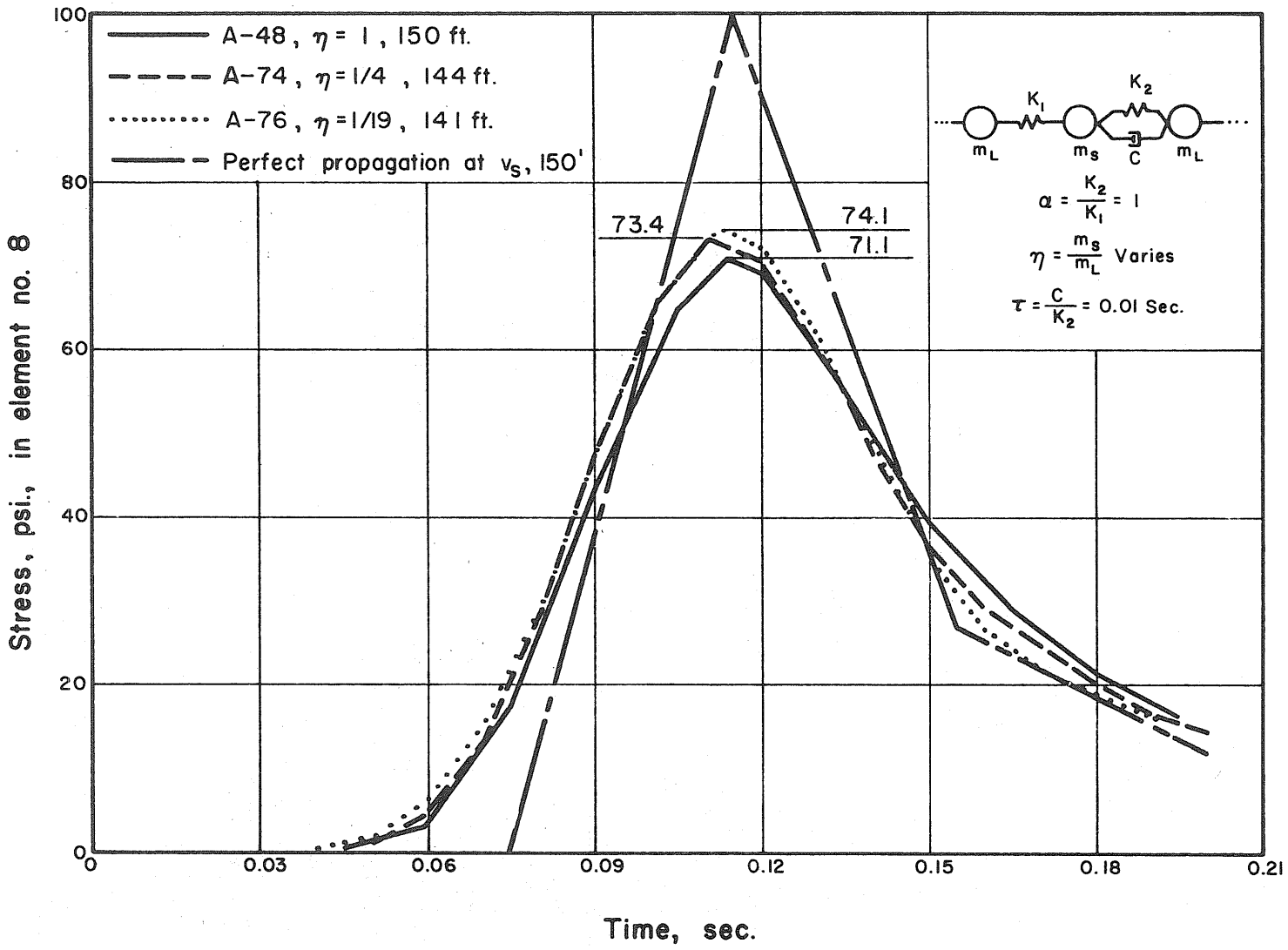

FIG. 19 STRESS VERSUS TIME AS A FUNCTION OF RATIO OF MASSES (η)
40 Kt WEAPON

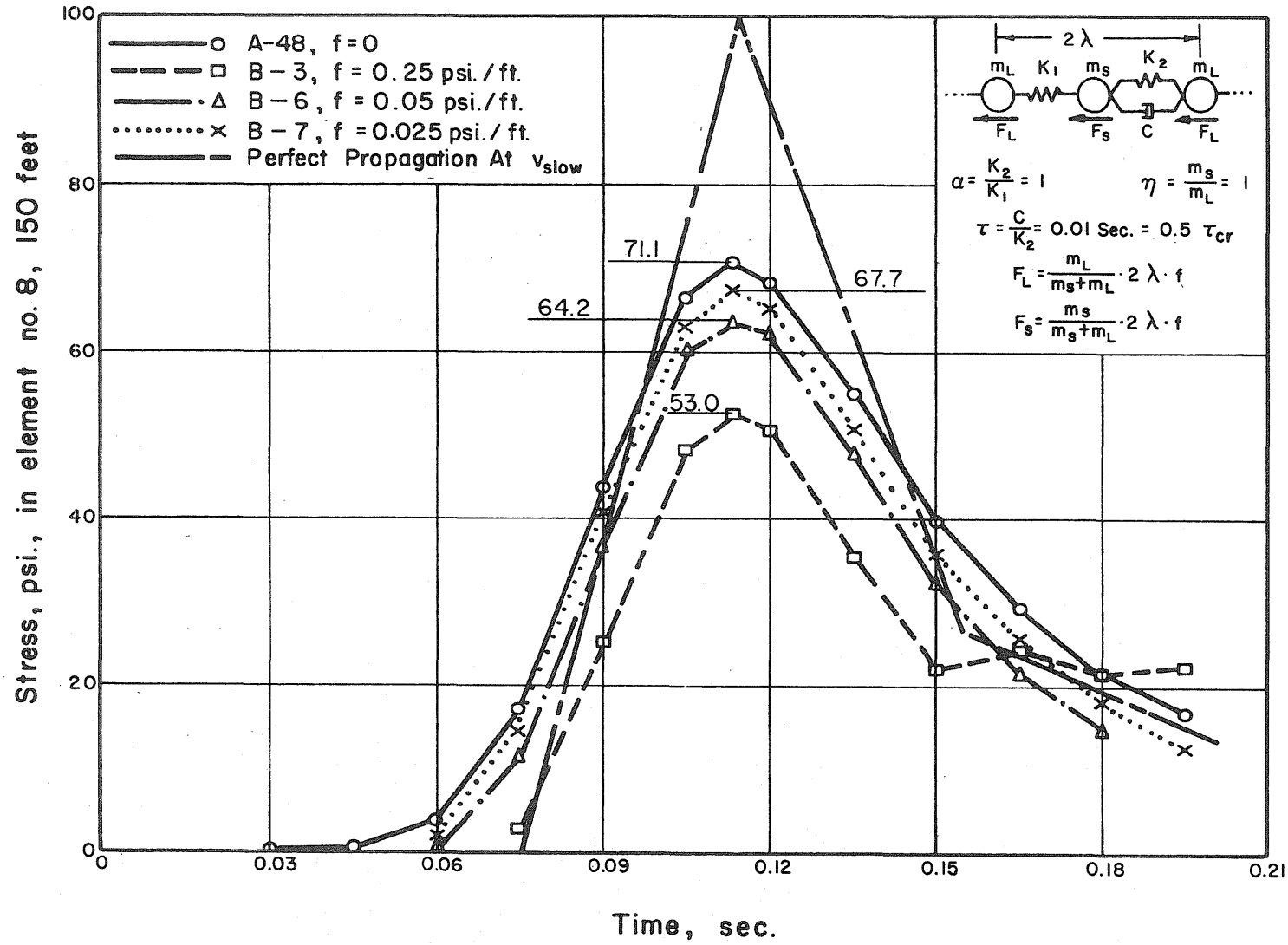

FIG. 20 STRESS VERSUS TIME AT 150 FEET AS A FUNCTION OF COULOMB DAMPING (f) — 40 Kt WEAPON

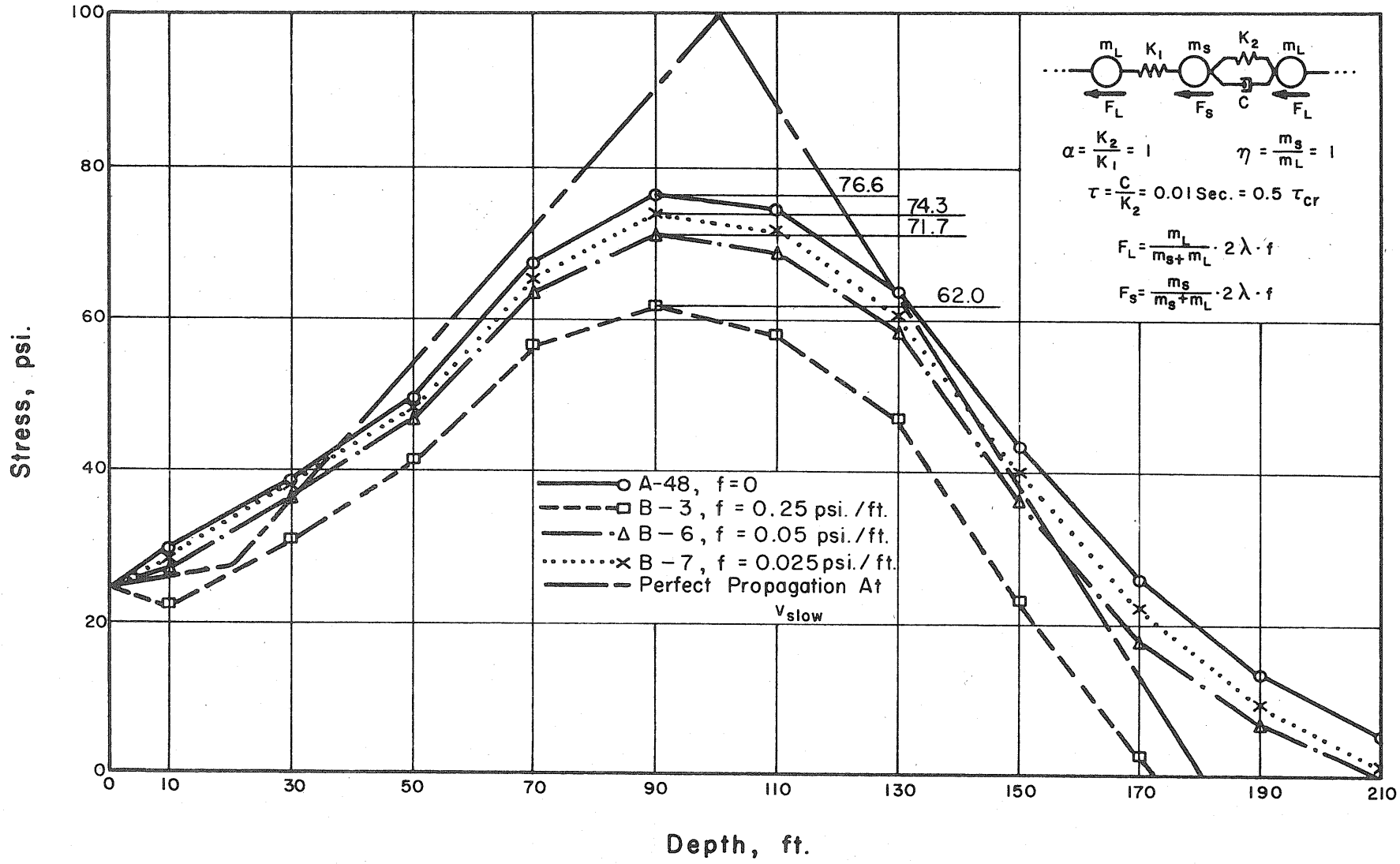

FIG. 21 STRESS DISTRIBUTION AS A FUNCTION OF COULOMB DAMPING (f) AT TIME = 0.09 SECONDS — 40 Kt WEAPON

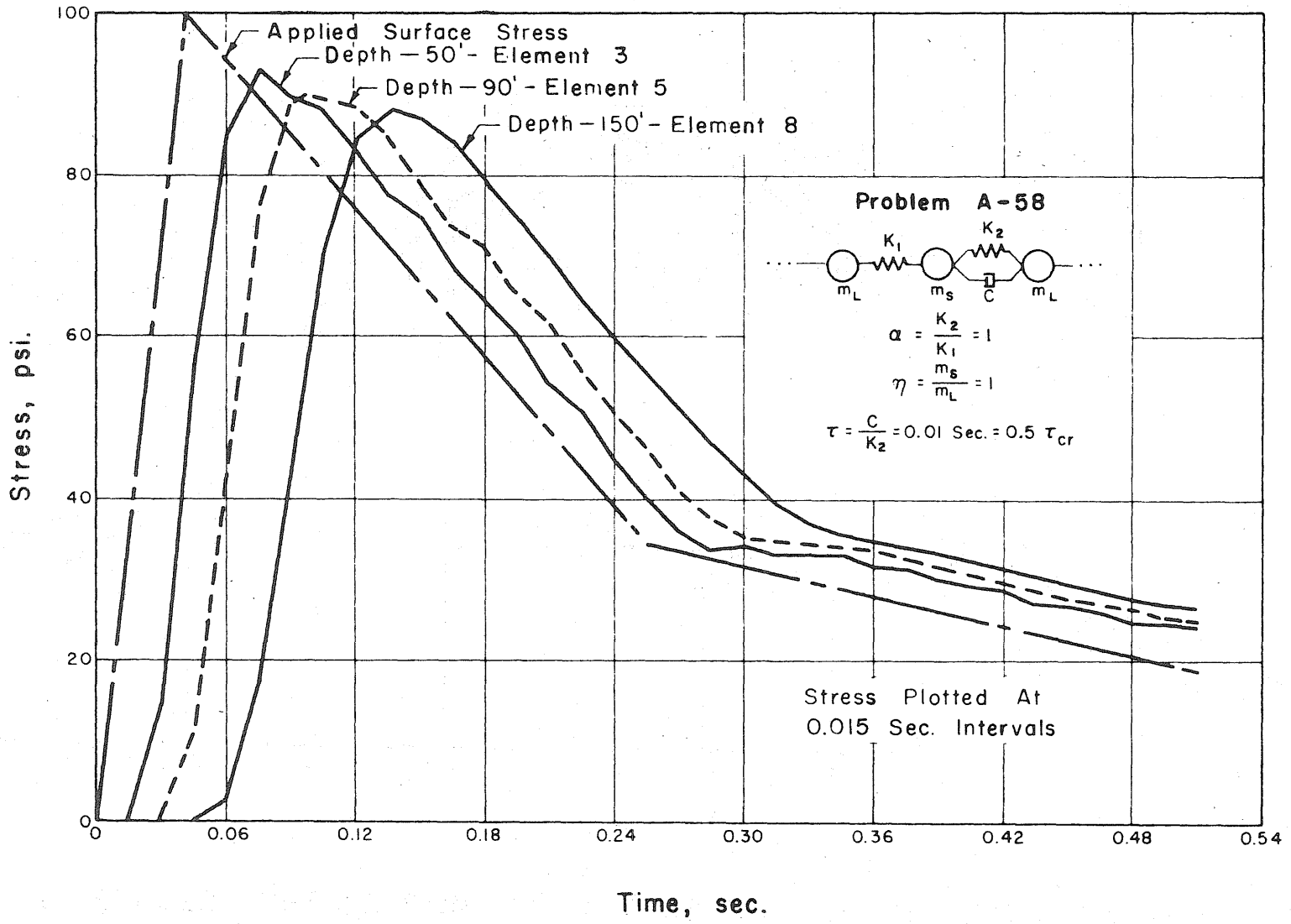

FIG. 22 STRESS VERSUS TIME AT VARIOUS DEPTHS
5Mt WEAPON

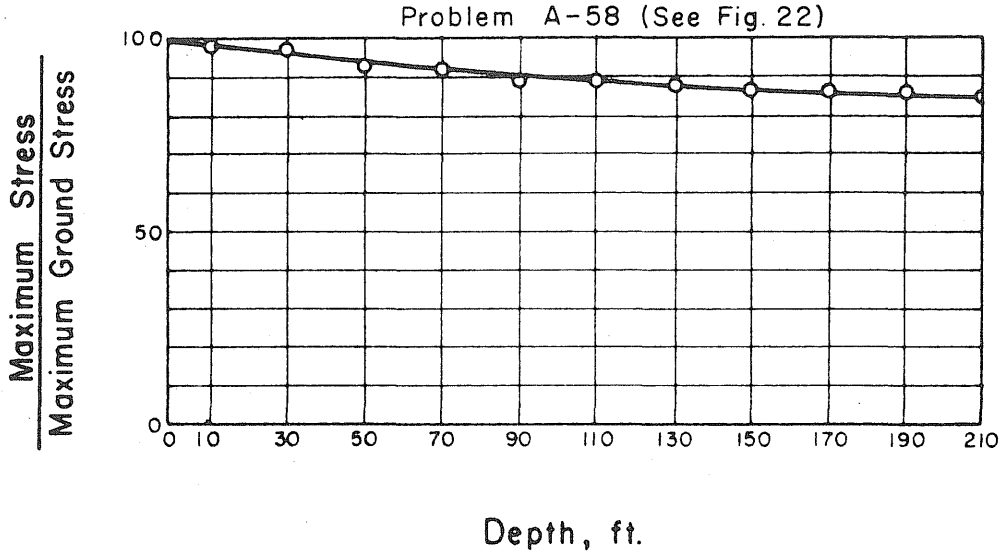

FIG. 23 VARIATIONS IN MAXIMUM STRESS WITH DEPTH— 5 Mt WEAPON

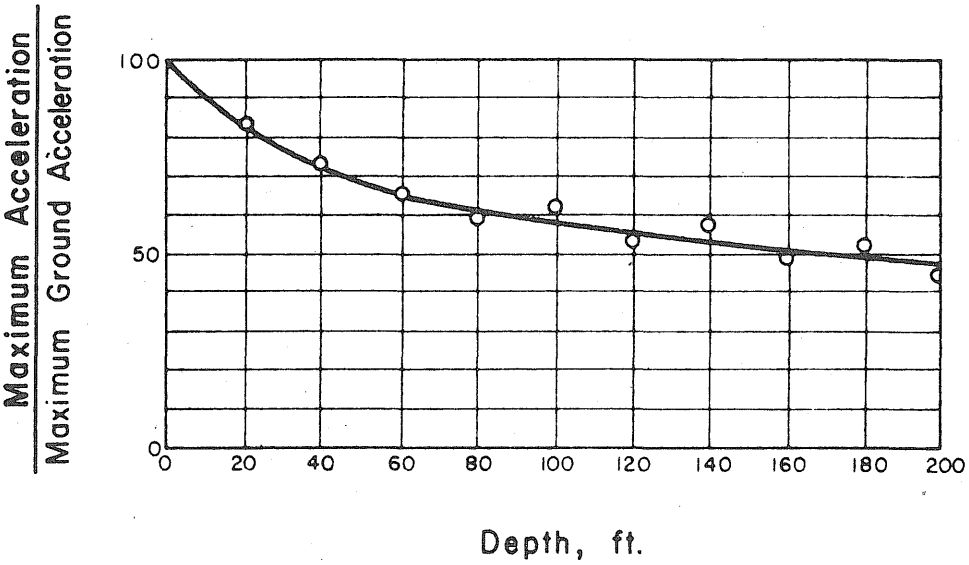

FIG. 24 VARIATIONS IN MAXIMUM ACCELERATION WITH DEPTH - 5 Mt WEAPON

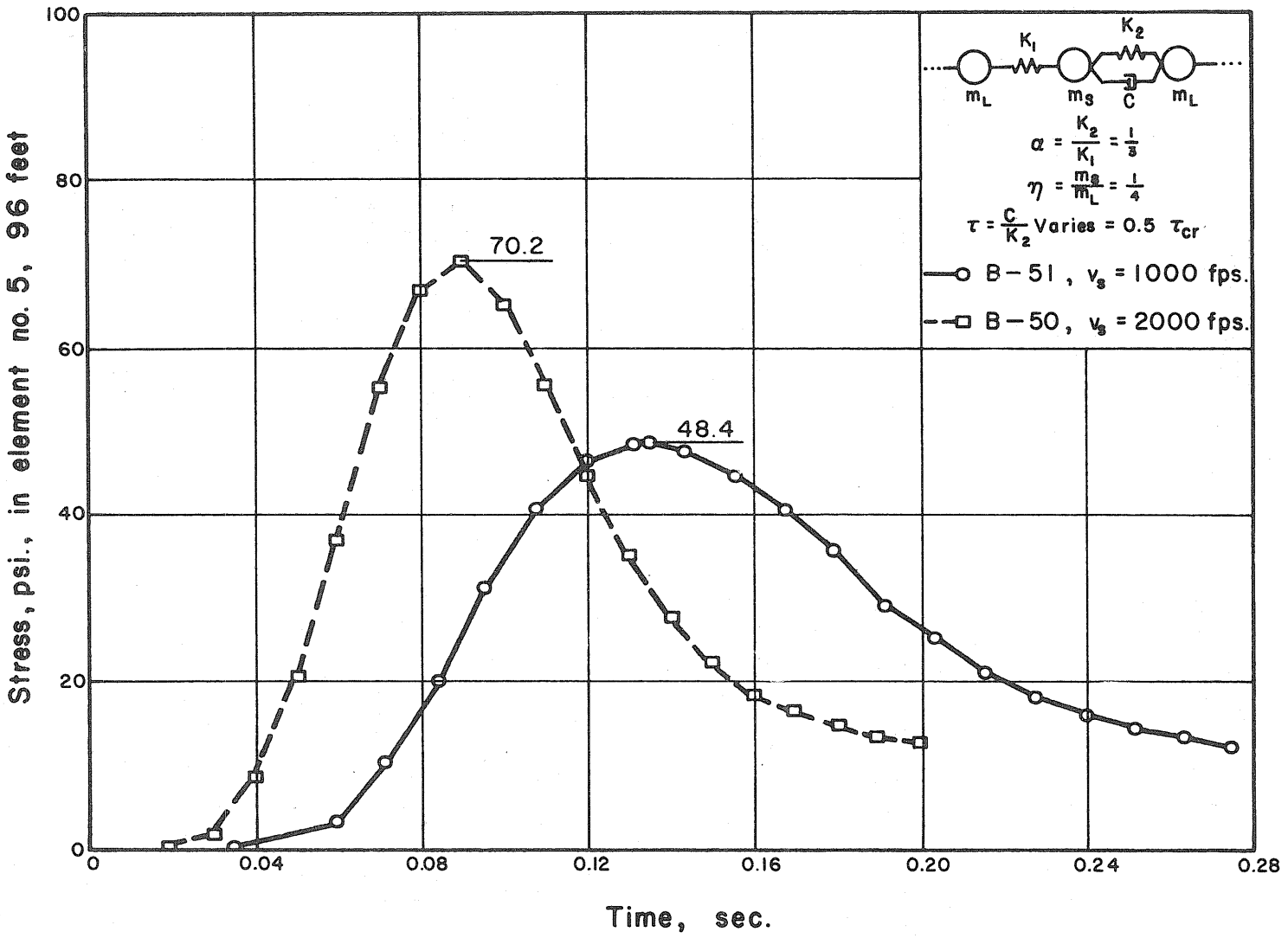

FIG. 25 STRESS VERSUS TIME AT 96 FEET FOR TWO ACOUSTIC VELOCITIES – 40 Kt WEAPON (FIG. 8)

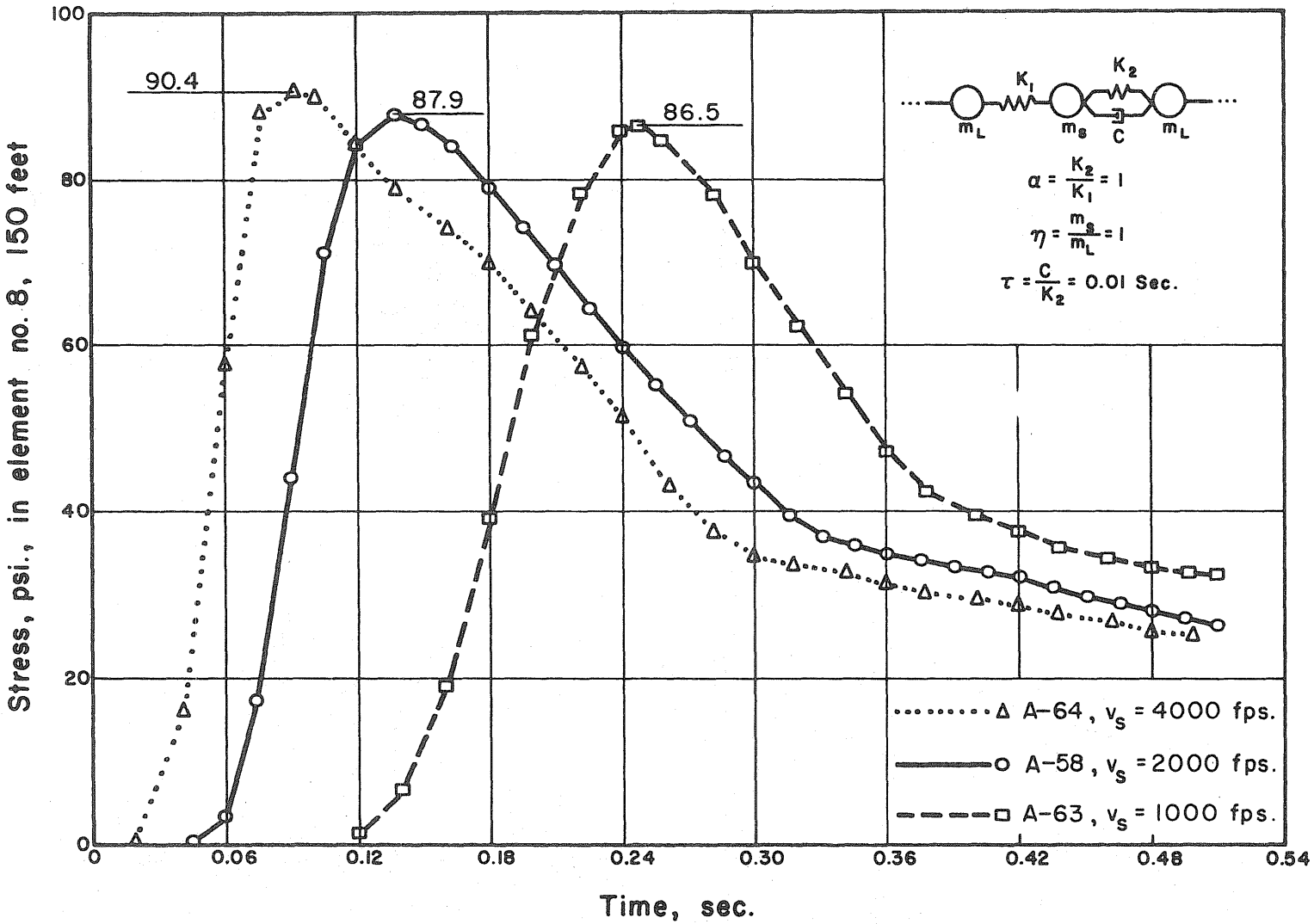

FIG. 26 STRESS VERSUS TIME AT 150 FEET FOR VARIOUS ACOUSTIC VELOCITIES — 5 Mt WEAPON

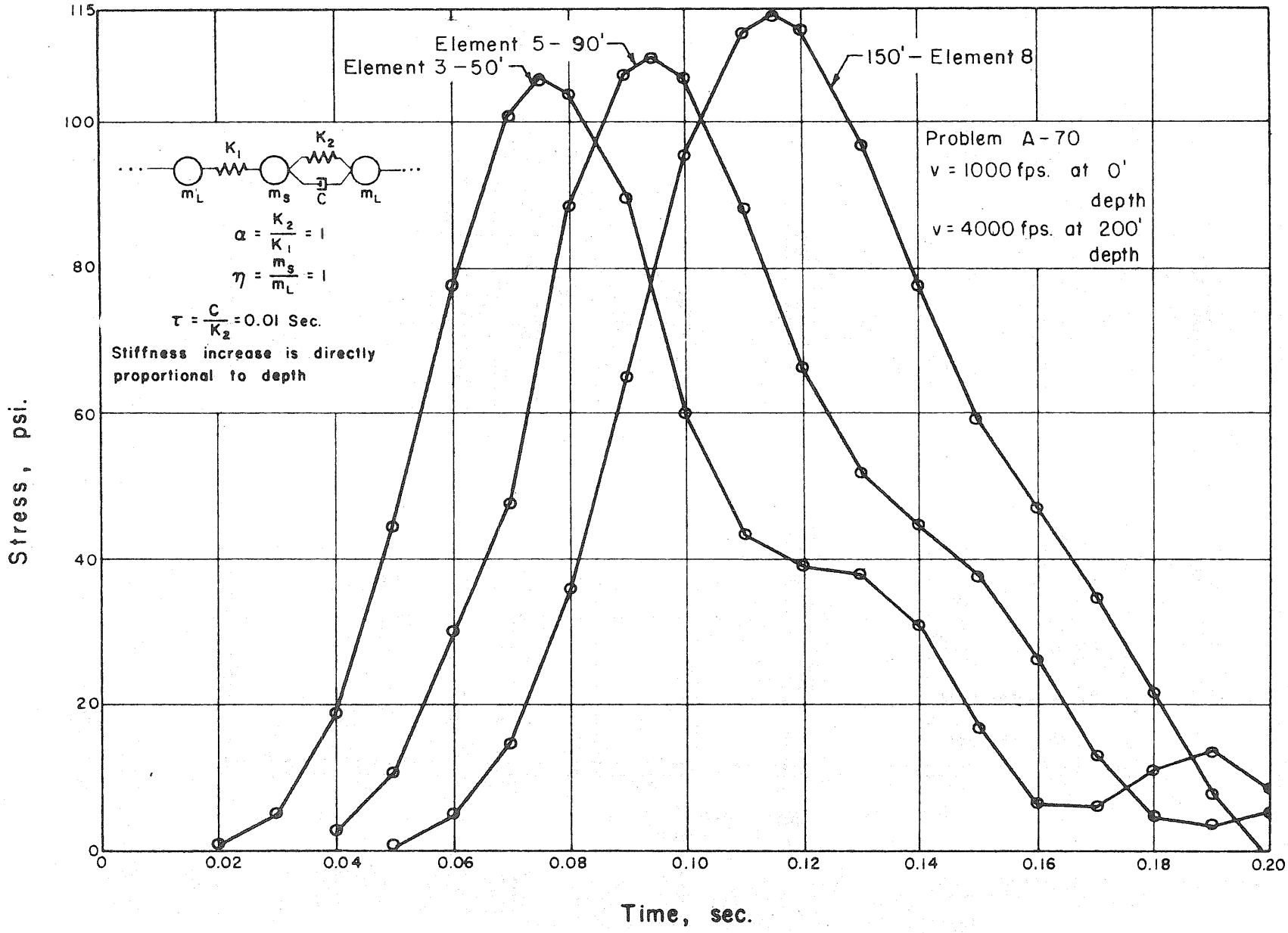

FIG. 27 STRESS VERSUS TIME FOR A SYSTEM WITH INCREASING STIFFNESS 40 Kt WEAPON (FIG. 8)

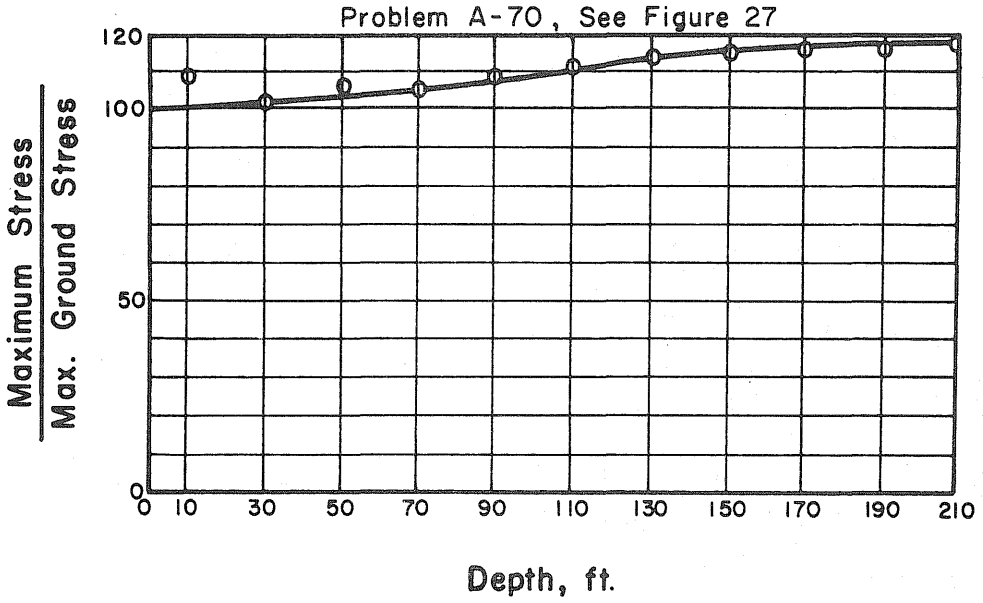

FIG. 28 VARIATIONS IN MAXIMUM STRESS WITH DEPTH IN A SYSTEM WITH INCREASING STIFFNESS

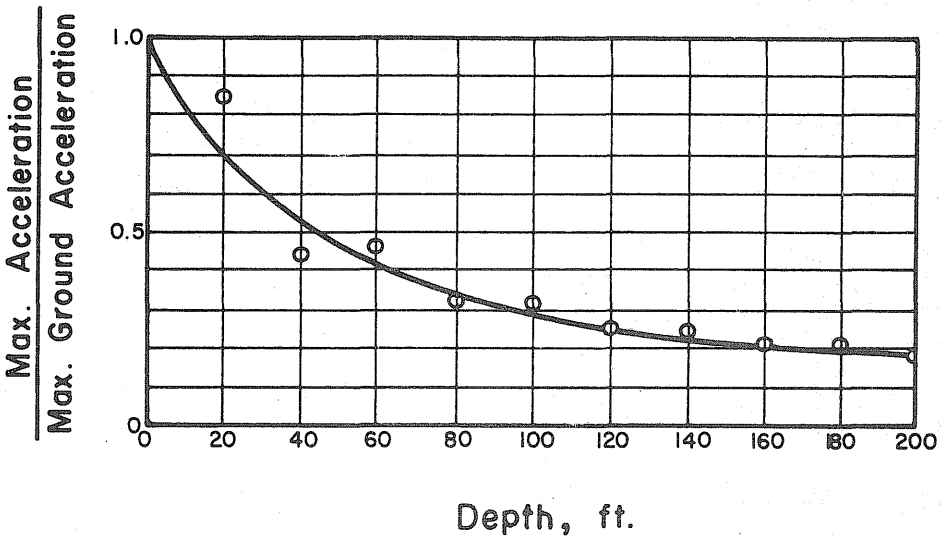

FIG. 29 VARIATIONS IN MAXIMUM ACCELERATION WITH DEPTH IN A SYSTEM WITH INCREASING STIFFNESS

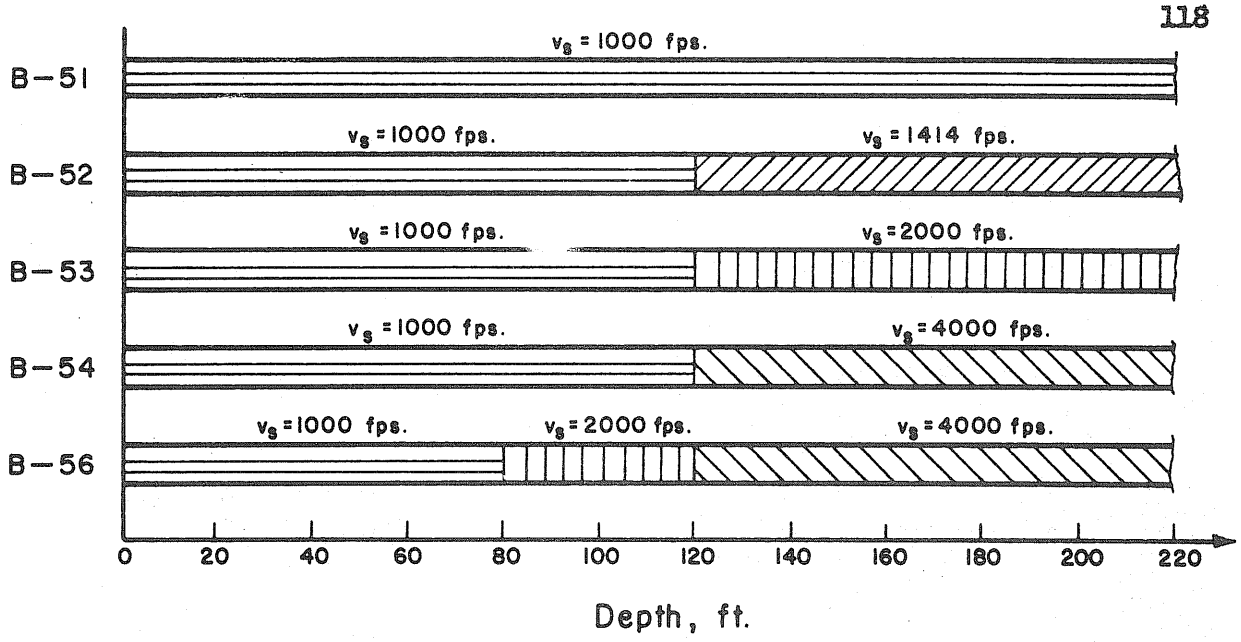

FIG. 30 SOIL PROFILES FOR PROBLEMS OF FIGURES 31 & 32

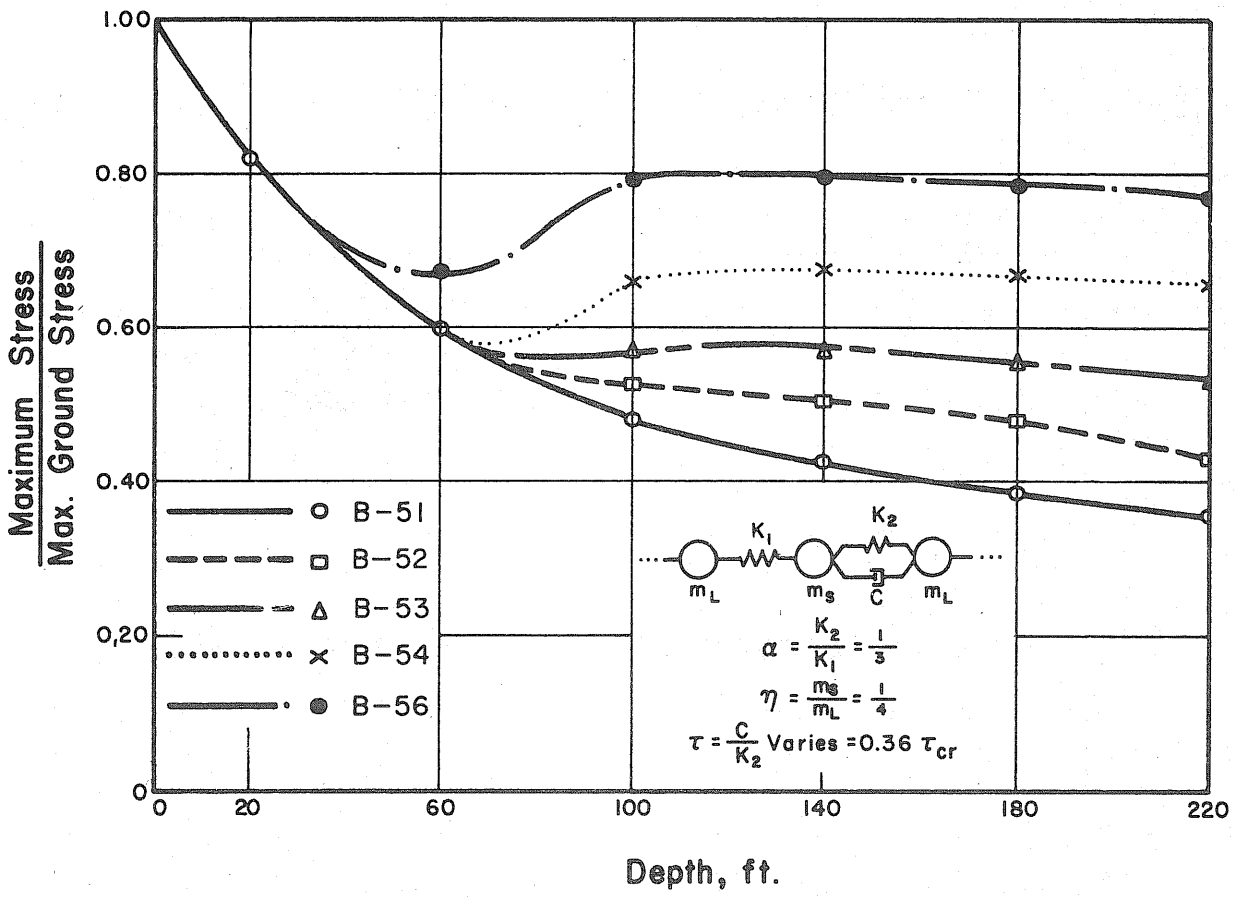

FIG. 31 MAXIMUM STRESS VERSUS DEPTH FOR STRATIFIED SOILS I — 40Kt WEAPON (FIG. 8)

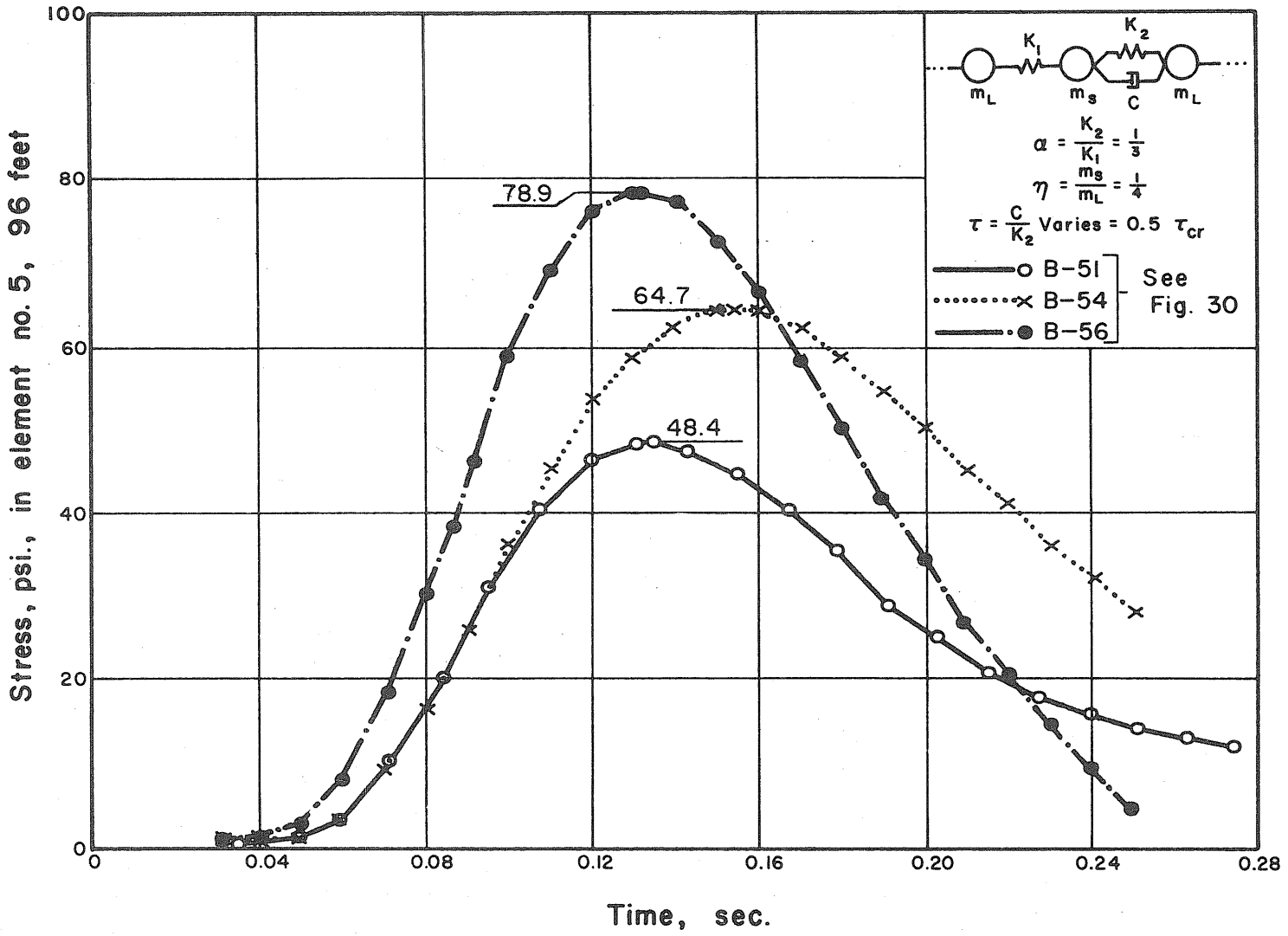

FIG. 32 STRESS VERSUS TIME AT 96 FEET IN STRATIFIED SOILS I 40 Kt WEAPON (FIG. 8)

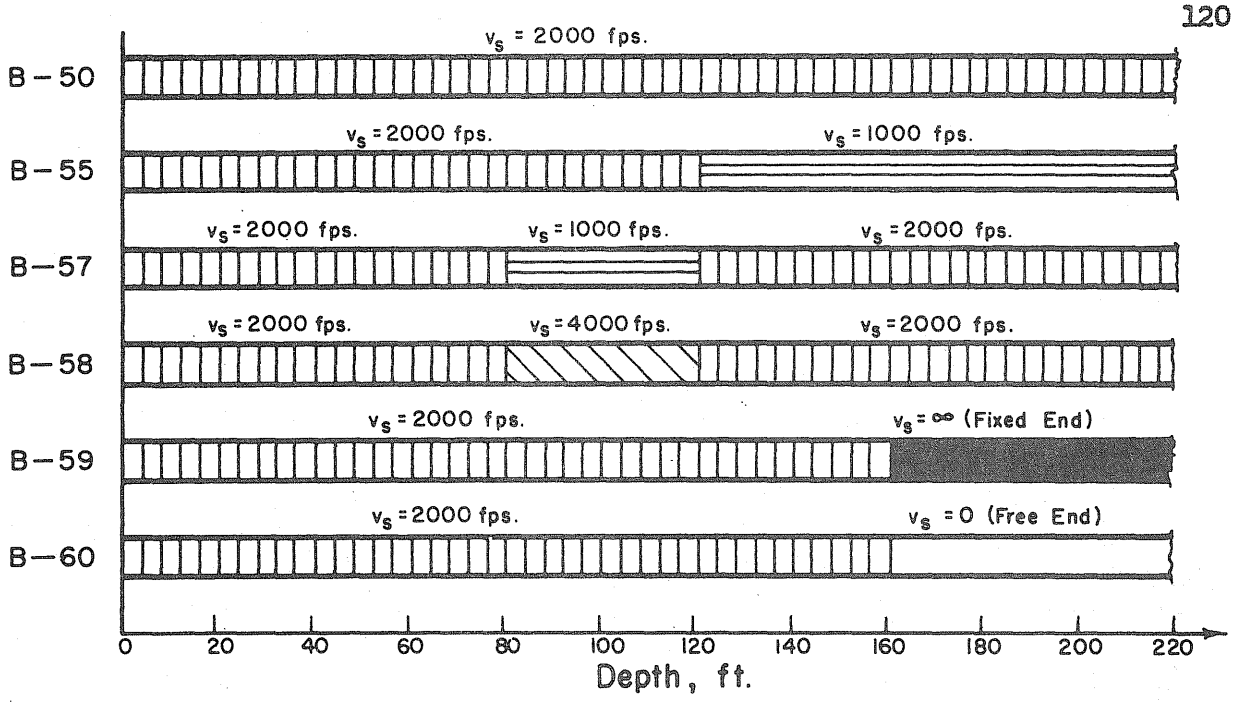

FIG. 33 SOIL PROFILES FOR PROBLEMS OF FIGS. 34 & 35

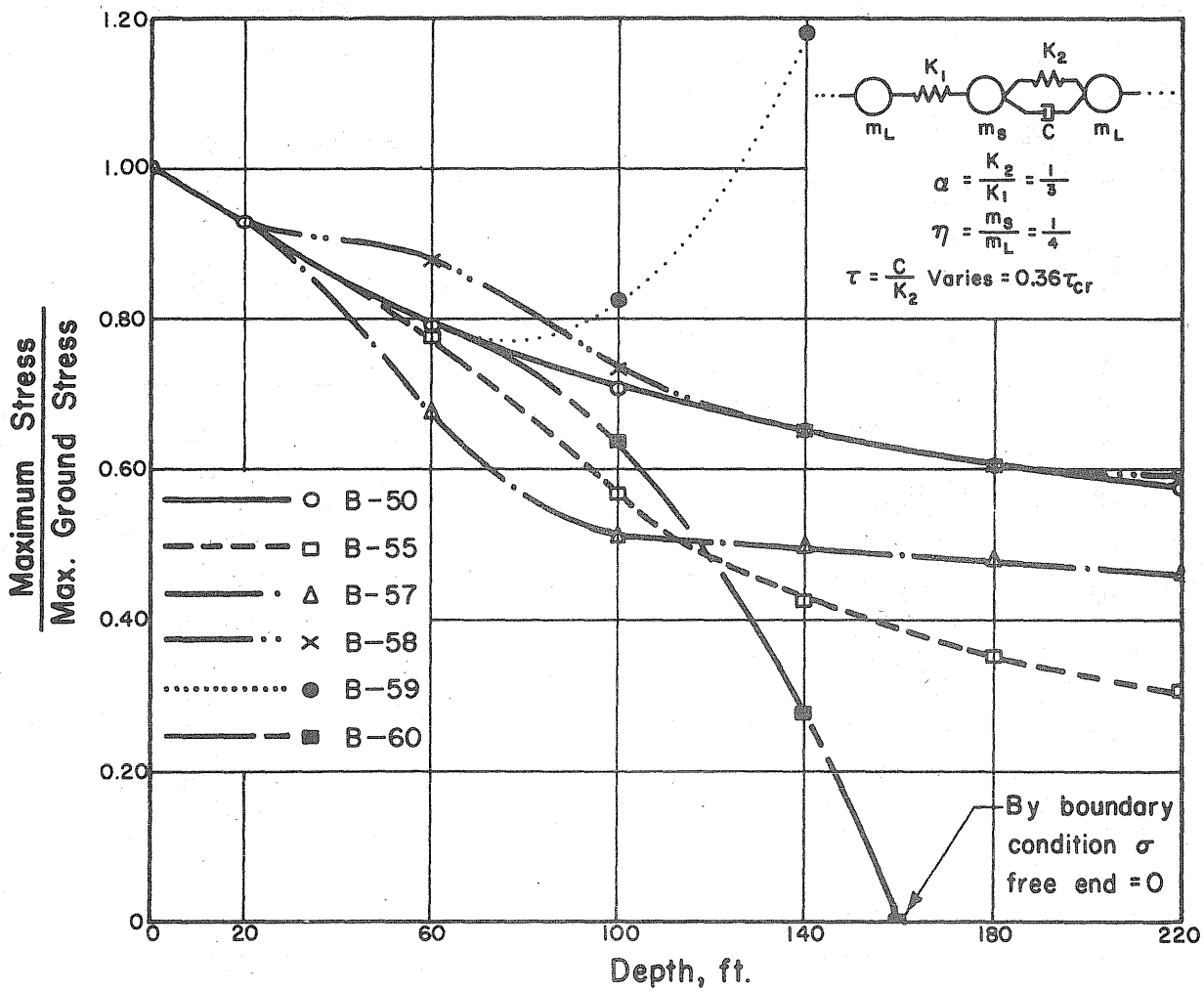

FIG. 34 MAXIMUM STRESS VERSUS DEPTH FOR STRATIFIED SOILS II – 40Kt WEAPON (FIG. 8)

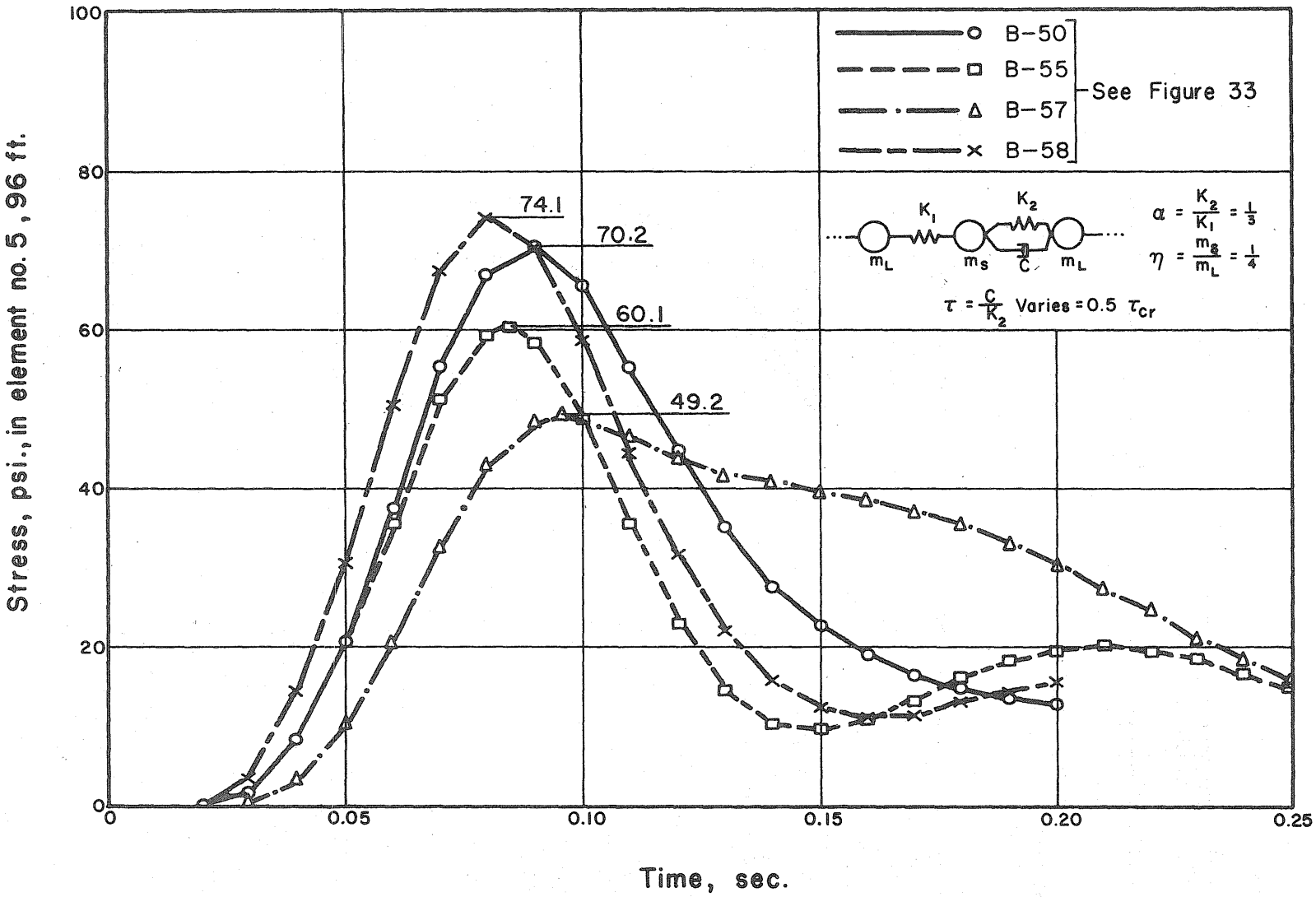

FIG. 35 STRESS VERSUS TIME AT 96 FEET IN STRATIFIED SOILS II
40 Kt WEAPON (FIG. 8)

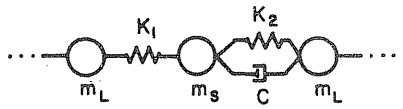

$\alpha = \frac{K_2}{K_1} = 1$ $\eta = \frac{m_s}{m_L} = 1$

$\tau = \frac{C}{K_2} = 0.01$ Sec. $= 0.5\ \tau_{cr}$

Springs Elasto-Plastic

As Shown Below

(a) Model For Problems B-30 and B-31

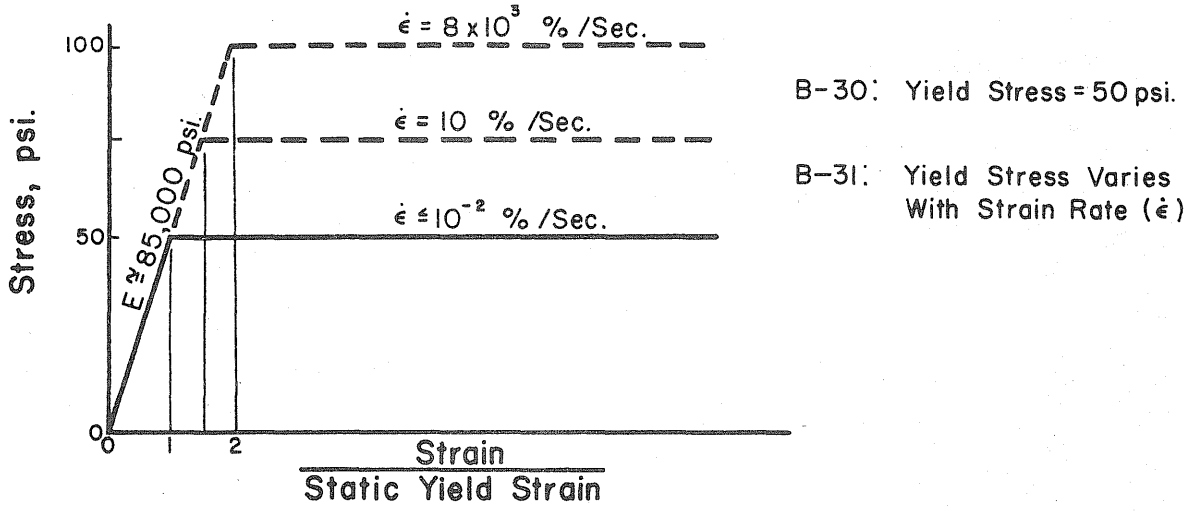

(b) Stress–Strain Curves For Problems B-30 and B-31

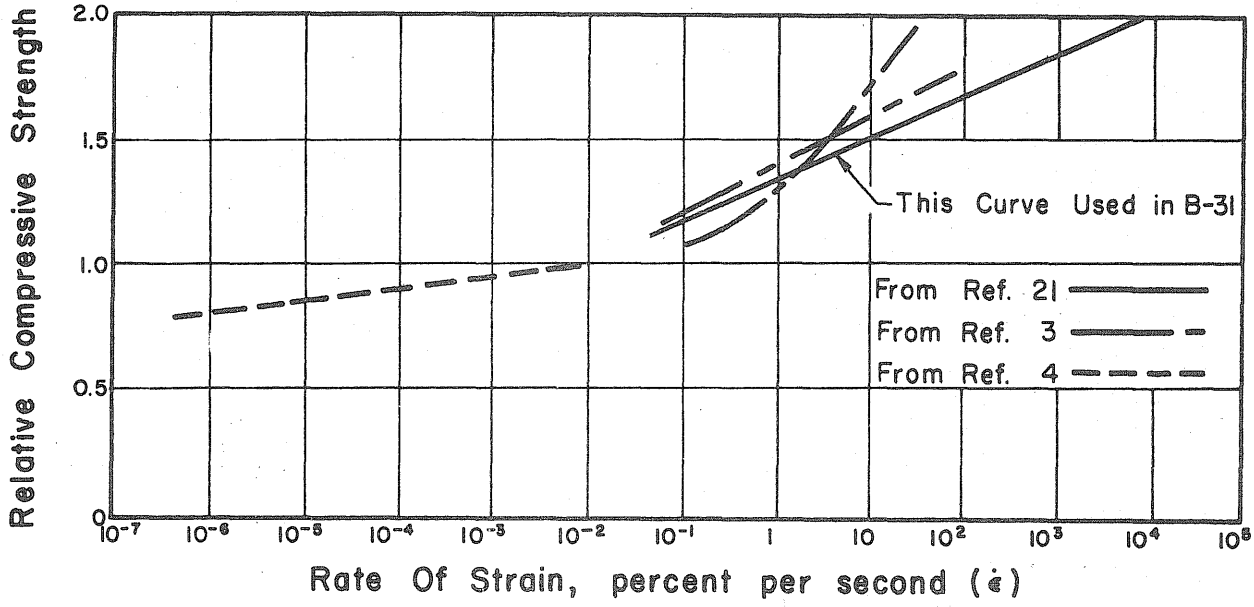

(c) Strain Rate Effect In Unconfined, Undisturbed Boston Clay (Figure from ref. 21)

FIG. 36 DATA ON MODEL USED FOR PROBLEMS B-30 AND B-31 CONCERNING STRAIN RATE EFFECT

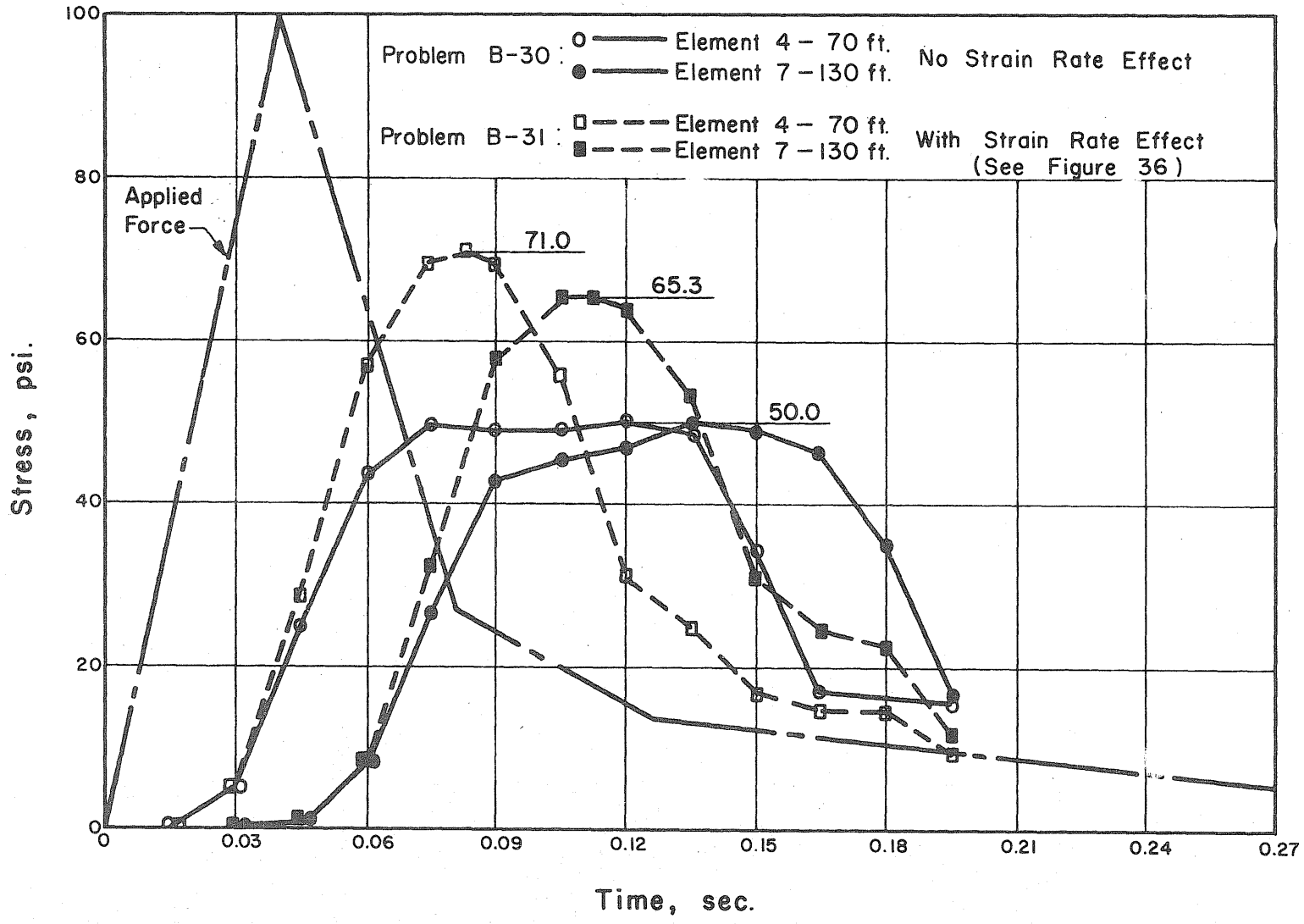

FIG. 37 STRESS VERSUS TIME AT 70 FT. AND 130 FT. SHOWING STRAIN RATE EFFECT
40 Kt WEAPON

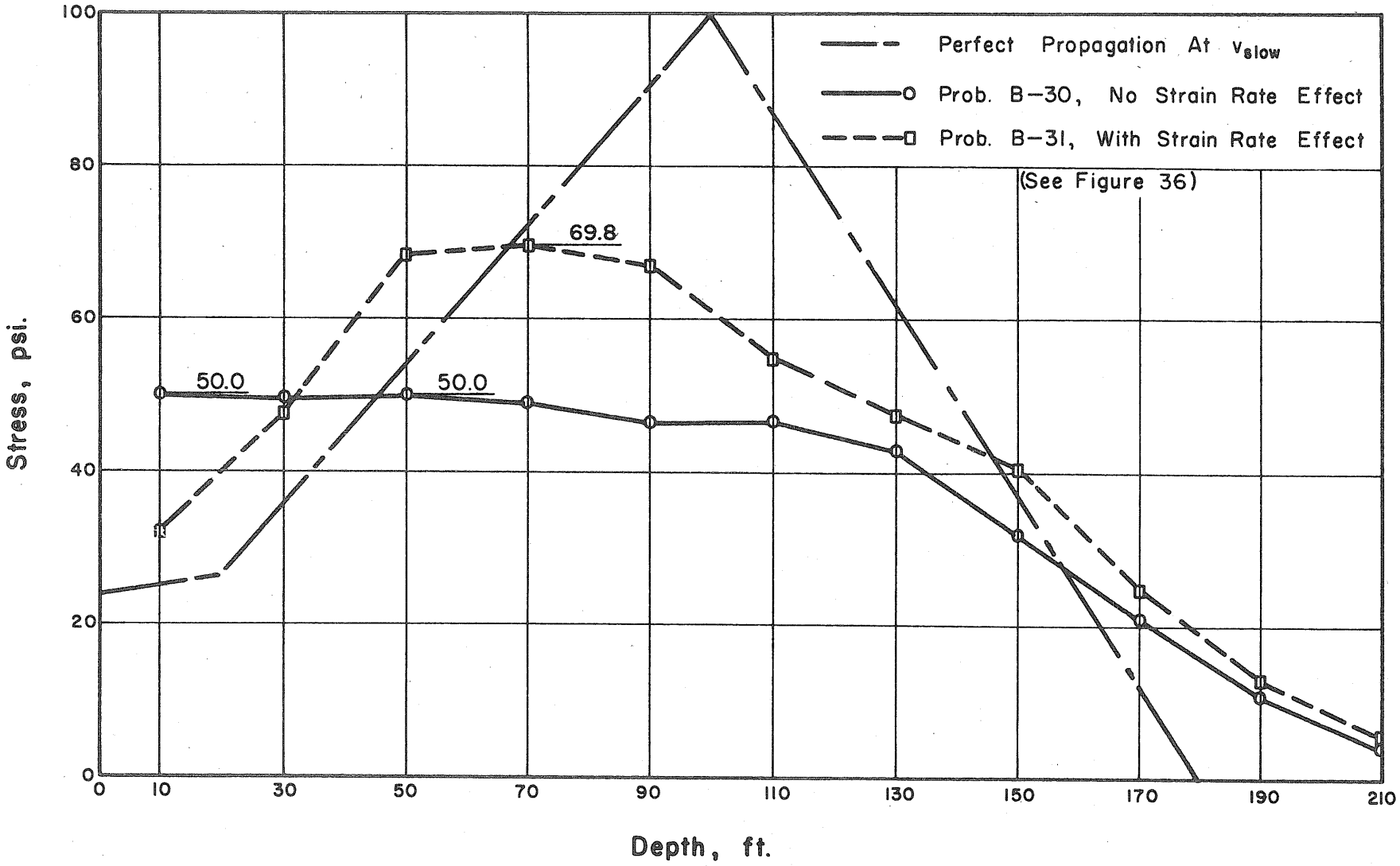

FIG. 38 STRESS DISTRIBUTION AT $t = 0.09$ SEC. SHOWING STRAIN RATE EFFECT
40 Kt WEAPON

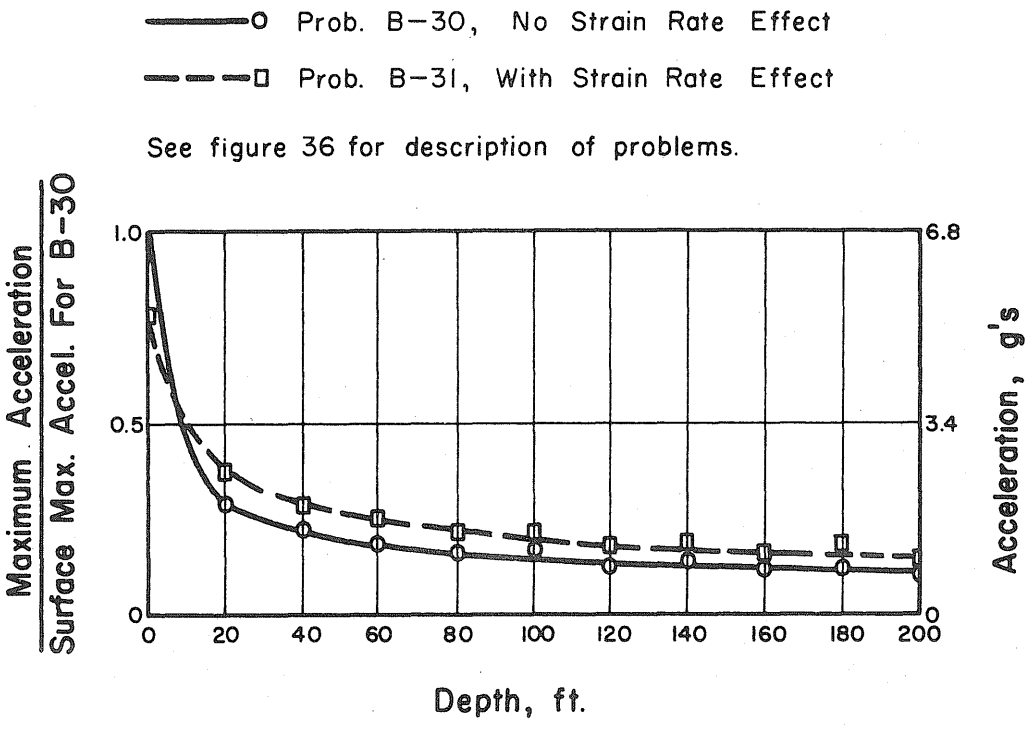

FIG. 39 STRAIN RATE EFFECT ON MAXIMUM ACCELERATION VERSUS DEPTH

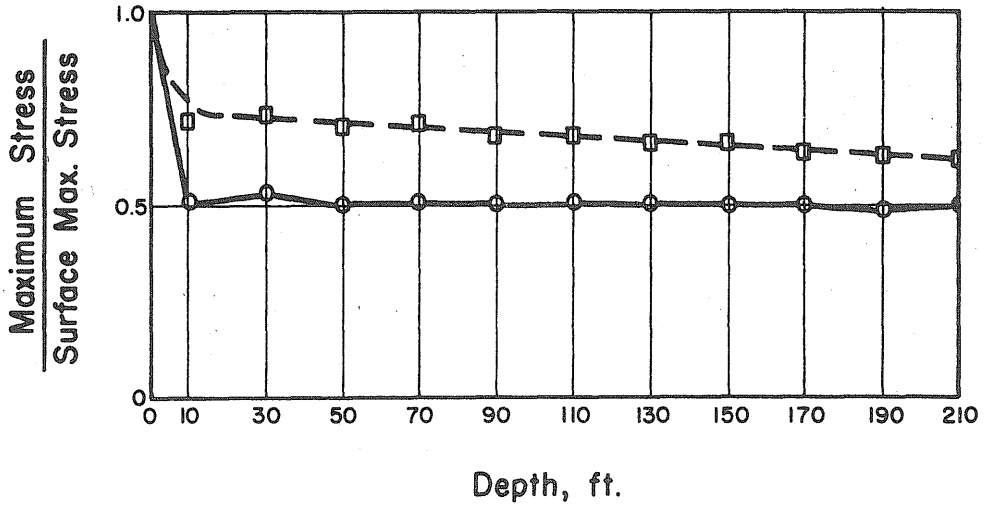

FIG. 40 STRAIN RATE EFFECT ON MAXIMUM STRESS VERSUS DEPTH

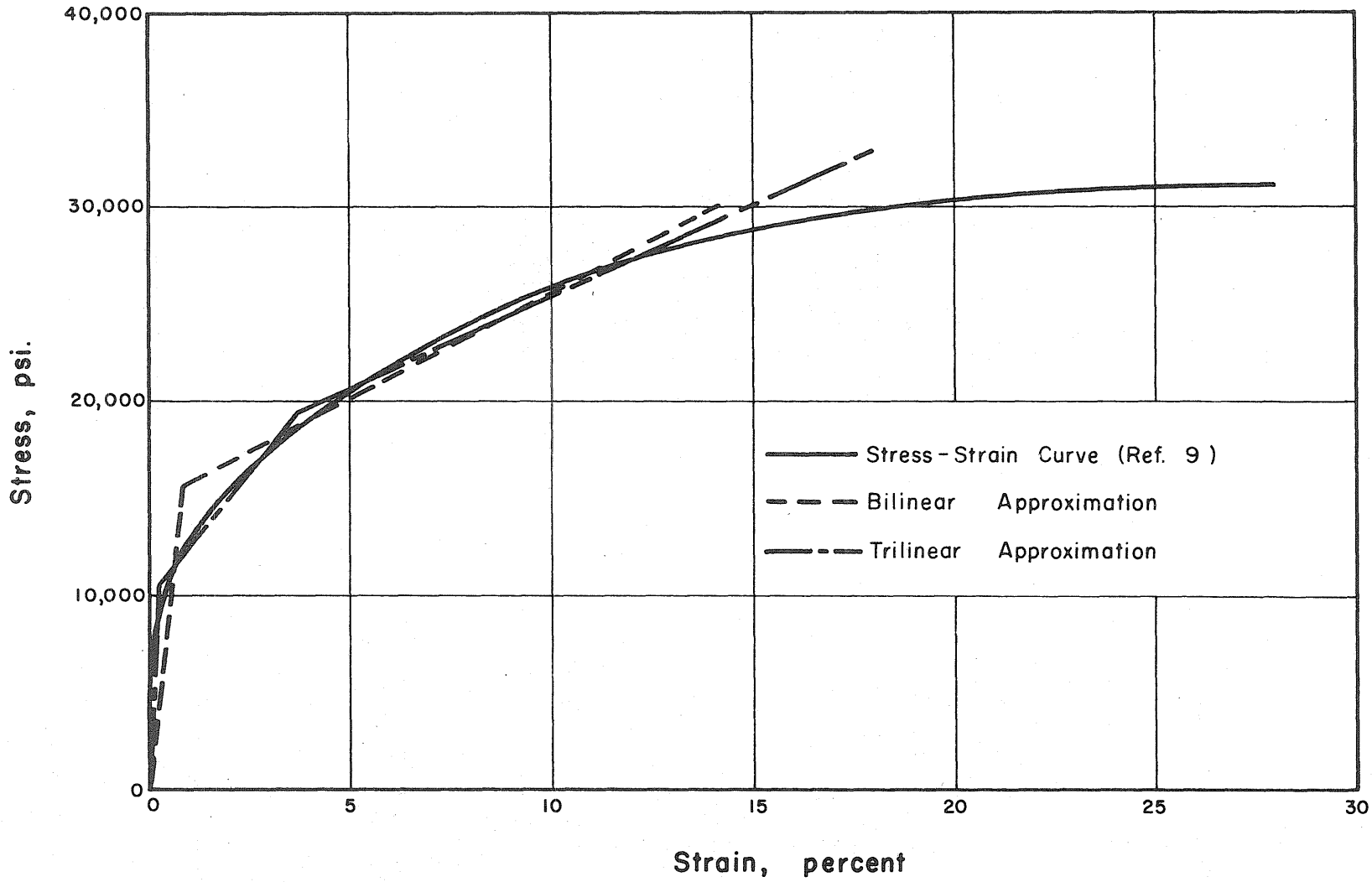

FIG. 41 STATIC STRESS-STRAIN CURVE FOR 80 INCH ANNEALED COPPER WIRE IN TENSION

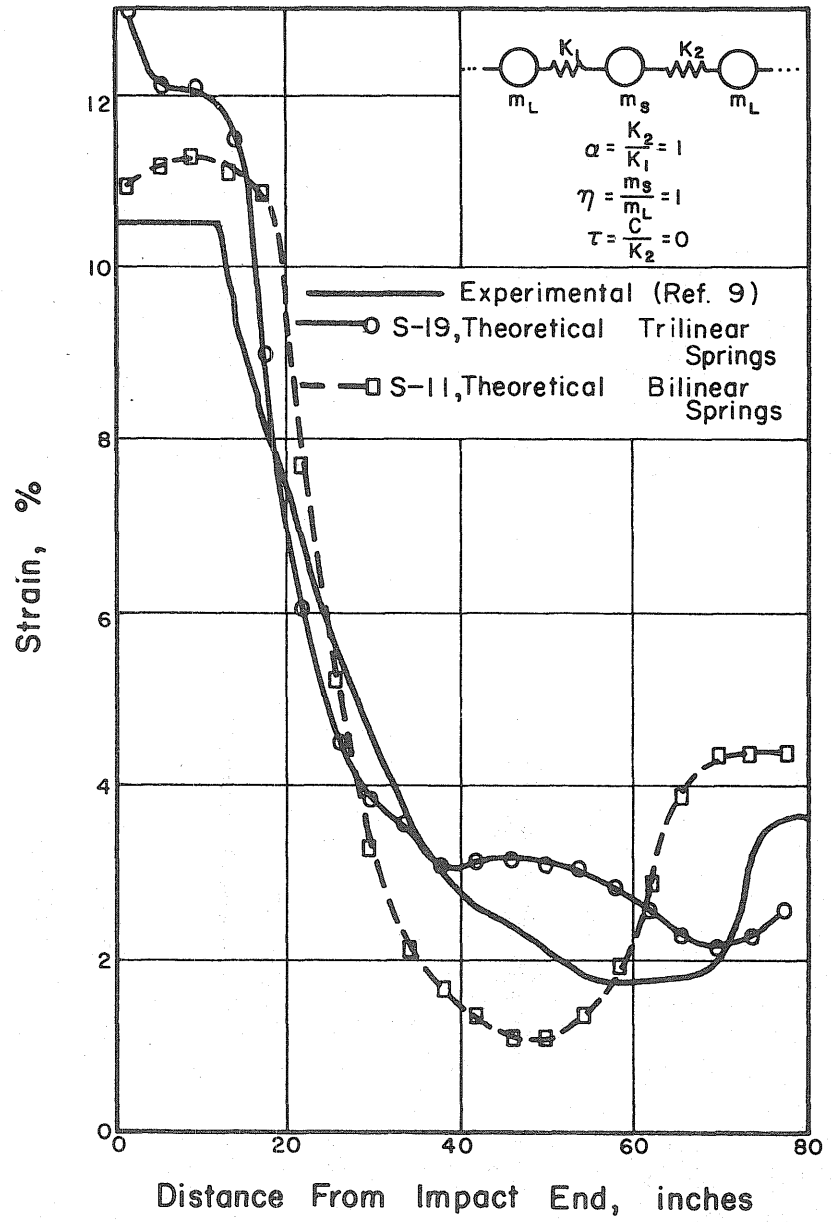

FIG. 42 STRAIN DISTRIBUTION FOR 80 INCH COPPER WIRE, $V_o = 145$ FT./SEC.

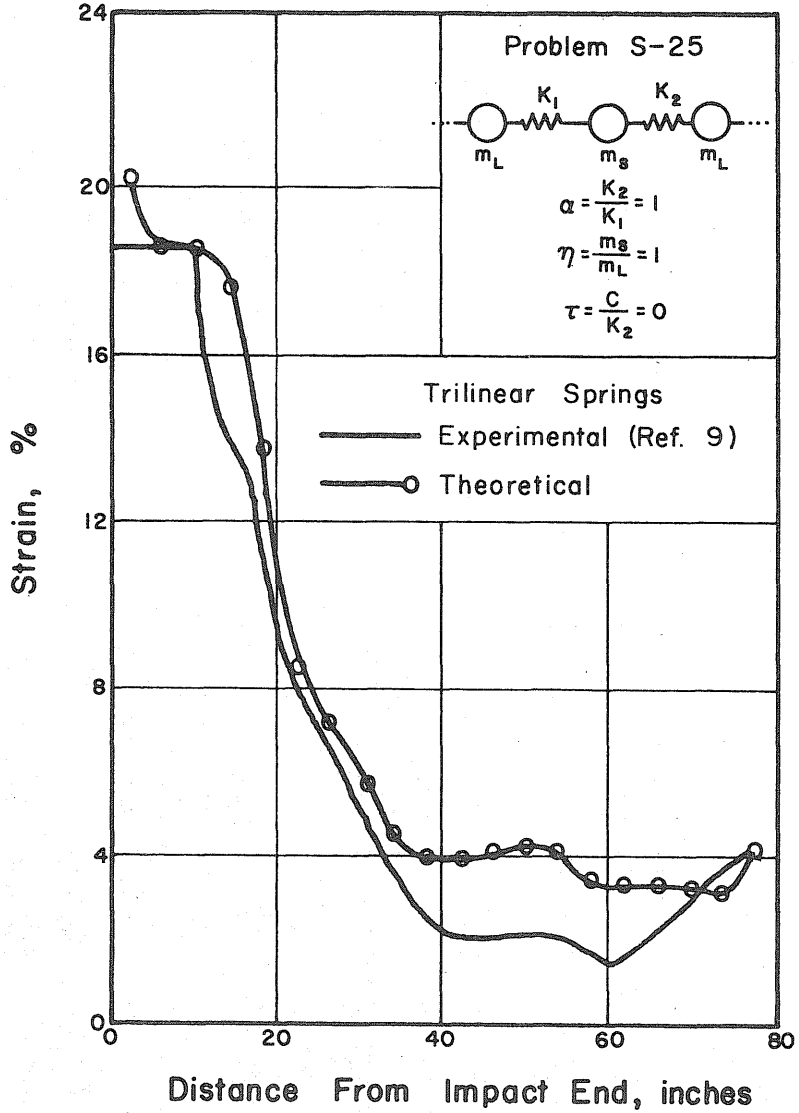

FIG. 43 STRAIN DISTRIBUTION FOR 80 INCH COPPER WIRE, $V_o = 201$ FPS.

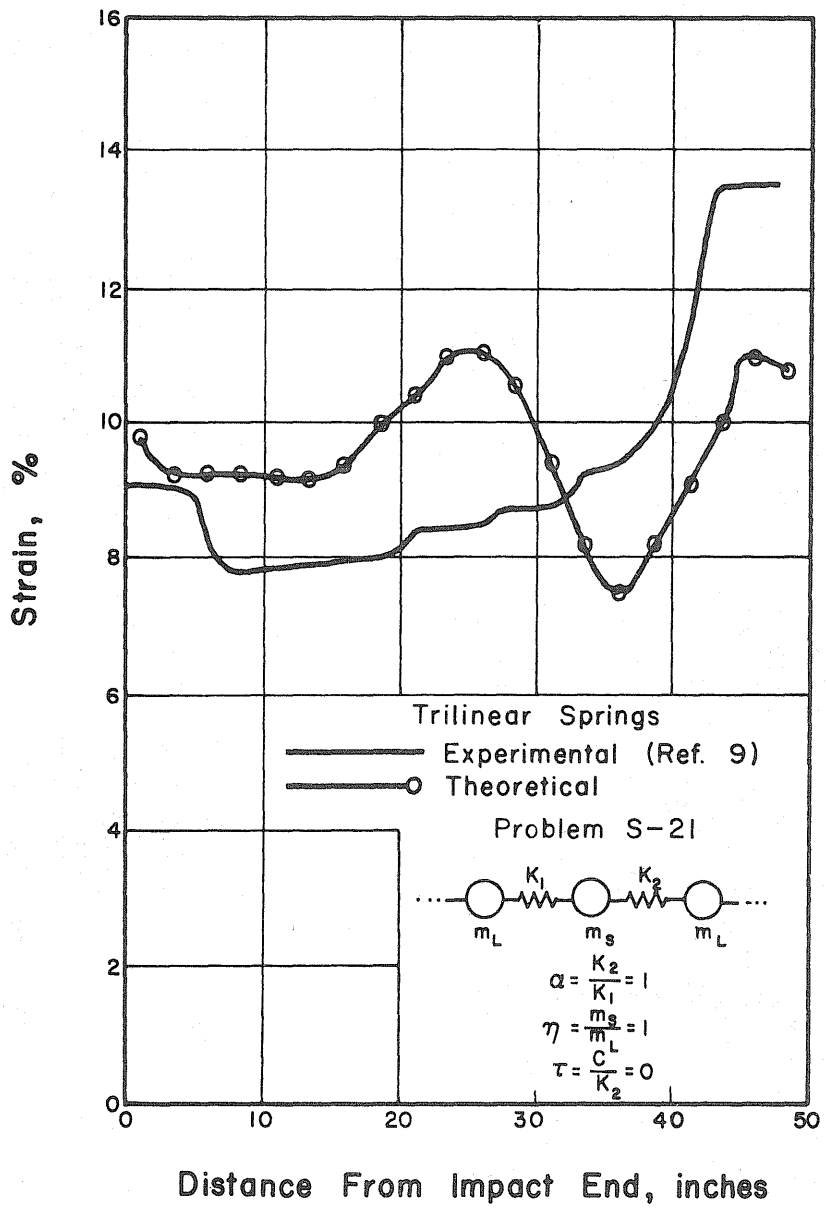

FIG. 44 STRAIN DISTRIBUTION FOR 50 INCH COPPER WIRE, V_o = 120 FT. PER SEC.

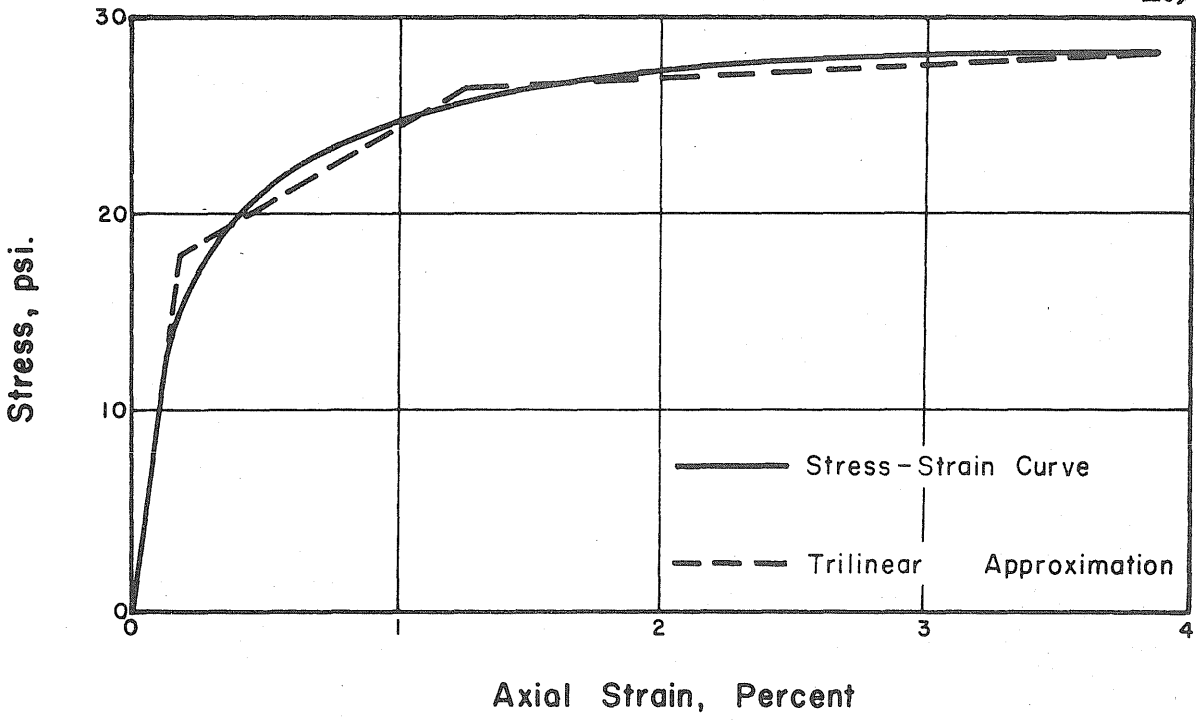

FIG. 45 STATIC STRESS–STRAIN CURVE FOR OTTAWA SAND (REF. 22)

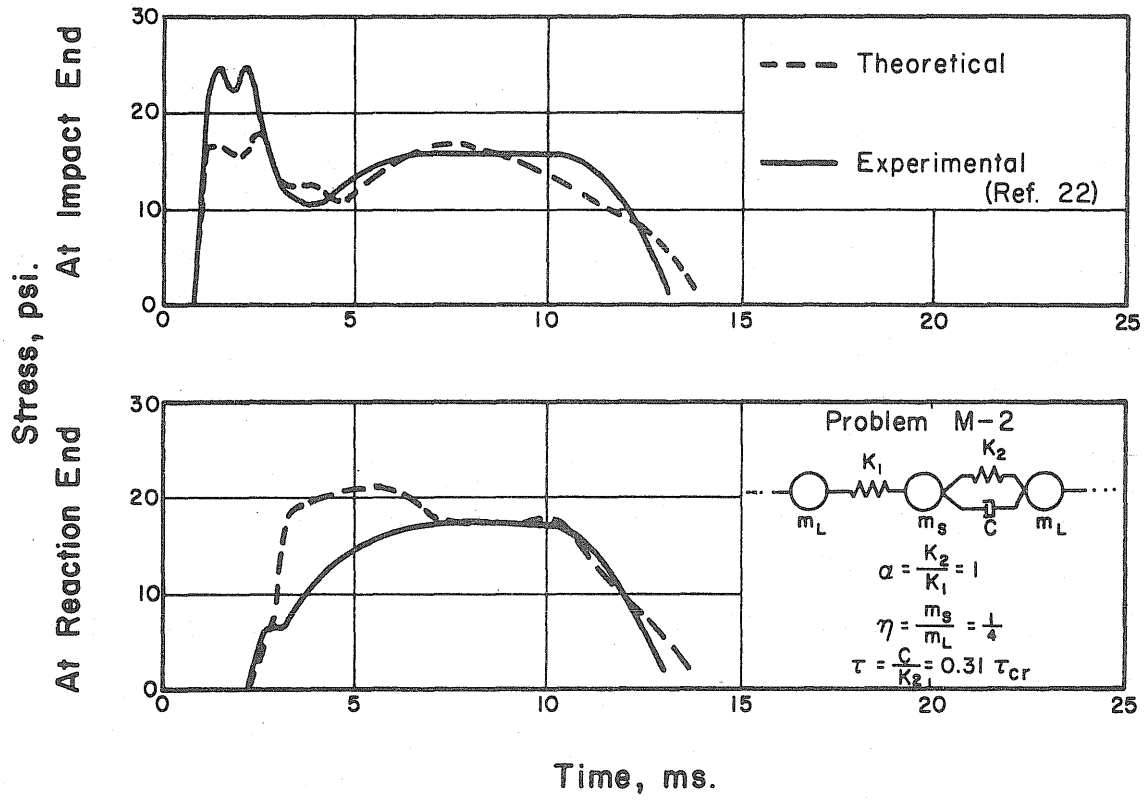

FIG. 46 STRESS VERSUS TIME FOR 20" OTTAWA SAND SPECIMEN, V_o = 15 IN. PER SEC.

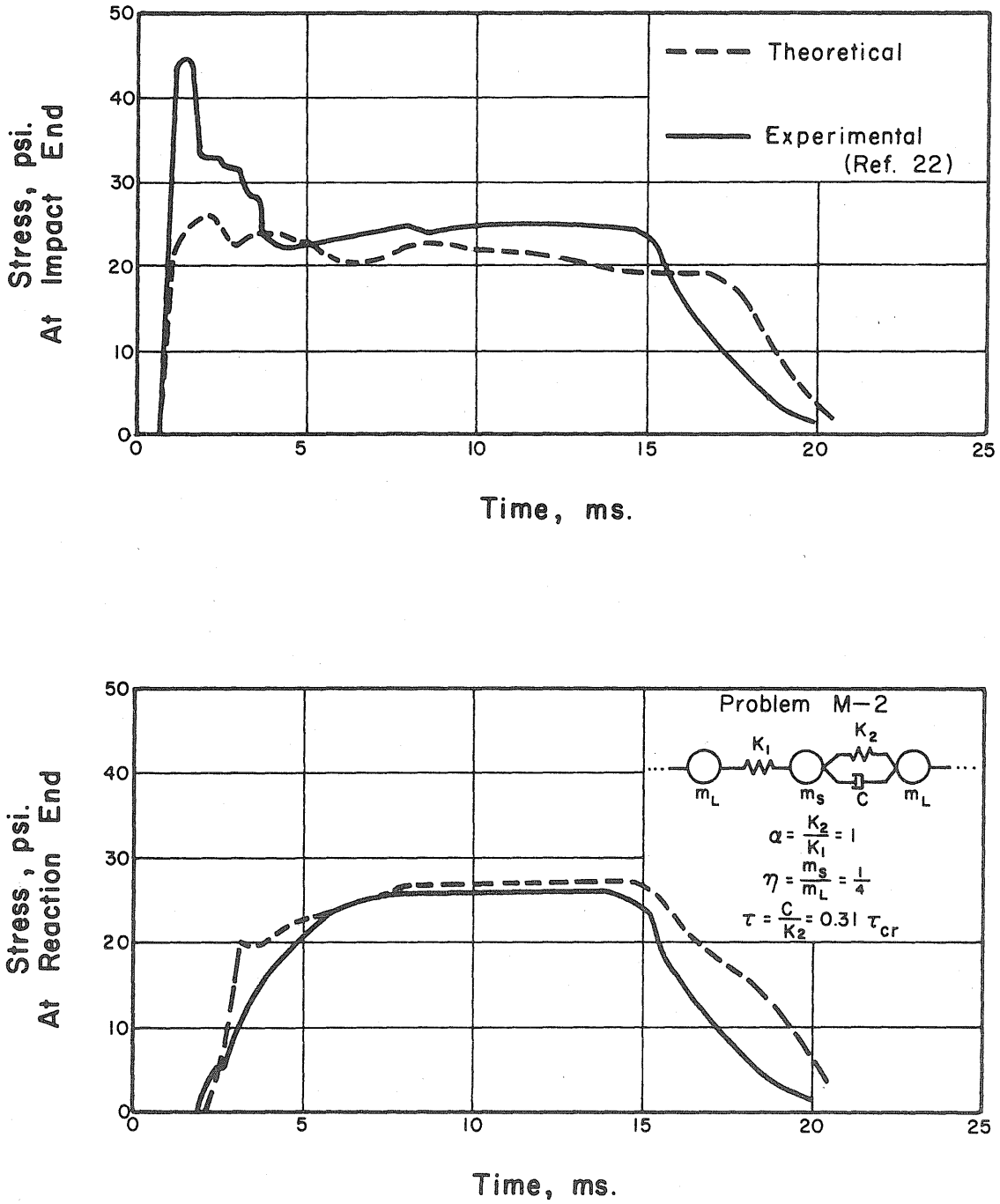

FIG. 47 STRESS VERSUS TIME FOR 20 INCH OTTAWA SAND SPECIMEN, V_o = 45 INCHES PER SEC.

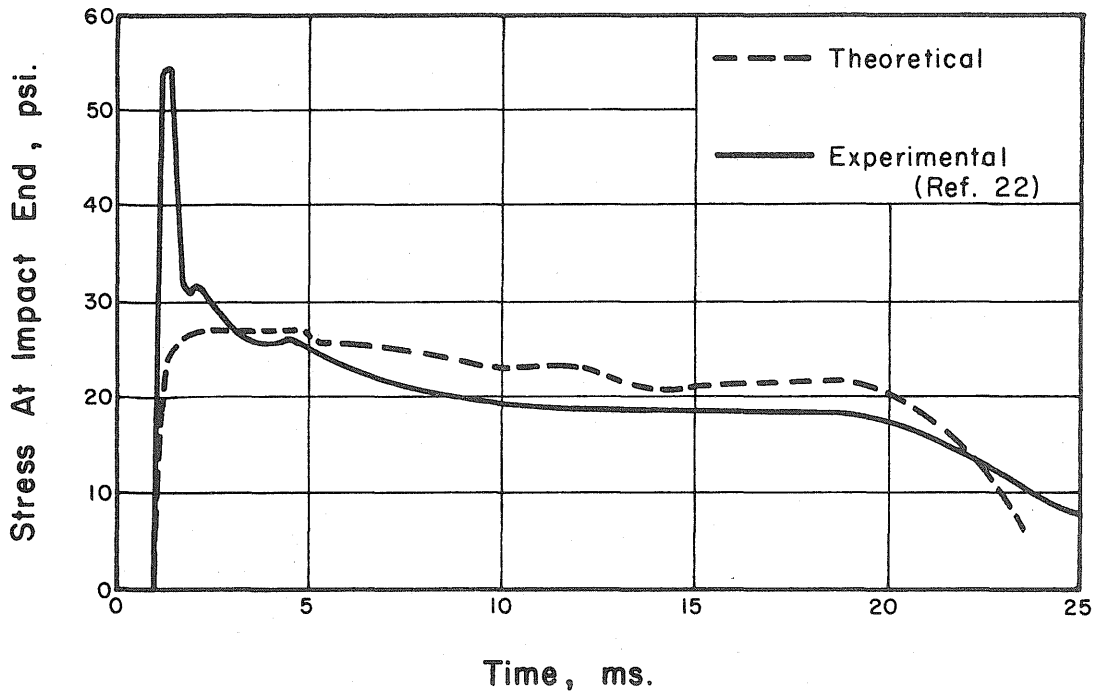

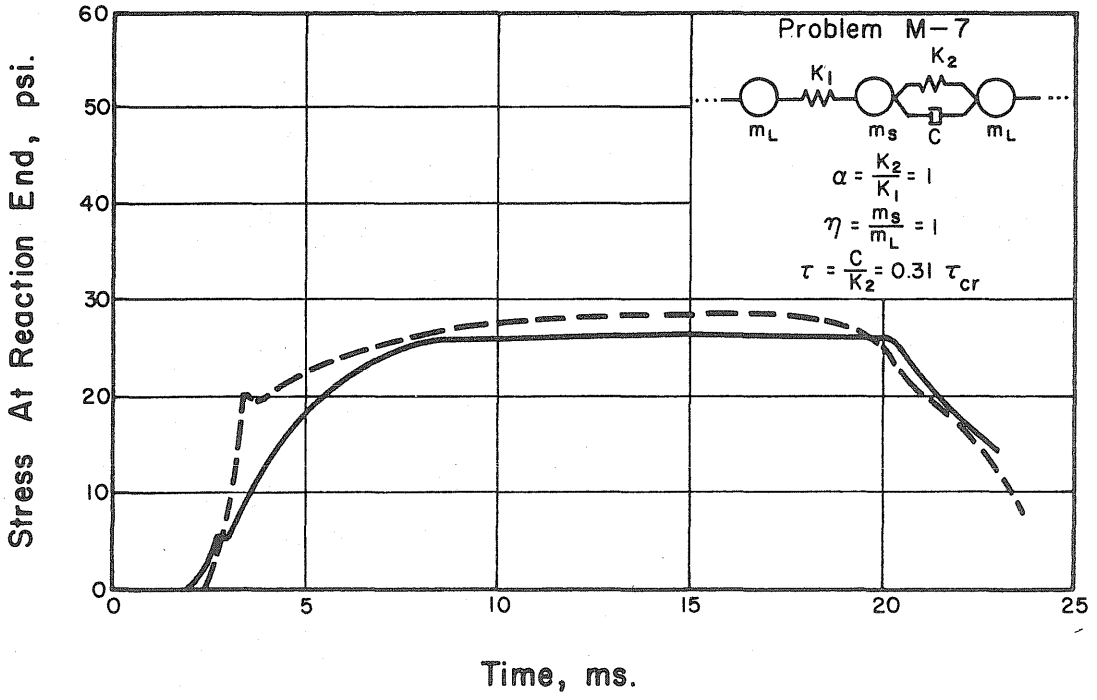

FIG. 48 STRESS VERSUS TIME FOR 20 INCH OTTAWA SAND SPECIMEN, V_o = 60 INCHES PER SEC.

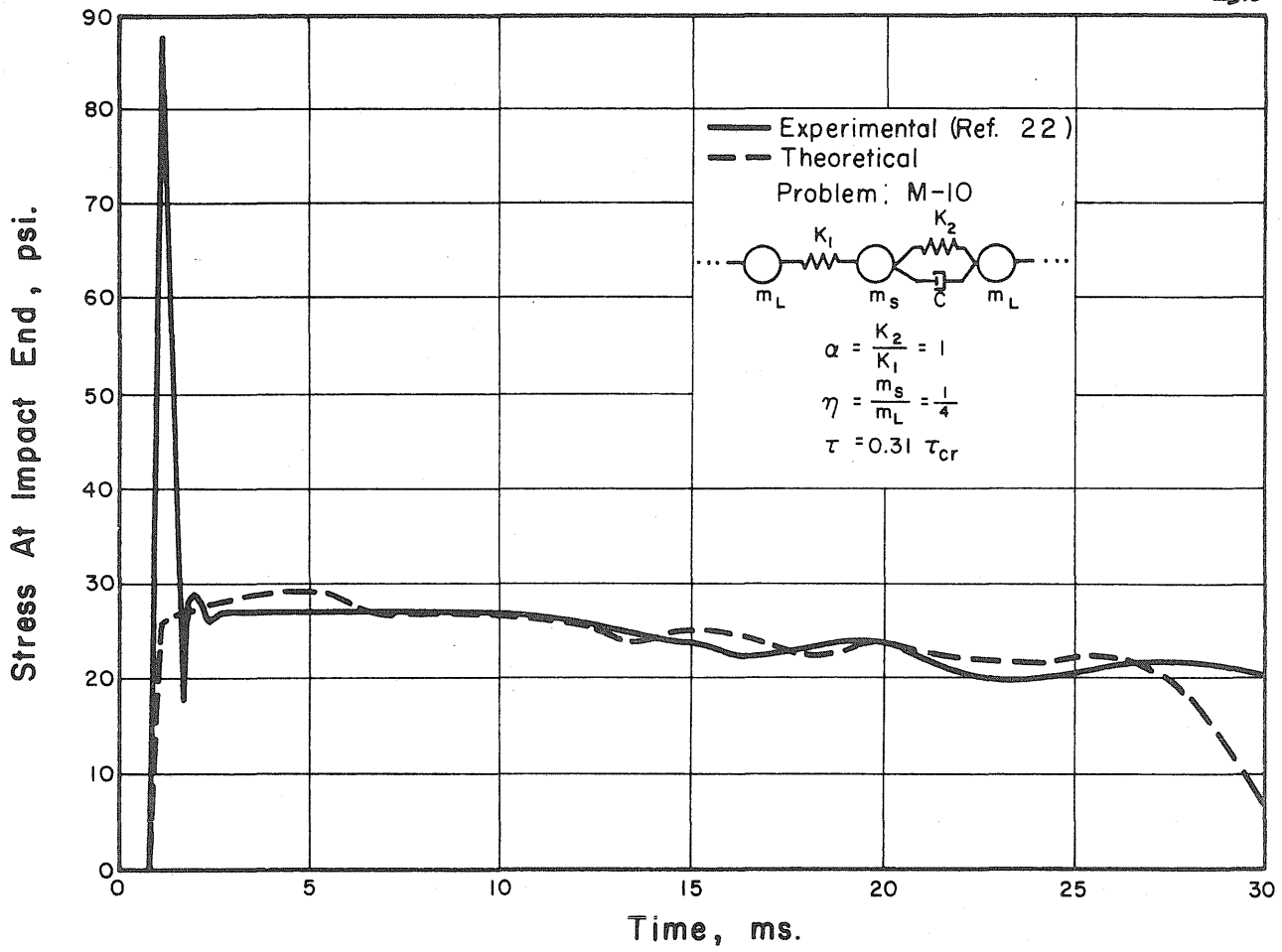

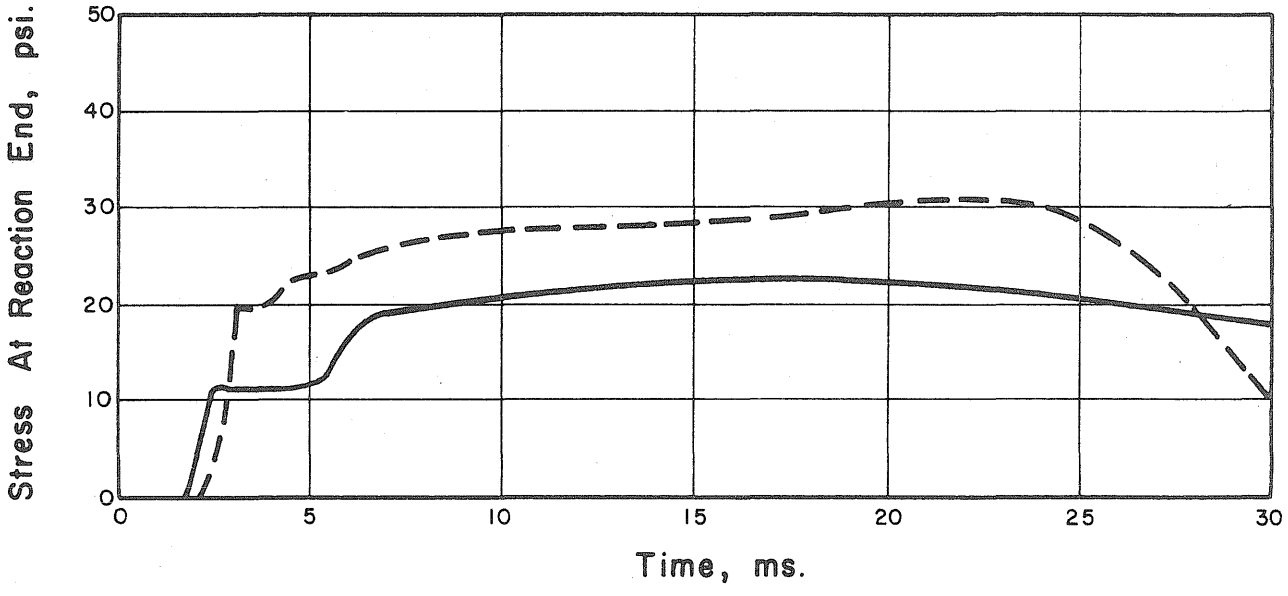

FIG. 49 STRESS VERSUS TIME FOR 20 INCH OTTAWA SAND SPECIMEN, V_o = 90 INCHES PER SEC.

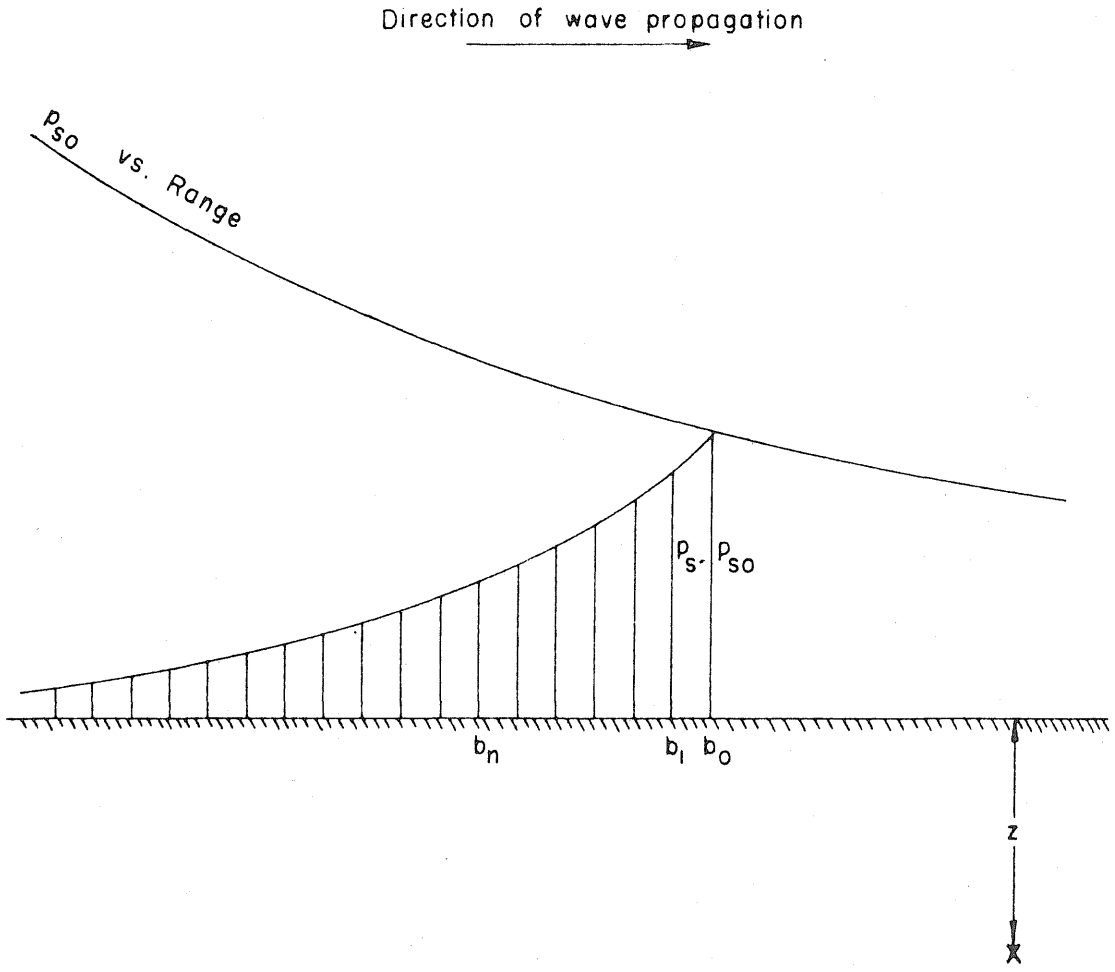

FIG. 50 ADVANCING PLANE WAVE

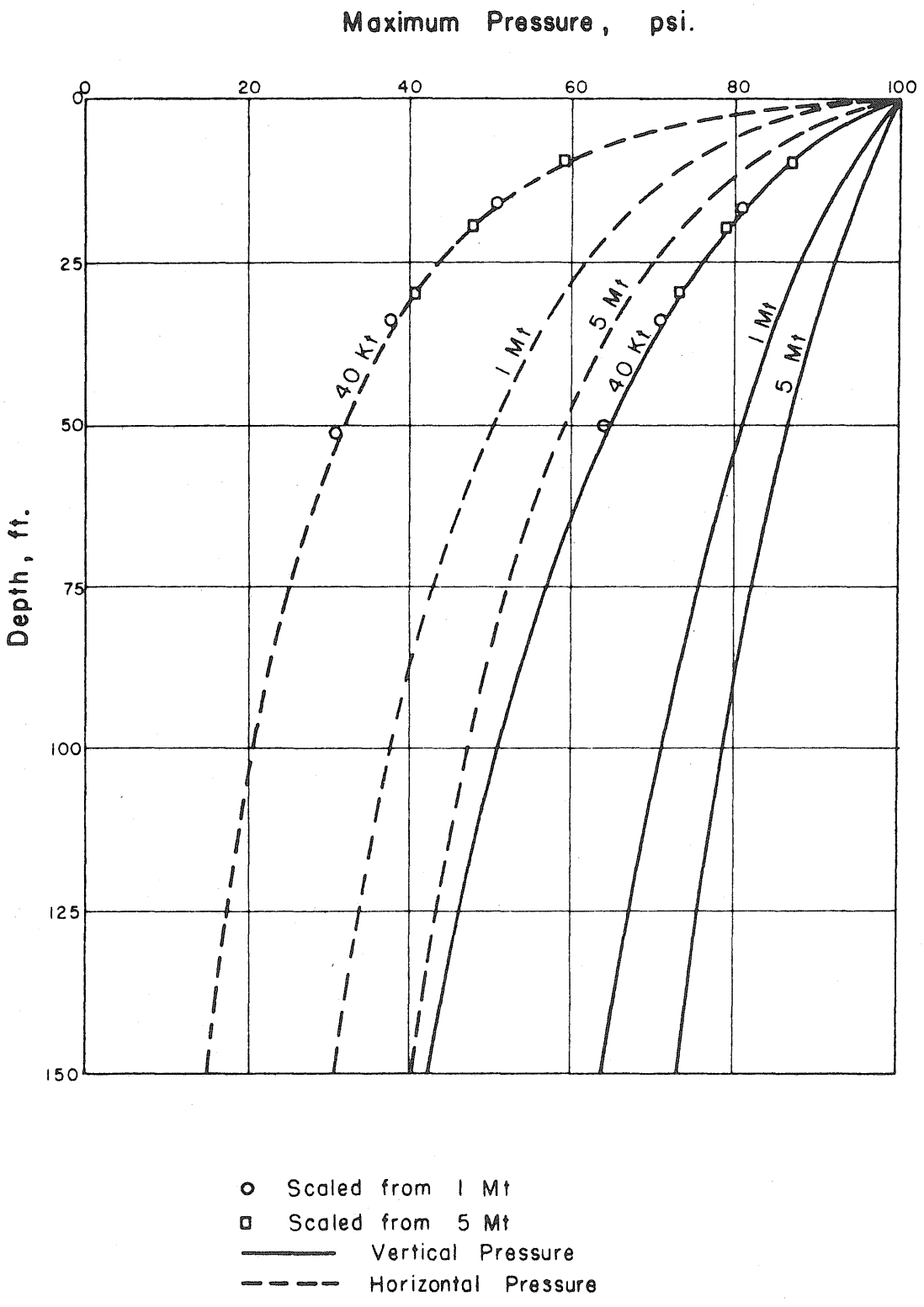

FIG. 51 MAXIMUM PRESSURE VERSUS DEPTH FOR 100 PSI. OVERPRESSURE

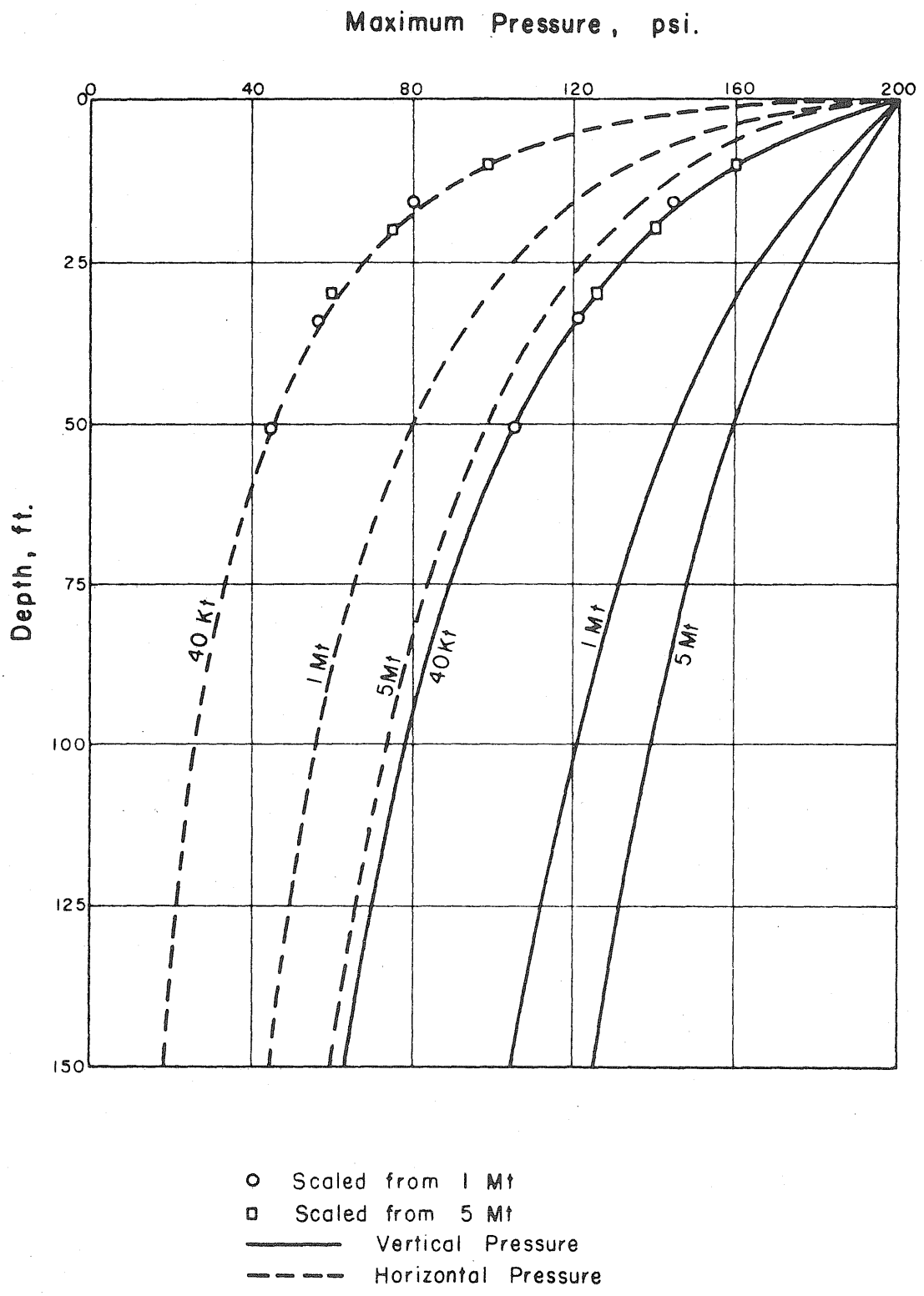

FIG. 52 MAXIMUM PRESSURE VERSUS DEPTH FOR 200 PSI. OVERPRESSURE

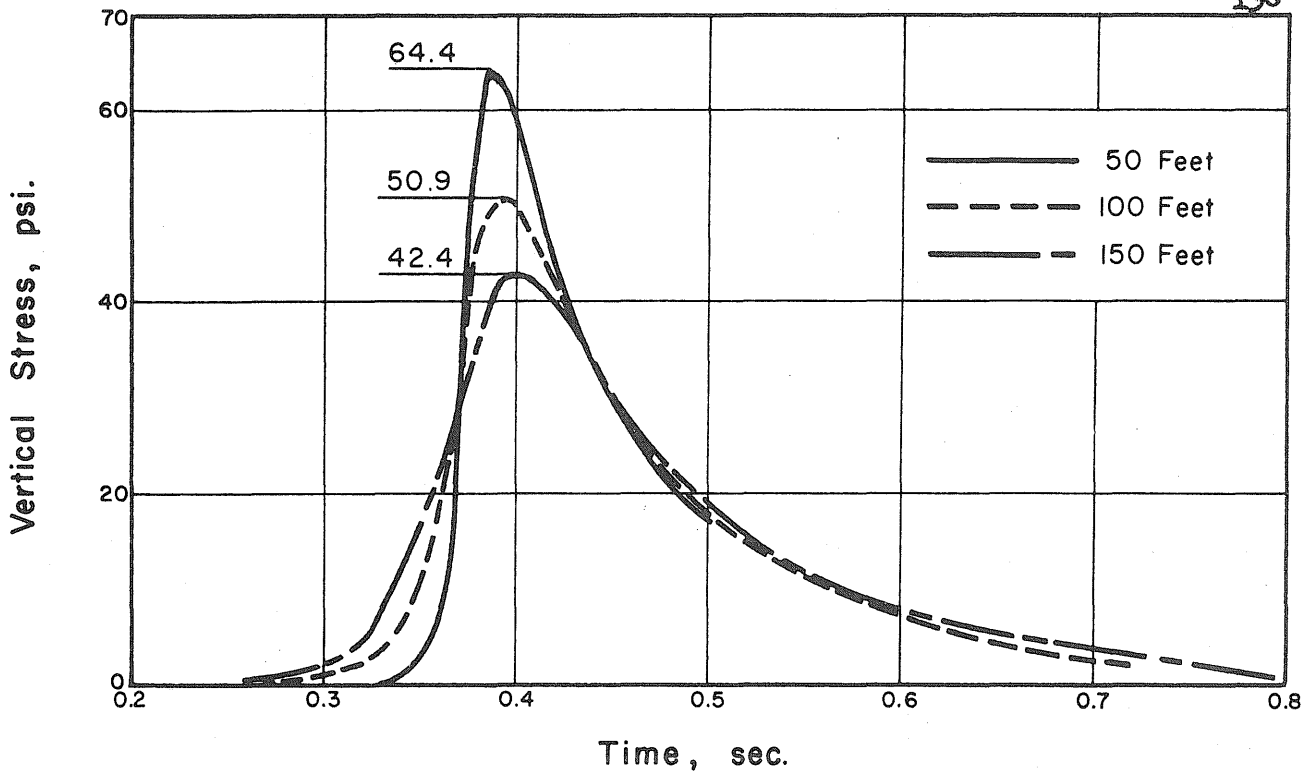

FIG. 53 VERTICAL STRESS VERSUS TIME, EFFECT OF SPATIAL DISPERSION — 40 Kt WEAPON

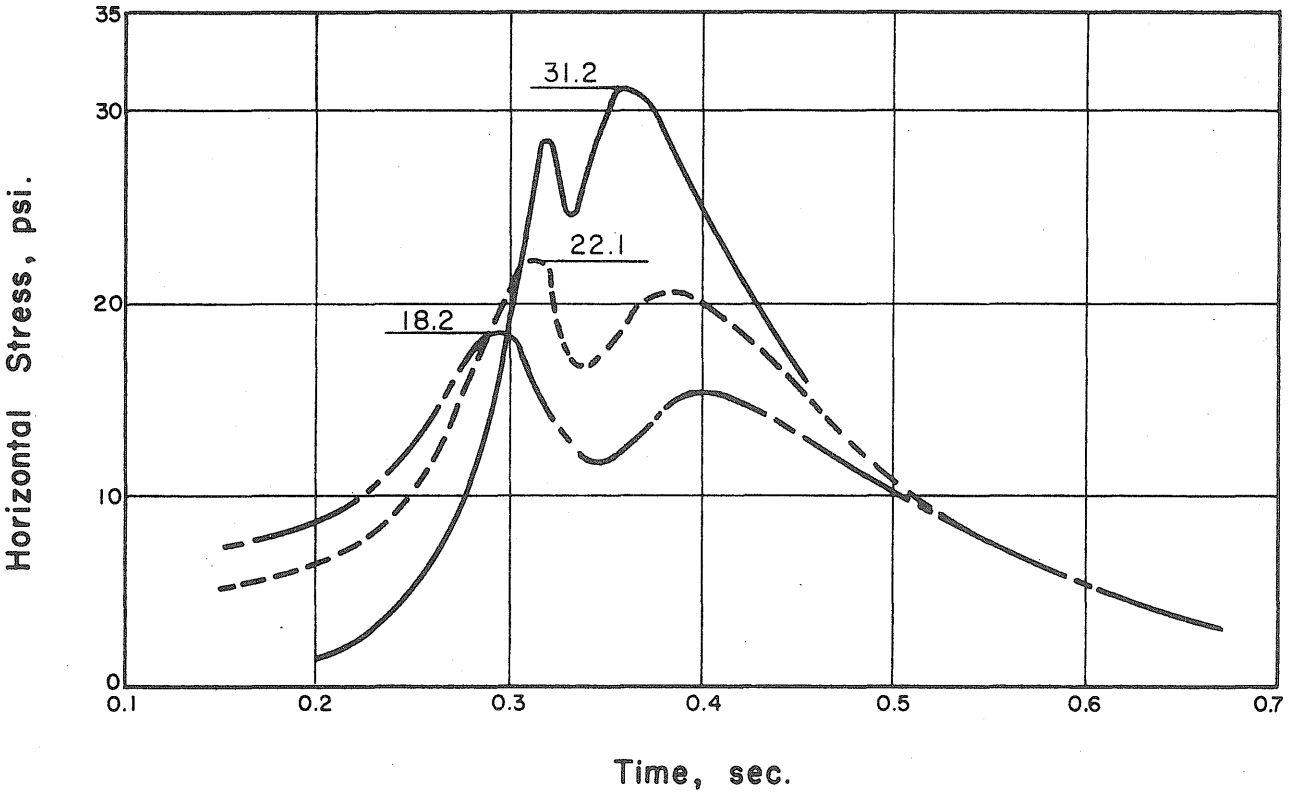

FIG. 54 HORIZONTAL STRESS VERSUS TIME, EFFECT OF SPATIAL DISPERSION — 40 Kt WEAPON